Mathematical optimization techniques for cognitive radar networks

Mathematical Optimization Techniques for Cognitive Radar Networks

Gaia Rossetti

Signal Processing and Networks Research Group
Wolfson School of Mechanical, Electrical
and Manufacturing Engineering

Loughborough University

A Doctoral thesis submitted in partial fulfilment
of the requirements for the degree of:

Doctor of Philosophy

19th July 2018

Certificate of Originality

This is to certify that I am responsible for the work submitted in this thesis, that the original work is my own except as specified in acknowledgements or in footnotes, and that neither the thesis nor the original work therein has been submitted to this or any other institution for a degree.

..... (Signed)

GAIA ROSSETTI (candidate)

To mamma, papà and Federica.

Who are always there for me.

Vi voglio bene.

Abstract

This thesis discusses mathematical optimization techniques for waveform design in cognitive radars. These techniques have been designed with an increasing level of sophistication, starting from a bistatic model (i.e. two transmitters and a single receiver) and ending with a cognitive network (i.e. multiple transmitting and multiple receiving radars). The environment under investigation always features strong signal-dependent clutter and noise. All algorithms are based on an iterative waveform-filter optimization. The waveform optimization is based on convex optimization techniques and the exploitation of initial radar waveforms characterized by desired auto and cross-correlation properties. Finally, robust optimization techniques are introduced to account for the assumptions made by cognitive radars on certain second order statistics such as the covariance matrix of the clutter.

More specifically, initial optimization techniques were proposed for the case of bistatic radars. By maximizing the signal to interference and noise ratio (SINR) under certain constraints on the transmitted signals, it was possible to iteratively optimize both the orthogonal transmission waveforms and the receiver filter. Subsequently, the above work was extended to a convex optimization framework for a waveform design technique for bistatic radars where both radars transmit and receive to detect targets. The method exploited prior knowledge of the environment to maximize the accumulated target return signal power while keeping the disturbance power to unity at both radar receivers.

The thesis further proposes convex optimization based waveform designs

for multiple input multiple output (MIMO) based cognitive radars. All radars within the system are able to both transmit and receive signals for detecting targets. The proposed model investigated two complementary optimization techniques. The first one aims at optimizing the signal to interference and noise ratio (SINR) of a specific radar while keeping the SINR of the remaining radars at desired levels. The second approach optimizes the SINR of all radars using a max-min optimization criterion.

To account for possible mismatches between actual parameters and estimated ones, this thesis includes robust optimization techniques. Initially, the multistatic, signal-dependent model was tested against existing worst-case and probabilistic methods. These methods appeared to be over conservative and generic for the considered signal-dependent clutter scenario. Therefore a new approach was derived where uncertainty was assumed directly on the radar cross-section and Doppler parameters of the clutters. Approximations based on Taylor series were invoked to make the optimization problem convex and subsequently determine robust waveforms with specific SINR outage constraints.

Finally, this thesis introduces robust optimization techniques for through-the-wall radars. These are also cognitive but rely on different optimization techniques than the ones previously discussed. By noticing the similarities between the minimum variance distortionless response (MVDR) problem and the matched-illumination one, this thesis introduces robust optimization techniques that consider uncertainty on environment-related parameters.

Various performance analyses demonstrate the effectiveness of all the above algorithms in providing a significant increase in SINR in an environment affected by very strong clutter and noise.

Statement of Originality

The contributions of this thesis mainly pertains the development of mathematical optimization techniques for cognitive radars. Specifically, various waveform optimization techniques based on convex optimization methods were developed. Additionally, in order to accommodate practical issues and uncertainties such as the availability of precise information of clutter parameters, robust optimization techniques have also been proposed for cognitive radars. The novelty of the contributions is supported by the following international journal and conference publications:

- In Chapter 4, a waveform optimization technique for bistatic cognitive radars has been proposed. This model is new to literature for the case of cognitive radars. The proposed technique works for the scenario of single receiving radar under signal-dependent clutter. The results of this work has been published in [2].

- The novelty introduced in Chapter 5 concerns three different waveform optimization techniques for two different multistatic radars models with centralized cognition. The first optimization criteria aims at maximizing the accumulated target return signal power while keeping the total disturbance power to unity. This model is suitable for small networks (possibly bistatic) with no specific target requirements. The second optimization criteria maximizes the signal power at a desired radar while keeping the SINR of all other radars at satisfactory level. This feature makes this algorithm suitable for applications where a

radar finds itself in a particularly advantageous position and it can also be used to counteract blockage effects. The third technique optimizes the SINR of all radar receivers equally and can be used for distributed surveillance in environments characterized by similar channels. The latter model is based on a max-min SINR criterion. Also, these last two optimization methods have been extended to an M number of radars. These works were published in [3] and [4].

- In Chapter 6, novel robust optimization techniques for a cognitive radar network have been proposed. The first two techniques employ traditional worst-case optimization and probabilistic (stochastic) optimization, respectively. These techniques, although well known to the literature, were not previously employed in the discussed scenario. Both methods are used for robust radar waveform design in the presence of uncertainty on the clutter-plus-noise covariance matrix. The third technique considers a completely novel approach where uncertainty is assumed directly on the radar cross-section and the Doppler of the clutter rather than on the clutter-plus-noise covariance matrix. The latter is solved using Taylor approximations and stochastic optimization. This work was published in [1].

- Chapter 7 introduces robust optimization techniques for a through-the-wall radar. The novelty introduced in this work is to apply robust minimum variance distortionless response (MVDR) optimization techniques to matched-illumination techniques. This work is ready for submission as a conference paper.

Jounal Paper

1. G. Rossetti, S. Lambotharan, "Robust Optimization Techniques for Cognitive Radar Networks," *IEEE Access*, Early Access Paper, Dec. 2017.

Conference Papers

2. G. Rossetti, A. Deligiannis, S. Lambotharan, "Waveform Design and Receiver Filter Optimization for Multistatic Cognitive Radar," *2016 IEEE Radar Conference (RadarConf)*, Washington DC, USA, 2016, pp. 1-5.

3. G. Rossetti, S. Lambotharan, "Waveform Optimization Techniques for Bi-Static Cognitive Radars," *2016 IEEE 12th International Colloquium on Signal Processing and Its Applications (CSPA)*, Malacca, Malaysia, 2016, pp. 115 - 118.

4. G. Rossetti, S. Lambotharan, "Coordinated Waveform Design and Receiver Filter Optimization for Cognitive Radar Networks," *2016 IEEE Sensor Array and Multichannel Signal Processing Workshop (SAM)*, Rio de Janeiro, Brazil, 2016, pp. 1-5.

5. G.Rossetti, S. Lambotharan, "Robust Matched-Illumination for Through-the-Wall Radar," to be submitted to an appropriate international conference.

Acknowledgements

I would like to thank Professor Sangarapillai Lambotharan for guiding me throughout my PhD. His advice and deep expertise have been fundamental to develop my research skills and my knowledge in the field of signal processing.

I would also like to thank Loughborough University and the EPSRC for providing me with the studentship and a beautiful campus filled with opportunities.

And a big thank you goes to my friends and colleagues Tasos, Anastasia, Kostas, Tien, Ben, Ye, Bokamoso, Ramadan and everyone else who is or has been part of the Signal Processing and Networks Research Group.

Moreover, this experience would not have been the same without my friends. Frazer, Lorraine and Anna. All my yogis, both my lovely SPY colleagues and my students, that warm my heart every time they take flight in their crows.

Distant in space but not in the heart, Christina and Sarika.

But mostly, thank you to my dear friend Eirini. Best flatmate I could have wished for and, most importantly, the best friend. She was there for weekend trips, funny Halloween costumes and evening movies. But she was also there to take endless pictures for my yoga plans and to support me with chocolate and kind words whenever I needed.

Patrick. I feel so lucky and grateful that this journey lead me to you. Simply, thank you.

Contents

List of Figures

List of Tables

List of Acronyms

AAF	Auto-Ambiguity Function
AF	Ambiguity Function
AWG	Arbitrary Waveform Generator
BTT	Bayesian Target Tracker
CAF	Cross-Ambiguity Function
CDF	Cumulative Distribution Function
CDMA	Code Division Multiple Access
CRB	Cramér-Rao Bound
CRN	Cognitive Radar Network
CS	Compressive Sensing
CS-MIMO	Compressive Sensing Multiple Input Multiple Output
DMRS	Distributed Multiple-Radar System
DOA	Direction-of-Arrival
DS	Direct Sequence
FPGA	Field Programmable Gate Array
i.i.d.	Independent and Identically Distributed
KA	Knowledge-Aided
KB	Knowledge-Based
LFM	Linear Frequency Modulated
LP	Linear Program

LS	Least Squares
MI	Matched-Illumination
MIMO	Multiple-Input Multiple-Output
MMSE	Minimum Mean Square Error
MVDR	Minimum Variance Distortionless Response
NP	Nondeterministic in Polynomial (time)
QCQP	Quadratically Constrained Quadratic Program
QP	Quadratic Program
RCS	Radar Cross-Section
RF	Radio Frequency
RSA	Radar Scene Analyzer
SDP	Semidefinite Programming
SINR	Signal to Interference Noise Ratio
SLA	Sense-Learn-Adapt
SNR	Signal to Noise Ratio
SOCP	Second Order Cone Program
STR	Separated Transmit Receive
TOA	Time-of-Arrival
TRS	Target Radar Signature
TWRI	Through-the-Wall Radar Imaging
ULA	Uniform Linear Array
UWB	Ultra-Wideband
WCR	Wideband Cognitive Radar

List of Symbols

Note: bold lowercase and bold uppercase letters represent vectors and matrices respectively.

$\odot$	Hadamard product
$(\cdot)^*$	conjugate operator
$(\cdot)^T$	transpose operator
$(\cdot)^H$	Hermitian operator
$\mathcal{CN}(\mu, \sigma^2)$	complex normal distribution (mean μ, variance σ^2)
$\mathbb{E}[\cdot]$	statistical expectation operator
$diag(\mathbf{A})$	diagonal of matrix $\mathbf{A}$
$\mathbf{dom}f$	domain of function f
$blkdiag(\mathbf{A})$	block diagonalization operator on matrix $\mathbf{A}$
$\mathcal{L}(\cdot)$	Lagrangian function
$Pr(\cdot)$	probability operator
$tr(\mathbf{A})$	trace of matrix $\mathbf{A}$
$rank(\mathbf{A})$	rank of matrix $\mathbf{A}$
$\succeq$ (or $\succ$)	generalized matrix inequality
$\|\mathbf{x}\|$	Euclidean norm of vector $\mathbf{x}$
$\|\mathbf{X}\|_{\mathcal{F}}$	Frobenius norm of matrix $\mathbf{X}$
$\mathbf{A}_{j,i,b_r}$	Subscript: signal transmitted by Radar-j, scattered by range-azimuth bin b_r, received at Radar-i

Chapter 1

Introduction

An overview on topics that are propaedeutic towards a full understanding of the research presented in this thesis is hereby provided. At first, the main principles on which radar systems are based (i.e. concepts such as *radar equation*, range resolution and Doppler frequency) are described. Next, some tools for waveform analysis (such as the matched filter and the ambiguity function), followed by a brief overview on minimum variance distortionless response (MVDR) beamformers are introduced. In the subsequent section the pros and cons of the most widely used radar waveforms such as the constant-frequency pulse, the linear frequency-modulated pulse, a train of pulses and phase-coded pulses are described. Furthermore, a thorough outline on cognitive radars is presented. Lastly, a brief overview on convex optimization techniques is provided followed by an outline of the remaining chapters.

1.1 Basic Radar Principles

The term radar finds its roots in the acronym of the expression RAdio Detection And Ranging. These systems work by exploiting the information contained in electromagnetic waves that propagate and reflect in a targeted environment. Radars can be used to evaluate distances, detect and track moving targets and create images. Being more specific, the principle is that a transmitter sends out a radio signal, which will scatter off any surface that it encounters and a small amount of energy is scattered back to a radio receiver, which is usually located near the transmitter. After amplification in the receiver, the signals are processed to sort out the required echoes from the the clutter [3]. The well known *radar equation* quantifies the process that connects the transmitted wave, the free space propagation, the incidence with the target and the received wave:

$$P_r = \frac{P_t G_t G_r \lambda^2}{(4\pi)^3 R^4} \sigma \tag{1.1}$$

The received power P_r is defined by three main features:

- The characteristics of the system (through the transmitted power P_t, the antenna features at the transmitter G_t and at the receiver G_r and the wavelength λ);
- Distance R between satellite and target (4π accounts for free space attenuation);
- Target properties represented by the radar cross-section (RCS) σ.

In fact, it is thanks to this dependence with R that the radar is able to evaluate the range distance of a target. By measuring the time τ_a after

which the signal reached the receiver, the range R can be calculated as:

$$R = \frac{c\tau_a}{2}$$

where c is the velocity of propagation, which is usually approximated with the speed of light. The problem is nevertheless not as straightforward since the pulse duration of the signal needs to be taken into account. The range resolution tells us how far apart two targets have to be before we can see that there are indeed two targets rather than a single large one [3]. The range resolution can also be called range bin which is a widely used term when considering target localization and tracking.

The targets contribution is accounted for in the radar equation by the radar cross-section σ. This is a complex coefficient that defines the scattering behavior of the target. It is defined as a measure of the power that a target scatters in a given direction when illuminated by an incident wave, normalized to the power density of the incident wave at the target. The normalization is necessary in order to remove the effects of the distance radar-target and the effects of the transmitter power level [4].

Another very important parameter in radar systems is the Doppler frequency. This is the change in the frequency of the radio signal caused by the motion of the target and it is equal to:

$$f_D = \frac{2v_r}{\lambda}$$

where v_r is the radial component of the target speed towards the radar and λ is the wavelength of the radio signal [3].

When talking about surveillance radars (i.e. radars that deal with localization and tracking activities such as air traffic control radars or air-borne

radar defence systems) another very important aspect that needs to be mentioned is clutter. This term is used to identify all the unwanted echoes that originate from elements in the environment under investigation: these are not targets but nevertheless contribute to the received signal. This additive disturbance cannot be confused with thermal noise which, for all practical radars, can be considered to be white [3].

1.2 Tools for Waveform Analysis

In order to design and analyze radar waveforms, a matched filter and an ambiguity function are necessary implementations.

1.2.0.1 Matched Filter

The filter used in radar to measure the delay of a returned known signal is usually the matched filter. The matched filter $h(t)$ concentrates the entire energy of the signal into an output peak at a predetermined additional delay t_0:

$$h(t) = Ks^*(t_0 - t)$$

where K is an arbitrary constant and s^* the conjugate of the transmitted waveform. The peak of the output of the matched filter is a function of the signal's energy and the output before and after the peak are strongly affected by the waveform. As previously mentioned, the pulse duration also needs to be taken into account and if the output level of the peak of the matched filter remains high over an extended delay, there will be an uncertainty as to which is the true delay. This would obviously be an undesired problem [5]. When considering a surveillance scenario, it is very likely to deal with signals that have been reflected by moving targets and that are therefore affected by

a Doppler frequency shift. Without exact knowledge of the Doppler shift, the radar receiver cannot modify its matched receiver to the new carrier frequency exactly and mismatch occurs. The response of a matched filter therefore needs to be studied in two dimensions: delay τ and Doppler ν. The tool for that is the ambiguity function.

1.2.0.2 Ambiguity Function

The ambiguity function (AF) represents the time response of a filter matched to a given finite energy signal when the signal is received with a delay τ and a Doppler shift ν relative to the nominal values expected by the filter. The definition provided by [5] is:

$$|\chi(\tau,\nu)| = \left| \int_{-\infty}^{\infty} u(t)u^*(t+\tau)\exp(j2\pi\nu t)\mathrm{d}t \right|$$

The three main AF properties are:

- Has a maximum (normalized to 1) in (0,0);
- Has constant volume (i.e. if we attempt to squeeze the AF to a narrow peak at the origin, the peak cannot exceed the value of 1 and the volume squeezed out of the peak must reappear somewhere else);
- It is symmetric with respect to the origin.

The AF has been derived (and thereafter widely used) as a tool to characterize the resolution performance of waveforms (in [6], [7] and many others) but, as it will be described in the following chapters, it has also been implemented in order to design waveforms with desired features (see for example [8], [9]).

1.3 MVDR Beamformers

In radar applications, array signal processing regards antenna elements that respond to incident electromagnetic waves. The requirement is to detect the source responsible for radiating the electromagnetic waves, estimate the angle of arrival of the waves, and extract information about the source [10]. In this scenario, beamforming has the purpose of distinguishing between the spatial properties of signal and noise. The beamformer has to satisfy two requirements:

- steering capability, whereby the target signal is protected;
- cancelation of interference, so that the output signal-to-noise ratio is maximized [10].

On method of satisfying these requirements is to minimize the variance (i.e., the average power) of the beamformer output, subject to the constraint that the $M \times 1$ weight vector $\mathbf{w}$ satisfies the condition:

$$\mathbf{w}^{\mathrm{H}}\mathbf{p}(\theta) = 1 \quad \text{with} \quad \theta = \theta_t, \tag{1.2}$$

where $\mathbf{p}(\theta) = [1, \mathrm{e}^{-j\theta}, \ldots, \mathrm{e}^{-j(M-1)\theta}]$ is the $M \times 1$ steering vector and $^{\mathrm{H}}$ denotes the Hermitian transposition and θ_t is the direction of the target. In Chapter 7, we will consider a similar model:

$$\mathbf{w}^{\mathrm{H}}\mathbf{v}(\theta) = 1 \quad \text{with} \quad \theta = \theta_t, \tag{1.3}$$

where $\mathbf{v}(\theta_t) = \alpha_t \mathbf{s} \odot \mathbf{p}(\theta_t)$ is the target's contribution and α_t is the radar cross-section of the target, $\mathbf{s}$ is the signal and $\odot$ identifies the Hadamard product.

The optimization problem of minimizing the variance of the interference and noise at the output of the adaptive beamformer while ensuring the distortionless response of the beamformer towards the direction of the target can be written as [11]:

$$\begin{aligned} \min_{\mathbf{w}} \quad & \mathbf{w}^{\mathrm{H}}\, \mathbf{R}\, \mathbf{w} \\ \text{s.t.} \quad & \mathbf{w}^{\mathrm{H}} \mathbf{v}(\theta_t) = 1, \end{aligned} \tag{1.4}$$

where $\mathbf{R}$ is the covariance matrix of the interference plus jammer and noise. The standard minimum variance distortionless response (MVDR) beamforming problem finds a solution in the following optimized value:

$$\mathbf{w}_{\mathrm{MVDR}} = \frac{\mathbf{R}^{-1}\mathbf{v}(\theta_t)}{\mathbf{v}^{H}(\theta_t)\mathbf{R}^{-1}\mathbf{v}(\theta_t)}.$$

The ability of an MVDR beamformer to reject interferers depends on the number of the antennae M the array has available. As a matter of fact, the MVDR has $(M-2)$ degrees of freedom to steer a beam towards the direction of the signal of interest or to place $(M-2)$ nulls to cancel $(M-2)$ independent interferences.

1.4 Radar Signals

The commonly known radar signals can be subdivided into four categories.

1.4.0.3 Constant-Frequency Pulse

A constant-frequency pulse is a single, unmodulated pulse:

$$u_{\mathrm{CFP}}(t) = \frac{1}{\sqrt{T}}\mathrm{rect}\left(\frac{t}{T}\right),$$

where rect(·) identifies the rectangular function. Due to its inefficient bandwidth occupation, the constant-frequency pulse provides poor performance in terms of both range and Doppler resolution. As a matter of fact, at zero-Doppler, the ambiguity function shows a triangular shape and, at zero-delay, it is the absolute value of a cardinal sine function [5].

1.4.0.4 Linear Frequency-Modulated Pulse

Linear frequency-modulated (LFM) pulse is a very popular pulse compression method, also known as *Chirp*. The complex envelope of an LFM pulse is given by:

$$u_{\mathrm{LFM}}(t) = \frac{1}{\sqrt{T}}\mathrm{rect}\left(\frac{t}{T}\right)\exp(j\pi kt^2)$$

Adding LFM increases the bandwidth and thus improves the range resolution of the signal by a factor equal to the time-bandwidth product. However the improved delay resolution of LFM comes with a penalty: delay-Doppler coupling (expressed by a diagonal ridge that will be seen in the ambiguity function.)

1.4.0.5 Coherent Train of Identical Unmodulated Pulses

This waveform is a coherent pulse train of identical, unmodulated pulses:

$$u_{\mathrm{T}}(t) = \frac{1}{\sqrt{T}}\sum_{n=1}^{N} u_{\mathrm{CFP}}[t-(n-1)T_r]$$

where u_{CFP} identifies a constant-frequency pulse, N is the number of identical pulses and T_r is the pulse repetition interval. The significant advantage of such waveform design is that the delay resolution is controlled by the pulse duration T, while the Doppler resolution is controlled by the total signal length NT_r. On the other hand, Doppler and delay ambiguities are

tied so a tradeoff still needs to be accepted [5].

1.4.0.6 Phase-Coded Pulses and Barker Codes

Phase-coded pulses are a single pulse of duration T which has been divided into M bits of identical duration $t_b = {}^{T}/_{M}$. Each bit is then assigned (i.e. coded) with a different phase value. The complex envelope of the phase-coded pulse is given by:

$$u_{\mathrm{PC}}(t) = \frac{1}{\sqrt{T}} \sum_{m=1}^{M} u_m \mathrm{rect}\left[\frac{t-(m-1)t_b}{t_b}\right]$$

where $u_m = \exp(j\phi_m)$ and the set of M phases $\left[\phi_1, \ \phi_2, \ \ldots \ \phi_m\right]$ is the phase code associated with $u_{\mathrm{PC}}(t)$. The advantage of this coding technique is that it lowers the main lobe width. In order to find a code with good resolution properties, it is sufficient to calculate the auto-correlation function of the code at integer multiples of the bit duration which is a more manageable problem than optimizing directly the ambiguity function. Probably the most famous family of phase codes is Barker codes. Originally, these were designed as sets of M binary phases yielding a peak-to-peak sidelobe ratio of M. An example of autocorrelation function of a 13-element Barker code can be seen in Figure 1.1.

1.4.1 Waveforms for MIMO Radars

In a MIMO radar, N_t antennas transmit N_t different waveforms simultaneously. These waveforms propagate in the environment, are reflected by the target and other scattering objects and are then received by N_r receive antennas. Each receiver is connected to a bank of filters, with one filter tuned to each of the transmitted waveforms [12]. These filters aim at can-

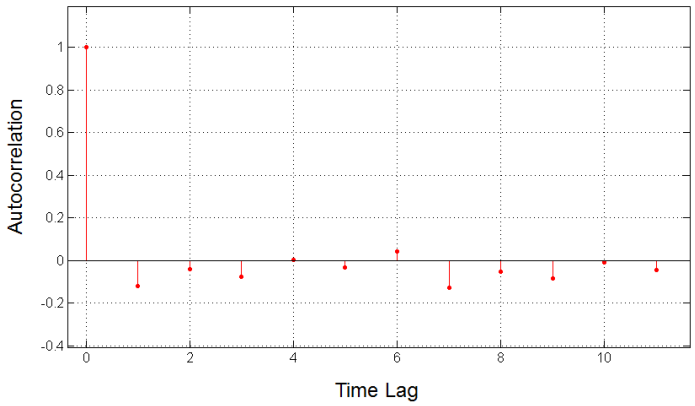

Figure 1.1: Autocorrelation function of a 13-element Barker code. As it can be seen, there is one single peak at zero time lag.

celing all waveforms that are not of interest to a specific radar. In order for this to work, perfectly orthogonal waveforms should be used. In practice, however, such waveforms do not exist and must be approximated. This in turn has prompted new research into the area of waveform design, with particular emphasis on minimizing waveform cross-correlation levels as well as autocorrelation sidelobe levels [12].

A work of particular interest, that has been implemented in the proposed work, is that of Clemente et al. [1]. In this paper the authors show how to obtain nearly orthogonal codes by modulating common minimum peak sidelobe waveforms with fractional Fourier transforms. As it can be seen in Figure 1.2, the resulting codes are characterized by very good autocorrelation and cross-correlation properties. The initial waveforms that have been selected are Barker 13, Frank 16, P4 25 (which are all phase-coded pulses) and Costas 7 (which are non-linearly frequency-modulated pulses). These are all well known radar waveforms with very good autocorrelation properties that have been designed for a single transmitting radar. By applying fractional Fourier transform to them, they will obtain the necessary combination of

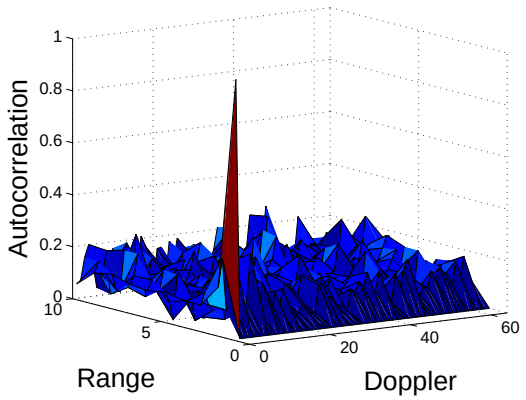

(a) AAF of s_1

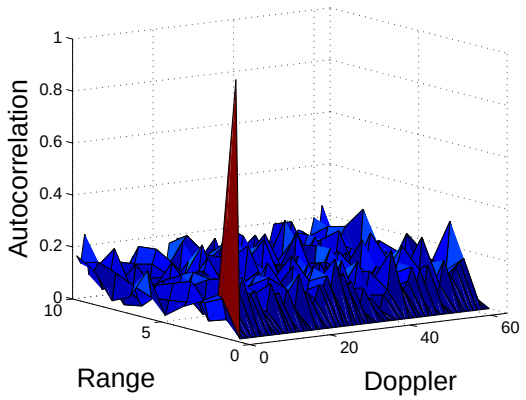

(b) AAF of s_2

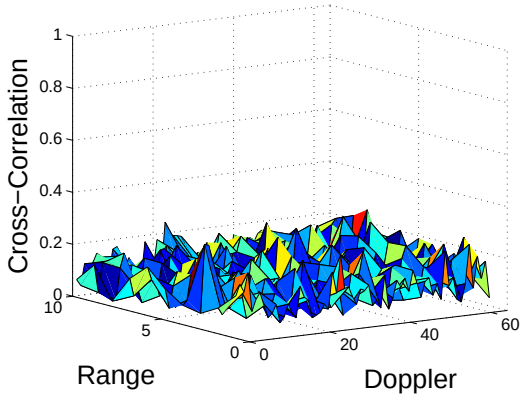

(c) CAF of s_1, s_2

Figure 1.2: Auto-ambiguity function (AAF) and cross-ambiguity function (CAF) of two nearly orthogonal waveforms $\mathbf{s}_1$ and $\mathbf{s}_2$ developed in [1]. They present very narrow autocorrelation peaks and small sidelobes proving their resolution in both range (τ) and Doppler (ν) domains. Furthermore, their cross-ambiguity function shows no significant interference between the two waveforms.

characteristics (i.e. good range resolution as well as orthogonality), making these codes ideal for MIMO applications. In order to deal with waveform diversity in a MIMO scenario, the authors in [13] subdivided the ambiguity function into an auto-ambiguity function (AAF) for each implemented signal and cross-ambiguity functions (CAF) between signals.

1.5 Cognitive Radars

Cognitive radars were first theorized in 2006 by Haykin [2], who was inspired by neurobiology and the success rate of target capture for echo-locating bats. They are characterized by three main aspects:

- Intelligent signal processing, achieved through the interactions of the radar with the surrounding environment (i.e. perception);
- Feedback from the receiver to the transmitter (i.e. intelligence);
- Preservation of the information content of radar returns (i.e. memory). This feature makes cognitive radars ideal candidates for target tracking which can be realized thanks to a Bayesian approach.

The inception of radars that mimic neuronal computations was justified by the increasing complexity of modern high performance radar challenges (e.g. targets embedded in complex clutter, competing background target settings, RF interference and so on) [14]. The block diagram in Figure 1.3 depicts the cognitive cycle which establishes the operating principles of such radars. The cycle begins with the transmitter illuminating the environment (left-hand side). The radar returns produced by the environment are fed at the receiver (right-hand side) into two functional blocks: the radar-scene analyzer and the Bayesian target-tracker (for those applications that require

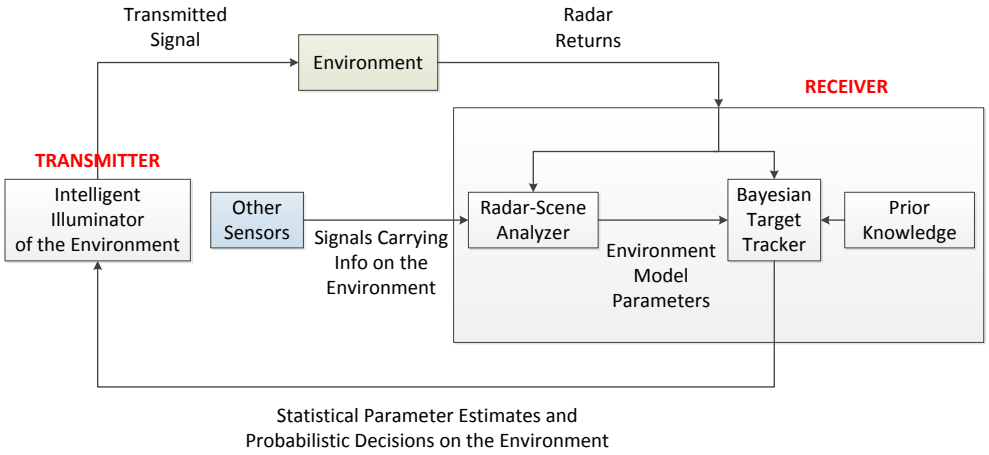

Figure 1.3: Block diagram of cognitive radar viewed as a dynamic closed-loop feedback system as described in [2].

such processing). The tracker makes decisions in light of information on the environment provided by the radar-scene analyzer. The transmitter, in turn, illuminates the environment in light of the decisions made on possible targets, which are fed back to it by the receiver. The cycle is then repeated over and over again [2]. The radar-scene analysis builds on two sources of information: radar returns and prior knowledge of the environment. In a surveillance scenario the interference is typically dominated by clutter and cognitive radars are very well suited to discern these unwanted echoes since possessing information on both the clutter acting alone (prior knowledge of the environment) and the clutter plus target (through the received signal).

Summarizing the characteristics that distinguish cognitive radars and that are of interest towards the research topic of this thesis are:

- Joint optimization of receiver and transmitter according to known information on the environment;
- Good clutter rejection capabilities.

1.6 Convex Optimization

In order to build a cognitive engine, advanced mathematical tools such as convex optimization, machine learning, random matrix theory and so on should be explored [15]. Convex optimization can be exploited to support waveform optimization ([15], [16], [17] and many others) as well as beamforming ([11]).

A mathematical optimization problem has the form:

$$\begin{aligned} &\text{minimize} && f_0(x) \\ &\text{subject to} && f_i(x) \leq b_i, \qquad i = 1, \ldots, m. \end{aligned}$$

where:

- Optimization variable: $x = (x_1, x_2, \ldots, x_n)$;
- Objective function: $f_0 : \mathbf{R}^n \to \mathbf{R}$;
- Constraint functions: $f_i : \mathbf{R}^n \to \mathbf{R}$;
- Limits or bounds of the constraints: $b_1, \ldots, b_m$

A convex optimization problem is one in which the objective function is convex and in which the constraints are convex sets. A function is convex if it satisfies the inequality [18]:

$$f_i(\alpha x + \beta y) \leq \alpha f_i(x) + \beta f_i(y)$$

Graphically, this can be represented as depicted in Figure 1.4. This implies that for a convex function if a local minimum exists, then the local minimum is also the global minimum. This is a very important piece of information

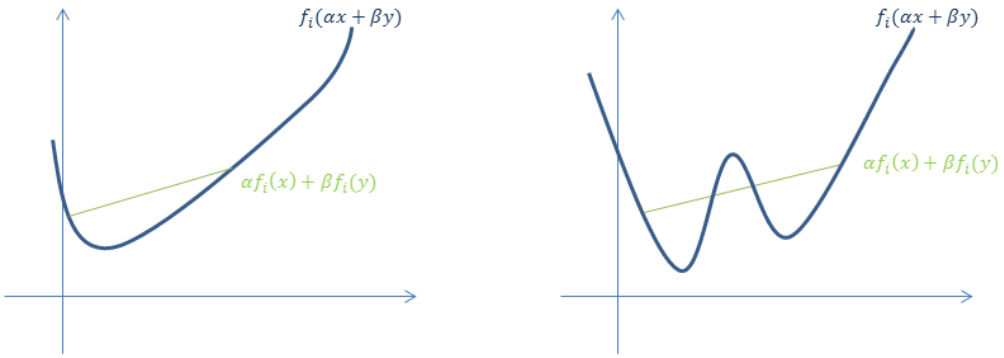

Figure 1.4: Graphic representation of a convex function (left-hand side) and non-convex function (right-hand side)

when dealing with optimization problems. In a convex optimization problem, the constraints are convex sets. A set C is convex if the line segment between any two points in C lies in C. It needs to be noted that this section has the aim of introducing the reader in an informal but accessible way to the main concept behind convex optimization. Due to the importance of this topic, the formal definitions of convex sets and convex functions will be introduced in Chapter 3.

1.7 Outline of the Thesis

The main problem discussed within this thesis, is the development of mathematical optimization techniques for waveform design in cognitive radars. These techniques have been designed with an increasing level of sophistication, starting from a bistatic model (i.e. two transmitters and a single receiver) and ending with a cognitive network (i.e. multiple transmitting and multiple receiving radars, one of which acting as centralized controller). The environment under investigation always features strong signal-dependent clutter and noise. All algorithms are based on iteratively optimizing the transmitted nearly-orthogonal waveforms and the receiver filter. The

waveform optimization techniques are based on convex optimization techniques and on the exploitation of initial radar waveforms characterized by desired auto and cross-correlation properties. Finally, robust optimization techniques are introduced to account for the assumptions made by cognitive radars on certain second order statistics such as the covariance matrix of the clutter. Indeed, an error on the assumed statistics can significantly deteriorate the SINR, leading to a reduced target interception performance.

The main contributions within this thesis are therefore the various waveform optimization techniques that have been developed for increasingly complex environments and scenarios.

More specifically, Chapter 2 discusses the relevant literature review. This includes two sections regarding a general overview on cognitive radars and tracking. Section 2.3 introduces waveform optimization techniques for cognitive radars. This is further subdivided into a discussion on the importance of the ambiguity function, waveform design for multiple-input multiple-output (MIMO) radars, and the available literature review on cognitive radars specifically. Section 2.4 outlines several contributions on robust optimization techniques, including methods developed specifically for beamformers. The following section discusses matched-illumination techniques. Finally, some concluding remarks will be provided.

Chapter 3 discusses convex optimization techniques. This is an overview of a rather general nature but it introduces the reader to optimization definitions and techniques that are fundamental towards a thorough understanding of this work. More specifically, Section 3.1 introduces a series of definitions, including affine and convex sets, cones and convex functions. Some practical examples are also provided. Furthermore, Section 3.2 discusses canonical optimization problems including linear programming, quadratic

programming and semidefinite programming.

Chapter 4 describes a methodology for waveform optimization for bistatic radars. The reader will be introduced to the system model under investigation, followed by the formulation of the iterative problem both in terms of filter optimization and waveform optimization. Finally, the performance of such algorithm will be analyzed and some conclusions will drawn. It needs to be noted how this chapter introduces the fundamental building block of all research discussed within this thesis. Concepts that could be rather confusing for the general case of M radars are here discussed for a bistatic model, making this chapter propaedeutic towards a thorough understanding of the subsequently discussed research.

Chapter 5 discusses waveform optimization techniques for coordinated networks. At first the radar system model is described alongside with a description of the main concepts behind the receiver filter optimization as well as the orthogonal waveform optimization methodology. The chapter is then divided into two main sections describing the different proposed iterative system optimization techniques. Section 5.2 discusses an optimization technique based on the accumulated power return. Section 5.3 introduces iterative methods suitable for a cognitive network. This section is further subdivided into Sub-Section 5.3.1, concerning selective optimization techniques and Sub-Section 5.3.2 regarding max-min optimization techniques. Both main sections include a performance analysis and some conclusions.

Chapter 6 introduces the reader to robust optimization techniques. The first section discusses worst-case optimization techniques and it is followed by a section on stochastic optimization. Section 6.4 introduces the novel topic of clutter-specific robust optimization techniques. The following section includes a thorough performance analysis of the three different methods as well

as comparisons between them. Finally, a concluding section is provided.

Chapter 7 presents robust matched-illumination techniques for through-the-wall radars. Initially an overview of the through-the-wall problem formulation is provided. This is followed by a section containing two proposed optimization techniques well suited for such environment. Furthermore, a performance analysis is outlined and followed by some conclusions.

Finally, Chapter 8 provides general conclusions and possible further developments for the work discussed within this thesis.

Chapter 2

Literature Review

In this chapter, the contents of the state of the art literature regarding cognitive radars are summarized. At first a general overview on the topic is presented, followed by a specific section on tracking. The latter isn't of direct interest towards the research discussed within this thesis but is a very important aspect of cognitive radars. In the main section, a detailed analysis on waveform design is provided. This is further arranged into two main categories: waveform design through ambiguity function shaping and waveform design for (cognitive) MIMO radars (i.e. with orthogonality constraints). It needs to be noted that the literature on cognitive radars is still developing so some of the papers discussed in this section do not regard cognitive radars specifically. Furthermore, a description about robust optimization techniques will be provided as well as one on matched-illumination techniques. Finally, some concluding remarks will be provided.

2.1 Overview on Cognitive Radars

In recent years cognitive radars have become an active field of research and many different aspects related to this topic have been discussed throughout the years. This Section has the aim of introducing the reader to the main concepts behind cognitive radars.

Some works provide a description of the system's features. The work in [2] is the first to theorize cognitive radars. This was followed in 2012 by an updated view on cognitive dynamic systems (radar, control and radio) [19]. This is also the case of [14] where a cognitive fully adaptive radar system is described. According to Guerci et al., cognition should be implemented via a sense-learn-adapt (SLA) approach. In order to "sense", transmit and receive functions are jointly optimized to enhance performance but they should also be utilized to enhance channel estimation. In order to "learn", there is a combination of novel sensing, knowledge-aided processing and expert systems techniques (rule based reasoning): such combined system essentially replicates the decision process of a human subject matter expert. Finally, in order to "adapt", a radar must select a spatio-temporal transmit and receive strategy and constantly incorporate more sophisticated techniques as they become available. To fully exploit cognition, a MIMO probing approach is introduced as a learning aid for signal-dependent channel effects.

Another very important system feature that has been discussed is the possibility of implementing more radars. A cognitive radar network (CRN) [20] is a system that incorporates several radars working together in a cooperative manner with the goal of realizing a remote-sensing capability far in excess of what the radar components are capable of achieving individually. To this end, the system incorporates a central base station to perform the

fusion of individual radar outputs. A CRN can operate in two modes: in a distributed cognitive network the individual radar components as well as the central base station are all cognitive whereas in a central cognitive network cognition is confined to a central base station. Some works refer to CRN as MIMO Cognitive Radars [21].

The work in [22] proposes a way to optimize scheduling and power allocation in a cognitive radar network aimed at multiple target tracking. The main idea around this paper is that to reduce the very high complexity of an adaptive system including multiple radars and multiple targets, a hybrid Bayesian filter and a posterior Cramér-Rao bound (CRB) should be implemented to partition the state space into smaller subspaces and subsequently find a suitable subset of antennae (and their transmit power) to be employed in each tracking interval.

Some works concentrate on the clutter problem. An example can be found in [23]. The objective of the method described in [23] is to provide useful information to the Bayesian target tracker (BTT) on the target-plus-clutter and clutter-alone data. A method based on the bivariate empirical mode decomposition (a data-driven time series analysis tool especially suited for non-linear, non-stationary data) is addressed to facilitate radar scene analysis for cognitive radars. The method exploits prior knowledge of the environment or, more specifically, on coherent sea clutter returns.

Many papers have been written on the topic of target tracking for cognitive radars, examples are [24] and [25]. This is a consequence of the fact that having prior and posterior probability information makes cognitive radars ideal candidates for target tracking through a Bayesian target tracker. A brief review of a couple of particularly interesting works is provided in the next section.

Waveform design is also of great interest in an adaptive system such as cognitive radars. This can be performed through ambiguity function shaping [8] and [9], by imposing similarity constraints on the code [26], by applying matched-illumination (MI) techniques on a target with known impulse responses [27], [28], and in many other ways. Several papers exploit convex optimization techniques for waveform optimization. Examples are [17], [21] and [15].

More specifically, in [17] the author develops a way to obtain a trade-off between competing design criteria: maximize the output SNR for a particular target impulse response and the mutual information between the received signal and a Gaussian ensemble of targets. In addition, constraints on the transmitted spectrum can be implemented. Haykin shows how the problem can be transformed into a convex optimization problem in the autocorrelation of the waveform. In order to make such algorithm feasible, the presence of a radar scene analyzer (RSA) was necessary.

2.2 Tracking with Cognitive Radars

As mentioned above, having prior and posterior probability information makes cognitive radars the ideal candidates for Bayesian target tracking. Due to this reason, tracking could be one of the natural further developments of the topics discussed within this thesis and will therefore be shortly outlined below.

Tracking has been implemented in cognitive radars right from the very start [2] and it has then evolved into many different ideas. Particularly related to the topics discussed within this thesis, are the works in [24] and [29]. These papers develop the problem of adaptive beamsteering for search-and-

track applications within a cognitive radar network. The aim of the analyzed platform is that of calculating two position parameters and two velocity parameters (both radial and tangential). The channel's resolution cells are represented so that each one contains the probability of a target being absent or present. In order to create such probabilistic representation of the radar channel, two radars are cooperating. These are positioned in a way that allows the system to never be blind towards neither azimuth nor range. In order to optimize the placement of the beam, the entropy of the channel has been calculated for every cell. Assumptions are made about which cells are more likely to see new targets. In addition to this searching strategy, a Kalman filter has been implemented to track the targets. Decisions on prioritizing searching or tracking activities are made according to the values of the beam-position entropy and tracked-target entropy.

This work is of particular interest towards this research due to similarities in the implemented systems: in both cases two separated radars are used and beamsteering is a key feature in the implementation of the algorithm.

2.3 Waveform Design for Cognitive Radars

The main contributions discussed within this thesis focus on waveform design. In the following subsection, further details will be given on state-of-the-art waveform optimization techniques. Due to the fact that cognitive radars are a rather new topic, not all of the papers that are described in the following section regard cognitive radars specifically, but all are important towards a general understanding of waveform techniques for radar applications.

2.3.1 Ambiguity Function Shaping

As described in Section 1.2, the ambiguity function (AF) was first introduced to characterize the local and global resolution properties of time-delay and Doppler for narrowband waveforms. The AF can therefore be used as a powerful tool to evaluate the properties of waveforms and this is how it has been utilised within this thesis. Nonetheless, the AF can also be used to directly design waveforms with desired features. This aspect has not been investigated within this thesis but it would be a point of extreme interest for further developments as it would allow to avoid the use of a known initial waveform to establish and maintain good auto and cross-correlation properties of the waveforms.

Originally, the AF was intended towards a single radar (i.e. single waveform) scenario. The advent of MIMO radars made it necessary to extend the initial idea to larger classes of waveforms and radar systems. In [30] San Antonio et al. extended the idea of waveform Ambiguity Functions to MIMO radars. MIMO Ambiguity Functions are developed so that they can simultaneously characterize the effects of array geometry and transmitted waveforms on resolution performance. The result is a function of range, Doppler and azimuth angle. This cube of data is not of immediate interpretation.

The work in [31] elaborates on the previously discussed work [30] and derives some mathematical properties of the MIMO AF. Additionally, Chen et al. implement an optimization technique using frequency-hopping waveforms based on the optimization of the MIMO ambiguity function. Summarizing their algorithm, they impose a structure on the pulses (i.e. the general definition of frequency-hopping pulses) and design the parameters (i.e. the frequency-hopping code) by selecting a cost function which puts penalties

on the peak values of the AF which are not at zero-range and imposing a constraint which will guarantee the orthogonality of the final waveforms. A similar work can be found in [32] which also describes an algorithm for adaptively designing orthogonal frequency-hopping waveforms according to the position of the target. The radar implemented in this work is a colocated uniform linear array (ULA) with separated transmit/receive (STR) capabilities. The proposed algorithm is feasible due to the fact that for a bistatic radar, geometry factors play an important role in the shape of the ambiguity function as the system configuration is varied: the closer the target to the baseline, the poorer the resolution performance the radar will be able to obtain: when the target is *on* the baseline neither one of the two radars will be able to provide any additional information as they will both only "see" along the range axis.

More interestingly, Aubry et al. worked on ambiguity function shaping for cognitive radar via complex quadratic optimization [8]. They devise an algorithm which, exploiting prior knowledge of the environment (e.g. geographic information system, meteorological data, clutter models and so on), locates the range-doppler bins where strong unwanted returns are foreseen and, consequently, transmit a waveform whose ambiguity function exhibits low values in those interfering bins.

2.3.2 Waveform Design for (Cognitive) MIMO Radars

In a cognitive radar network (CRN), several radars could work together in a cooperative manner [20] combining the benefits of both cognition and diversity offered by MIMO radars. These radar systems employ multiple transmit waveforms and have the ability to jointly process signals received at multiple receiver antennae [33]. Distributed radars provide potential ad-

vantages such as enlarging coverage areas, improving detection performance and many others [34]. The disadvantages of such radar networks are the interference among radar transceivers, the requirement of precise location information of sensing nodes, synchronization and the need for data fusion [34].

From a waveform design point of view, the disadvantages of MIMO radars imply that there is a strong requirement to develop orthogonal or nearly-orthogonal waveforms. All contributions within this thesis consider nearly-orthogonal waveforms.

Furthermore, in recent years many works considered both cognitive radars and MIMO systems however, unlike this thesis, not much work has been carried out about the added value of merging these two concepts. This subsection provides an overview of the relevant techniques that can be found within literature.

Optimization of waveform lies at the heart of radar design. Various criteria have been used for waveform design. For example, one of the earlier works [35] considered mutual information for waveform design. Further developments of this concept can be found in [36] and [37], where the mutual information between subsequent radar returns is used as a figure of merit for ultra-wideband waveform optimization. In [38] maximization of mutual information between the target impulse response and the received echoes is used to improve the target detection and feature extraction performance. The works in [21] and [39] are aimed at sequentially designing a desired waveform by minimizing the Bayesian Cramér-Rao bound [40] under some constraints such as constant-modulus and peak-to-average-power ratio for the transmit beamforming. Finally, [34] provides a methodology for the design of a family of frequency-selective orthonormal wavelets. Within

the context of cognition, matched-illumination has been proposed in [41] and [28]. A comprehensive outline of signal to noise ratio SNR-based and matched-illumination-based waveform design techniques has been proposed in [41] for both known and stochastic targets, in a monostatic radar scenario. Furthermore, the work in [42] proposes an optimal waveform design method and a fast hierarchical optimization method to optimize a wideband cognitive radar (WCR) waveform for joint target radar signature (TRS) estimation and target detection. In this work the authors reflect on the fact that cognitive radars strongly rely on prior knowledge of the surrounding environment. This is viewed as long-term memory, and it can be used in transmit waveform design for a relative long time. In contrast, the target radar signature of the wideband radar is target-radar orientation sensitive and it varies alongside with the relative motion between the radar and the target. In this case, the TRS estimation update is needed as a feedback. Otherwise, the mismatch between the outdated and the actual TRS may degrade the radar performance significantly, i.e., detection and tracking performance degradation resulting from output signal to clutter plus noise ratio (SCNR) loss. Hence, in the waveform design, the TRS estimation performance should also be considered for the case of wideband cognitive radars, which is a key difference between WCR waveform design and the traditional one.

Huleihel et al. propose in [21] two different methods to iteratively estimate desired waveforms. The first method consists in minimizing the CRB of the estimation performance. This can be solved with convex optimization techniques. It is computationally fast but for low SNRs and/or number of observations, large errors can occur. The second method consists in minimizing the Reuven-Messer bound of the estimation performance. This problem

is non-convex and was solved with the steepest descent method (due to this design choice, the solution depends on the initialization of the covariance matrix). This method is computationally more complex but obtained better results than the first waveform design method. In order to solve this problem, the paper assumes both range and Doppler information on the target as known. The Reuven-Messer bound, although less used or known than the Cramér-Rao bound, is also one of the minimal available bounds on the mean square error (MSE) and is therefore used in order to predict the best achievable performance of an estimator for a given observation model [43], [44].

The majority of works on waveform design for MIMO radars though do not specifically regard cognitive radars. The work in [45] proposes a set of nearly orthogonal waveforms based on de-ramping of linear frequency modulated (LFM) pulses for MIMO systems. The de-ramping processing technique is a frequency-domain method of range measurement that is used for compression of LFM signals: an incoming signal is mixed with a replica of the transmitted chirp. As soon as both inputs have the same rate of frequency change, the output frequencies are constant tones. The input signals are linear, so there is a mapping of time offset onto frequency offset. In other words, targets at different ranges give echoes on different beat frequencies. Two interesting examples can be found in communication systems. The authors in [46] and [47] describe a method for modifying Walsh-Hadamard sequences to achieve correlation properties suited for asynchronous direct sequence (DS) code division multiple access (CDMA) applications. Walsh-Hadamard codes are easy to generate and orthogonal, but only in the case of perfect synchronization. As a matter of fact, the cross-correlation between two Walsh-Hadamard sequences can rise considerably in magnitude if there is a non-zero delay shift between them. In order to solve this problem, the

authors suggest the use of orthogonal polyphase spreading sequences. Another work that implements Walsh-Hadamard sequences is the previously mentioned [13]. Here the authors code each of the transmitted LFM waveforms with a Hadamard sequence to obtain orthogonality.

In [15] the authors developed and demonstrated for the first time an ultrawideband (UWB) MIMO cognitive radar. In fact, the experiment scenario comprises a computing engine (a computer running the Matlab code), a field programmable gate array (FPGA) transmitter and a digital phosphor oscilloscope receiver with corresponding radio frequency (RF) components (two transmission antennae and two receiving). A narrowband interference is generated by an arbitrary waveform generator (AWG).
The signal-processing problem discussed therein is of a dual nature: at first the (single or multiple) target's position needs to be estimated. Subsequently, both the waveform and the receiver filter are optimized with convex optimization techniques. The problem is formulated as a quadratically constrained quadratic program (QCQP) that is then relaxed into a semidefinite programming (SDP) problem. More specifically, for the estimation of target locations in two-dimensional space, the estimation algorithm is based on multilateration. The equations for both single target localization and multiple targets localizations are derived. Since these are both based on time of arrivals (TOA), it is of primarily importance for this implementation to design waveforms with very good auto-correlation properties. In fact, while designing the optimization problem, the authors impose both a maximization of the correlation peak and a constraint on the correlation sidelobes. The other constraints imposed by the optimization problem are good cross-correlation properties (given the MIMO nature of the system), a constraint on the energy of both the transmitter waveform and the receiving

filter and noise suppression.

Also of great importance are the works [16], and [48]. These are quite similar to one another and are the initial building block of the research discussed within this thesis. In these studies the authors consider the problem of cognitive transmit signal and receiver filter design for a point-like target embedded in a highly reverberating environment (i.e. the clutter is considered to be signal-dependent and quite strong: as a matter of fact they assume to have 100 different sources of clutter for each range ring). The optimization procedure devised by the authors of [16] consists of iteratively optimizing both the transmit signal and receiver filter. They use the SINR as objective function of the optimization and impose two constraints on the waveform. The first one is to ensure finite energy. The second one is to ensure that the optimized waveform does not deviate significantly from an initial waveform that has certain desired characteristics (they chose Barker 20). In this research the authors of [16] implement a monostatic radar and assume to have knowledge of the environment through national land cover data combined with RCS clutter models for the terrain types declared by the digital terrain map. The optimization problem, which is originally non-convex, can be modified into a semidefinite programming (SDP) problem thanks to the work developed in [49]. In order to evaluate the performance of the estimated waveform, a key role has been given to the ambiguity function.

2.4 Robust Optimization Techniques

Cognitive radars heavily rely on previous knowledge. The clutter environment is determined by prior information such as previous radar measure-

ments, land cover databases or by using estimates based on training signals. However, it is difficult to obtain an exact description of the clutter. Therefore, radar waveform design should take into account uncertainties associated with environmental parameters. Traditionally, this can be done in two ways: with worst-case optimization techniques [50–52] and with stochastic optimization techniques [53].

This thesis implements both traditional worst-case and stochastic optimization techniques and additionally introduces a completely novel robust optimization technique for radars in signal-dependent clutter (as described in Chapter 6). This section introduces the reader to a more thorough understanding of the state-of-the-art techniques within this field.

An interesting example of robust radar waveform in the presence of signal-dependent interference can be found in [54]. This work deals with the robust iterative optimization of the transmit signal and receive filter bank for the case of a monostatic radar and assumes unknown Doppler shift of the target. In this work the worst-case SINR at the output of the filter bank is used as a figure of merit for the optimization. A suitable iterative reformulation of the initial non-convex max-min problem, monotonically improves the worst-case SINR. In [55], an algorithm for robust waveform design of wideband cognitive radar for extended target detection was developed. The work proposes a max-min approach to design the waveform by considering the worst-case SINR over the uncertainty region (which was bound by a Frobenius norm). This was then re-formulated into a convex optimization problem. Furthermore, in [56] a robust method for jamming power allocation strategy for MIMO radar based on minimum mean square error (MMSE) and mutual information is presented. The robustness was introduced when the target, environment or waveform information were not

perfectly known. The worst case performance was optimized considering two different cases of uncertainty. Due to the fairly recent introduction of cognitive radars, not many works can be found on robust techniques aimed at optimizing them specifically.

2.4.1 Robust MVDR Optimization Techniques

In literature, robust optimization techniques have been extensively developed for the case of MVDR beamformers. By noticing the similarities between the MVDR beamformer problem and the matched-illumination problem for through-the-wall radars, such techniques have been used in Chapter 7 for cognitive radars. This subsection introduces the reader to an overview of the available techniques.

In [57] Stoica et al. propose robust optimization techniques for capon beamforming. The authors model the uncertainty on the steering vector of the signal-of-interest as belonging to an uncertainty ellipsoid. This way they were able to directly obtain a robust estimate of the power of the signal of interest without any intermediate calculation of the weight vector. In [58] the authors propose robust adaptive beamforming using worst-case performance optimization via second-order cone programming. The authors assume the steering vector distortions to be bounded by some known constant. This work was then further developed in [59], where a good overview on robust adaptive beamforming using worst-case performance optimization was provided. The method used in the second paper is diagonal loading. The key idea behind traditional diagonal loading is to regularize the solution for the weight vector by adding quadratic penalty term to the objective function. In this work, Gershman et al. propose to introduce uncertainty sets and optimize the worst-case performance. This

leads to a "distortionless response constraint" which, for all mismatched steering vectors, guarantees that the array response is not smaller than one. The work in [60] shows how a natural extension of the Capon beamformer to the case of uncertain steering vectors, also belongs to the class of diagonal loading and that the amount of diagonal loading necessary can be precisely calculated based on the uncertainty set of the steering vector.

In [61], an extension of minimum variance beamforming that explicitly takes into account variation or uncertainty in the array response is presented. The uncertainty is modeled via an ellipsoid. The robust weight selection was cast as a SOCP that can be solved efficiently using Lagrange multiplier techniques. It was proven that, if the ellipsoid reduces to a single point, the method coincides with Capon's method. Particular detail is given in [61] about ellipsoidal modeling and anisotropic uncertainty.

In [38] an improved approach to the worst-case robust adaptive beamforming for general-rank signal models is proposed. The method works by taking into account the positive semidefinite constraint for the mismatched signal covariance matrix. The problem is solved iteratively by using semidefinite programming.

In [62] an overview of previous robust beamforming techniques can be found. These include diagonal loading, the eigenspace-based beamformer method and covariance matrix reconstruction. Subsequently the authors in [62] propose a method based on the analysis of the direction of arrival (DOA) matrix structure for the case of uniform linear array.

In [63] robust MVDR beamforming techniques are proposed for a colocated MIMO radar in the presence of powerful jamming signals. A method was designed for known jammers in the sector of interest by imposing a distortionless response towards the direction of interest while placing nulls

in the directions of the jammers. A second method concerned unknown in-sector jammers and/or out-of-sector interfering sources. Both problems were solved by using convex optimization techniques.

Furthermore, in the last couple of years the following works have been published with additional developments. In [64], a robust MIMO radar waveform design is proposed. The aim is to improve the worst-case estimation accuracy in the presence of clutter by exploiting the Cramér-Rao bound of the angle of arrival. To tackle the resultant NP-hard problem, a new diagonal loading based iterative method is developed to design the waveform covariance matrix for improving the worst-case accuracy. Each step is formulated as a convex optimization problem, and hence can be solved efficiently. An optimal solution to the initial issue is obtained via the least squares (LS) fitting of the solution acquired by the iterative algorithm.

In [65], Aubry et al. propose a constrained design of radar Doppler filters by considering the output SINR as performance measure. To account for possible mismatches between the design and the operative conditions, some specific uncertainty sets have been associated with both the target Doppler frequency and the interference covariance matrix and introduced as constraints of the optimization problem. Additionally, a constraint on the filter sidelobe response is enforced to control the amount of interference energy produced by targets lying in the same range cell as the target of interest. The problem, initially formulated as a constrained non-convex max-min optimization problem, is then solved with a polynomial-time technique exploiting the representation of non-negative trigonometric polynomials via linear matrix inequalities, the spectral factorization theorem, and the duality theory.

In [66], the joint robust design of the transmit waveform and filtering struc-

ture for a polarimetric radar is proposed. In this work the worst case signal-to-interference plus noise ratio (SINR) is considered as the figure of merit to optimize under both a similarity and an energy constraint on the transmit signal. The developed procedure is of an iterative nature.

In [67], a robust design method is proposed to optimize a compressive sensing multiple-input multiple-output (CS-MIMO) radar system in the presence of clutter. One of the drawbacks of MIMO radars is high computational complexity of signal processing due to the large amount of received data from all receive antennas. To cope with this problem, compressive sensing (CS) techniques can be exploited to reduce the amount of received data using a measurement matrix. In their work, Shahbazi et al. propose to consider uncertainty on this measurement matrix. A maxmin optimization problem was devised to maximize the worst-case signal-to-clutter-plus-noise ratio.

Some works also developed robust stochastic techniques rather than worst-case ones. An example is [68] where robust transmit beamforming techniques for multi-user MIMO systems are developed through a probabilistic constraint approach. The suggested method maximizes the average signal power while keeping the leakage power below an acceptable level. The probabilistic constraint is transformed to a deterministic convex one through the application of the Markov inequality.

In probability theory Markov's Inequality gives an upper bound for the probability that a non-negative function of a random variable is greater than or equal to some positive constant:

$$Pr(X \geq a) \leq \frac{\mathbb{E}\{X\}}{a}, \tag{2.1}$$

where Pr indicates the probability operator, X is a non-negative random

variable, $a > 0$ is a constant, and $\mathbb{E}$ indicates the expected value.

In [69] a joint robust transmit/receive adaptive beamforming for MIMO radar based on probability-constrained optimization approach is developed in case of both complex Gaussian and arbitrary distributed mismatches. The complex Gaussian probability is transformed into a deterministic constraint thanks to the cumulative distribution function (CDF). This is a distribution giving the probability that a random variable is less than given values. For the case of arbitrary distribution, the authors transform the probabilistic constraint thanks to the Chebyshev inequality. This states that for any zero-mean random variable τ with variance σ_τ^2 and positive real number α:

$$Pr\{|\tau| \geq \alpha\} \leq \frac{\sigma_\tau^2}{\alpha^2}. \tag{2.2}$$

The thus formulated probability-constrained robust beamforming problem is initially non-convex and NP-hard. However, the authors reformulate its cost function into a bi-quadratic function while splitting the probability constraint into transmit and receive parts. Subsequently, a block coordinate descent method based on second-order cone programming is developed to address the problem.

2.5 Matched-Illumination Techniques

A technique that utilizes a priori information is matched-illumination (MI) as it exploits known information about the properties and characteristics of the target to improve target detection and classification. It is very important to not confuse matched-illumination with mutual information techniques. The latter, also abbreviated as MI within the literature, is a probability theory tool and it is a measure of the mutual dependence between the two random

variables.

Matched-illumination techniques have been considered within this thesis in Chapter 7. These have been introduced to provide the reader with a different example of cognitive radar and the way that robust techniques can improve its performance. This section outlines the available literature on the topic.

MI is a rather new concept and it has been proposed in only a limited amount of works. The work in [28] discusses matched-illumination waveform design for a multistatic through-the-wall radar system where the target is assumed to be stationary and with a known impulse-response and inspired the work in Chapter 7. Furthermore, a comprehensive outline of SNR-based and matched-illumination-based waveform design techniques has been proposed in [41] for both known and stochastic targets, in a monostatic radar scenario. In addition the problem of matched waveform design in signal-dependent interference is extensively addressed within.

In [70], the impact of wall-target interaction on matched-illumination waveforms for through-the-wall radar imaging is examined via finite-difference time-domain simulation. In this work the authors are mainly concerned about how matched-illumination theory depends on the a priori knowledge of the target and environment. Usually, an assumption of minimal interaction between target and wall is made for most waveform design techniques. The target return from this matched-illumination waveform design is called primary-wave target response. The target return from a matched-illumination waveform determined by including all wave physics is called fullwave target response. In their work the authors consider returns from various wall–target scenarios as a function of the target-to-wall separation in order to examine the effectiveness of the primary-wave target response

in the matched-illumination implementation. The primary-wave target response is shown to effectively maximize the SINR in through-wall radar applications where the wall–target interaction is minor. The ability of the primary-wave target response to maximize the SINR can be degraded by relatively minor errors in the wall-target transfer function caused by the incomplete wall-target physics inherent to the scheme. In such cases, the resulting matched-illumination waveform spectrum was generally characterized by narrowband energy concentrated at suboptimal frequencies.

In [71], ambiguity functions are obtained for a radar using matched-illumination transmit signals for the detection of range-spread targets in the presence of clutter. The transmit signals are adapted to target and interference spectra and are filtered optimally in the receiver; they are designed to maximize SINR power ratios at the receiver's output. The authors proved that ambiguity functions resulting from using optimal MI constant envelope waveforms demonstrate superior resolution characteristics compared to the classic linear frequency-modulated (LFM) signals employing optimal pulse compression.

2.6 Conclusions

In recent years cognitive radars have become an active field of research. Their sense-learn-adapt approach makes them an invaluable tool for effective target detection and tracking in complex environments. Waveform design is a key aspect of any signal processing optimization for radar applications. Signals that feature excellent auto and cross-correlation properties are of particular importance in MIMO systems. Furthermore, due to the fact that cognitive radars strongly rely on prior knowledge, which is not available

precisely, it is of paramount importance to implement robust optimization techniques. However, unlike the case of robust beamforming techniques, still not many works have been carried out on cognitive radars specifically. This thesis therefore introduces and further develops concepts and techniques that haven't been fully exploited for cognitive radars.

Chapter 3

Convex Optimization

The use of optimization methods is of paramount importance for signal processing applications. Amongst the different available techniques, convex optimization is a computational tool of central importance in engineering, thanks to its ability to solve very large, practical problems reliably and efficiently in polynomial time [72].

Convex optimization techniques are based on the minimization of a convex objective function subject to convex constraints. In this context, a local optimum is also a global optimum [73]. This makes it a very powerful tool to solve optimization problems and several numerical algorithms have been developed to solve such problems efficiently. Examples of available Matlab toolboxes are CVX Software for Disciplined Convex Programming [74], SeDuMi [75] and Yalmip [76]. This makes such optimization techniques even more attractive for many engineering applications.

Majority of optimization problems are not originally in convex form. It is therefore of primary importance to gain the skills and knowledge necessary to recognize which problems could be reformulated in convex form.

In the following chapter the basic optimization concepts, frameworks and

tools that are most relevant towards the understanding of this thesis will be outlined. The first section includes the definitions of convex sets and convex functions. The second section outlines some canonical optimization problems such as linear programming, quadratic programming, second order cone programming and semidefinite programming. The third section introduces Lagrangian multipliers. Finally, a concluding summary will be provided.

3.1 Fundamental Convex Definitions

In order to recognize convex optimization problems, it is of great importance to gain knowledge on basic concepts and models such as affine and convex sets, cones and functions.

3.1.1 Affine Sets

A set $C \subseteq \mathbf{R}^n$ is affine if the line through any two distinct points in C lies in C, i.e. for any $\mathbf{x}_1$,$\mathbf{x}_2 \in C$ and $\theta \in \mathbf{R}$, it is true that $\theta\mathbf{x}_1 + (1-\theta)\mathbf{x}_2 \in C$. In other words, C contains the linear combination of any two points in C, provided the coefficients in the linear combination sum to one [18]. This can be well understood by looking at Figure 3.1. Generalizing to more than two points:

> A point in the form $\theta\mathbf{x}_1 + \cdots + \theta_k\mathbf{x}_k$, where $\theta_1 + \cdots + \theta_k = 1$ is referred to as an affine combination of the points $\mathbf{x}_1, \ldots, \mathbf{x}_k$. An affine set contains every affine combination of its points [18].

Every affine set is also convex.

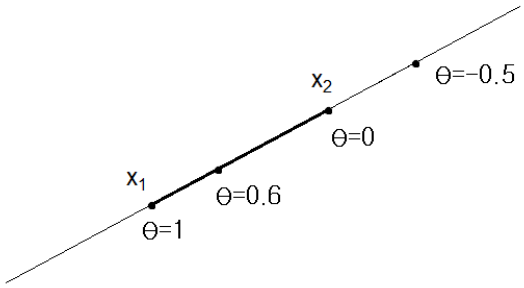

Figure 3.1: Representation of an affine set C. As it can be seen, the line through any two distinct points in C, lies in C. In other words, for any $\mathbf{x}_1$,$\mathbf{x}_2 \in C$ and $\theta \in \mathbf{R}$, $\theta\mathbf{x}_1 + (1-\theta)\mathbf{x}_2 \in C$. Values of θ between 0 and 1 correspond to the line segment between $\mathbf{x}_1$ and $\mathbf{x}_2$.

3.1.2 Convex Sets

A set C is convex if the line segment between any two points in C lies in C, i.e. if for any $\mathbf{x}_1, \mathbf{x}_2 \in C$ and any θ with $0 \leq \theta \leq 1$, it is true that $\theta\mathbf{x}_1 + (1-\theta)\mathbf{x}_2 \in C$. Generalizing to more than two points:

> A point in the form $\theta\mathbf{x}_1 + \cdots + \theta_k\mathbf{x}_k$, where $\theta_1 + \cdots + \theta_k = 1$ *and* $\theta_i \geq 0 \quad$ with $\quad i = 1, \ldots, k$ is referred to as a convex combination of the points $\mathbf{x}_1, \ldots, \mathbf{x}_k$. A convex combination of points can be thought of as a weighted average of the points. A set if convex if every point in the set can be seen by every other point, along an unobstructed straight path between them [18].

This fact can be well appreciated by looking at Figure 3.2. A convex combination can be generalized to include infinite sums, integrals and probability distributions.

3.1.3 Convex Cones

A set C is called a cone, or nonnegative homogeneous, if for every $\mathbf{x} \in C$ and $\theta \geq 0$, it is true that $\theta\mathbf{x} \in C$. A set C is a convex cone if it is convex

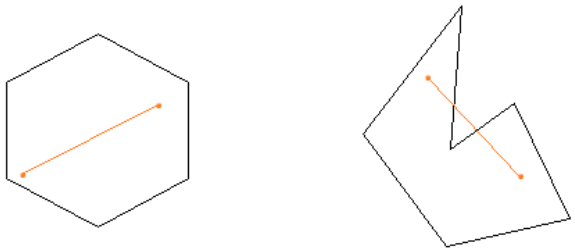

Figure 3.2: Representation of a convex and a non-convex set. A hexagon which includes its boundary (to the left) is a convex set: every point in the set can be seen by every point along an unobstructed straight path between them. The shape to the right is a non-convex set. As it can be clearly seen from the image, the line segment between the two points in the set is not entirely contained in the set.

and a cone, which means that for any $\mathbf{x}_1, \mathbf{x}_2 \in C$ and $\theta_1, \theta_2 \geq 0$, it is true that $\theta_1\mathbf{x}_1 + \theta_2\mathbf{x}_2 \in C$. Generalizing to more than two points:

> A point in the form $\theta\mathbf{x}_1 + \cdots + \theta_k\mathbf{x}_k$ with $\theta_i \geq 0 \quad$ with $\quad i = 1, \ldots, k$ is refereed to as a conic combination of the points $\mathbf{x}_1, \ldots, \mathbf{x}_k$. If $\mathbf{x}_i$ are in a convex cone C, then every conic combination of $\mathbf{x}_i$ is in C. Conversely, a set C is a convex cone if and only if it contains all conic combinations of its elements [18].

3.1.4 Positive Semidefinite Cones

The convex cone $\mathbf{S}_+^n$ should be defined as a set of symmetric positive semidefinite matrices:

$$\mathbf{S}_+^n = \{\mathbf{X} \in \mathbf{S}^n | \mathbf{X} \succeq 0\}$$

If $\theta_1, \theta_2 \geq 0$ and $\mathbf{A}, \mathbf{B} \in \mathbf{S}_+^n$, then $\theta_1\mathbf{A} + \theta_2\mathbf{B} \in \mathbf{S}_+^n$. As a matter of fact, from the definition of semidefiniteness, for any $\mathbf{x} \in \mathbf{R}^n$:

$$\mathbf{x}^{\mathrm{H}}(\theta_1\mathbf{A} + \theta_2\mathbf{B})\mathbf{x} = \theta_1\mathbf{x}^{\mathrm{H}}\mathbf{A}\mathbf{x} + \theta_2\mathbf{x}^{\mathrm{H}}\mathbf{B}\mathbf{x} \geq 0, \tag{3.1}$$

if $\mathbf{A} \succeq 0$, $\mathbf{B} \succeq 0$ and $\theta_1, \theta_2 \geq 0$. For instance, a positive semidefinite cone in $\mathbf{S}^2$ is:

$$\mathbf{X} = \begin{bmatrix} \mathbf{x} & \mathbf{y} \\ \mathbf{y} & \mathbf{z} \end{bmatrix} \in \mathbf{S}_+^2 \tag{3.2}$$

with $\mathbf{x} \geq 0$, $\mathbf{z} \geq 0$ and $\mathbf{xz} \geq \mathbf{y}^2$.

3.1.5 Examples on Sets and Cones

A few practical examples are as follows:

- The empty set, a single point, a line and the whole space $\mathbf{R}^n$ are affine;
- A line segment is convex.

A convex set is more restrictive than an affine set since it also includes the condition that $\theta_i \geq 0 \quad \text{with} \quad i = 1, \ldots, k$. Other sets are hyperplanes and halfspaces, Euclidean balls and ellipsoids, norm balls and norm cones and polyhedra. For further details on these sets, the reader can refer to [18], [72] and [73].

3.1.6 Convex Functions

A function $f : \mathbf{R}^n \to \mathbf{R}$ is convex if $\mathbf{dom}f$ is a convex set and if for all $\mathbf{x}$, $\mathbf{y} \in \mathbf{dom}f$, and θ with $0 \leq \theta \leq 1$, it is true that:

$$f(\theta\mathbf{x} + (1-\theta)\mathbf{y}) \leq \theta f(\mathbf{x}) + (1-\theta) f(\mathbf{y}), \tag{3.3}$$

where $\mathbf{dom}f$ denotes the domain of function f. Geometrically, this inequality means that the line segment between $(\mathbf{x}, f(\mathbf{x}))$ and $(\mathbf{y}, f(\mathbf{y}))$ lies above the graph of f. This can be well appreciated by looking at Figure 3.3.
f is concave if $-f$ is convex [18].

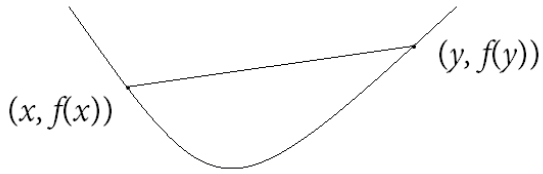

Figure 3.3: Graph of a convex function. As it can be seen, the line segment (i.e. the chord) between $(\mathbf{x}, f(\mathbf{x}))$ and $(\mathbf{y}, f(\mathbf{y}))$ lies above the graph of f. This is true for any two points.

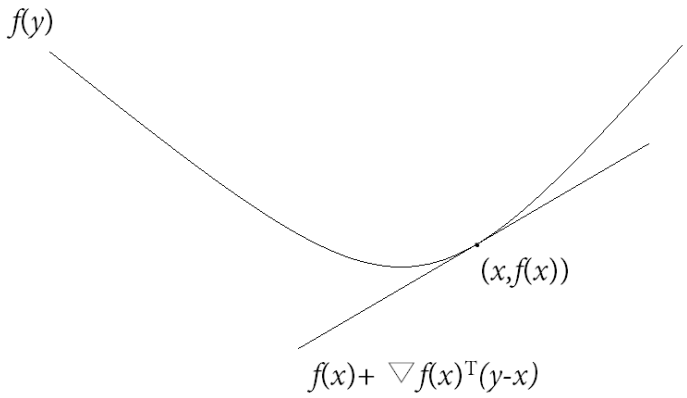

Figure 3.4: Geometrical interpretation of a first-order condition. If f is convex and differentiable, then $f(\mathbf{y}) \geq f(\mathbf{x}) + \nabla f(\mathbf{x})^{\mathrm{H}}(\mathbf{y} - \mathbf{x})$ for all $\mathbf{x}, \mathbf{y} \in \mathbf{dom} f$. If f was non-convex, the first order derivative would at some point intersect the function.

For an affine function there is equality in Equation (3.3). An affine function is both convex and affine.

3.1.6.1 First-Order Conditions

If f is differentiable (i.e. its gradient ∇f exists at each point in $\mathbf{dom} f$), then f is convex if and only if $\mathbf{dom} f$ is convex and:

$$f(\mathbf{y}) \geq f(\mathbf{x}) + \nabla f(\mathbf{x})^{\mathrm{H}}(\mathbf{y} - \mathbf{x}), \tag{3.4}$$

holds for all $\mathbf{x}, \mathbf{y} \in \mathbf{dom} f$ [18] This can be easily understood by looking at the geometrical interpretation in Figure 3.4.

3.1.6.2 Second-Order Conditions

If f is twice differentiable (i.e. its Hessian or second derivative $\nabla^2 f$ exists at each point in $\mathbf{dom} f$), then f is convex if and only if $\mathbf{dom} f$ is convex and its Hessian is positive semidefinite for all $\mathbf{x} \in \mathbf{dom} f$:

$$\nabla f(\mathbf{x})^2 f(\mathbf{x}) \succeq 0. \tag{3.5}$$

A clear example of this is a quadratic function $f : \mathbf{R}^n \to \mathbf{R}$ with $\mathbf{dom} f = \mathbf{R}^n$:

$$f(\mathbf{x}) = \mathbf{x}^{\mathrm{H}}\mathbf{P}\mathbf{x} + \mathbf{q}^{\mathrm{H}}\mathbf{x} + \mathbf{r}, \tag{3.6}$$

with $\mathbf{P} \in \mathbf{S}^n$, $\mathbf{q} \in \mathbf{R}^n$, and $\mathbf{r} \in \mathbf{R}$.
f is convex if and only if $\mathbf{P} \succeq 0$ and concave if and only if $P \preceq 0$ (and strictly convex if $\mathbf{P} \succ 0$ [18].

3.1.7 Examples on Convex Functions

Examples of convex functions on $\mathbf{R}$ are:

- Exponential function, $\exp(a\mathbf{x})$ is convex on $\mathbf{R}$, for any $a \in \mathbf{R}$;
- Power function, $\mathbf{x}^a$ is convex on $\mathbf{R}_{++}$ when $a \geq 1$ or $a \leq 0$ and concave for $0 \leq a \leq 1$;
- Logarithm.

Examples of convex functions on $\mathbf{R}^n$ are:

- Norms;
- Max-functions, $f(\mathbf{x}) = \max\{\mathbf{x}_1, \ldots, \mathbf{x}_n\}$;
- Geometric mean.

3.2 Canonical Optimization Problems

In this section some fundamental optimization problems are described. Solution codes and toolboxes are available for these categories of optimization problems. Thus, if any problem at hand can be cast into one of these forms, then it can be solved efficiently. There are several techniques that can be used to reformulate problems in standard form (e.g. change of variables, eliminating or introducing equality constraints and so on). However, these methods are outside the scope of this introductory chapter. The reader can refer to [18] or [72] for further details.

3.2.1 Linear Programming (LP)

When the objective and constraint functions are all affine, the problem is called a linear program (LP). A general linear program has the form:

$$\begin{aligned} \text{minimize} \quad & \mathbf{c}^{\mathrm{H}}\mathbf{x} + \mathbf{d} \\ \text{subject to} \quad & \mathbf{G}\mathbf{x} \succeq \mathbf{h} \\ & \mathbf{A}\mathbf{x} = \mathbf{b}, \end{aligned} \tag{3.7}$$

where $\mathbf{G} \in \mathbf{R}^{m \times n}$ and $\mathbf{A} \in \mathbf{R}^{p \times n}$ [18].

3.2.2 Quadratic Programming (QP)

A convex optimization problem is called quadratic program (QP) if the objective function is (convex) quadratic, and the constraint functions are

affine. This can be expressed in the form:

$$\begin{array}{ll} \text{minimize} & \frac{1}{2}\mathbf{x}^T\mathbf{P}\mathbf{x} + \mathbf{q}^T\mathbf{x} + \mathbf{r} \\ \text{subject to} & \mathbf{G}\mathbf{x} \preceq \mathbf{h} \\ & \mathbf{A}\mathbf{x} = \mathbf{b} \end{array} \tag{3.8}$$

where $\mathbf{P} \in \mathbf{S}_+^n$ and $\mathbf{G} \in \mathbf{R}^{m \times n}$, and $\mathbf{A} \in \mathbf{R}^{p \times n}$ [18].
In a quadratic program the aim is to minimize a convex quadratic function over a polyhedron (i.e. the feasible affine set).

3.2.3 Quadratically Constrained Quadratic Program (QCQP)

A convex optimization problem is called a quadratically constrained quadratic program (QCQP) if the objective as well as the inequality constraint functions are (convex) quadratic. This can be represented in the form [18]:

$$\begin{array}{lll} \text{minimize} & \frac{1}{2}\mathbf{x}^T\mathbf{P}_0\mathbf{x} + \mathbf{q}_0^T\mathbf{x} + \mathbf{r}_0 & \\ \text{subject to} & \frac{1}{2}\mathbf{x}^T\mathbf{P}_i\mathbf{x} + \mathbf{q}_i^T\mathbf{x} + \mathbf{r}_i \leq 0, & i = 1, \ldots, m \\ & \mathbf{A}\mathbf{x} = \mathbf{b} & \end{array} \tag{3.9}$$

where $\mathbf{P}_i \in \mathbf{S}_+^n$, $i = 1, \ldots, m$. This type of problem can be relaxed in a semidefinite programming problem (SDP).

3.2.4 Second-Order Cone Programming

A second-order cone program (SOCP) is a convex optimization problem in the form:

$$\begin{array}{ll} \text{minimize} & f^T\mathbf{x} \\ \text{subject to} & \|\mathbf{A}_i\mathbf{x}+\mathbf{b}_i\|_2 \leq \mathbf{c}_i^T\mathbf{x}+\mathbf{d}_i, \qquad i=1,\ldots,m \\ & \mathbf{F}\mathbf{x}=\mathbf{g} \end{array} \tag{3.10}$$

where $\mathbf{x} \in \mathbf{R}^n$ is the optimization variable, $\mathbf{A}_i \in \mathbf{R}^{n_i \times n}$, and $\mathbf{F} \in \mathbf{R}^{p \times n}$. A constraint in the form:

$$\|\mathbf{A}\mathbf{x}+\mathbf{b}\|_2 \leq \mathbf{c}^T\mathbf{x}+\mathbf{d}$$

is defined as a second-order cone constraint.

3.2.5 Semidefinite Programming (SDP)

In semidefinite programming, one minimizes a linear function subject to the constraint that an affine combination of symmetric matrices is positive semidefinite. Such a constraint is nonlinear and non-smooth, but convex, so semidefinite programs are convex optimization problems. Semidefinite programming unifies several standard problems (i.e. linear and quadratic programming) and finds many applications in engineering and combinatorial optimization [77]. These are in the form:

$$\begin{array}{ll} \text{minimize} & \mathbf{c}^T\mathbf{x} \\ \text{subject to} & \mathbf{x}_1\mathbf{F}_1+\cdots+\mathbf{x}_n\mathbf{F}_n+\mathbf{G} \preceq 0 \\ & \mathbf{A}\mathbf{x}=\mathbf{b} \end{array}$$

where $\mathbf{G}, \mathbf{F}_1, \ldots, \mathbf{F}_n \in \mathbf{S}^k$, and $\mathbf{A} \in \mathbf{R}^{p \times n}$. A standard form SDP has linear equality constraints and a matrix non-negativity constraint on the variable X [18]:

$$\begin{array}{lll} \text{minimize} & \text{tr}(\mathbf{CX}) & \\ \text{subject to} & \text{tr}(\mathbf{A}_i\mathbf{X}) = \mathbf{b}_i, & i = 1, \ldots, m \\ & \mathbf{X} \succeq 0, & \end{array}$$

where $\mathbf{C}, \mathbf{A}_1, \ldots, \mathbf{A}_p \in \mathbf{S}^n$, and $\mathbf{A} \in \mathbf{R}^{p \times n}$.

3.3 Lagrangian Multipliers

Lagrangian multipliers are a way to solve a system of equations or inequalities within an optimization problem by writing the objective function and constrains as a series of weighted sums. Suppose the optimization problem at hand is in the form:

$$\begin{array}{lll} \text{minimize} & f_0(\mathbf{x}) & \\ \text{subject to} & f_i(\mathbf{x}) \leq 0, & i = 1, \ldots, m \\ & h_i(\mathbf{x}) = 0, & i = 1, \ldots, p, \end{array} \tag{3.11}$$

with variable $\mathbf{x} \in \mathbf{R}^n$. Then the associated Lagrangian $\mathcal{L}$ can be defined as:

$$\mathcal{L}(\mathbf{x}, \lambda, \nu) = f_0(\mathbf{x}) + \sum_{i=1}^{m} \lambda_i f_i(\mathbf{x}) + \sum_{i=1}^{p} \nu_i h_i(\mathbf{x}), \tag{3.12}$$

where:

- λ_i is the Lagrange multiplier associated with the ith inequality constraint $f_i(\mathbf{x}) \leq 0$;
- ν_i is the Lagrange multiplier associated with the ith equality (affine) constraint $h_i(\mathbf{x}) = 0$.

The Lagrange dual function is the minimum value of the Lagrangian over $\mathbf{x}$. Since the dual function is the pointwise infimum of a family of affine functions it is concave, even when the initial optimization problem (3.11) is not convex [18].

3.4 Conclusions

In this chapter various convex optimization definitions and problems have been outlined. These are all of fundamental relevance in order to fully understand the problems and equations developed within this thesis. Furthermore, they are of a general importance towards many engineering problems since they can be solved efficiently and with freely available toolboxes.

Chapter 4

Waveform Design for Bistatic Radars

The following analysis, inspired by [16] and [48], develops the design of transmit signals and receiver filter for the case of a bistatic cognitive radar. The environment is that of signal-dependent clutter and the figure of merit that is used is the SINR at the receiver filter. In order to estimate the transmission codes, a similarity constraint is imposed. This method is well established in the literature and examples can be [78] and [26]. However, thanks to the introduction of bistatic features to the model, the work discussed within this chapter has been published in [79]. It needs to be noted that this chapter introduces the reader to the main concepts of the multistatic cognitive model and sets itself at the foundation of a progressively more sophisticated framework that will peak in Chapter 6 with the development of robust optimization techniques for a cognitive radar network.

This chapter is organized as follows. In Section 4.1 the system model is described and the equations characterizing both the observations and their statistics is presented. In Section 4.2 the problem is formulated. More

specifically, the figure of merit is explained alongside with the needed constraints. Specific sub-sections describe the receiver filter optimization and subsequent optimization of the orthogonal codes. In Section 4.3 the performance of the proposed algorithm is analyzed. Finally, some conclusions are provided.

4.1 System Model

A bistatic cognitive radar system where each radar transmits a coherent burst of N pulses is considered.

$$\mathbf{s}_1 = [s_1(1), s_1(2), \dots s_1(N)]^T \in \mathbb{C}^N,$$

$$\mathbf{s}_2 = [s_2(1), s_2(2), \dots s_2(N)]^T \in \mathbb{C}^N,$$

denote the two radar codes, on which unit norm is imposed: $\|\mathbf{s}_1\| = 1$, and $\|\mathbf{s}_2\| = 1$. Also, in order to avoid unwanted correlation between the two signals, $\mathbf{s}_1$ and $\mathbf{s}_2$ are assumed to be orthogonal to each other: $\mathbf{s}_1^{\mathrm{H}}\mathbf{s}_2 = 0$.
In the considered model, both radars transmit but only Radar-1 receives and processes the signals. Hence Radar-1, which is the central radar where cognition is confined, determines the most appropriate waveforms for the subsequent transmission and instructs the second radar as appropriately through a local backbone communication network. In this model, depicted in Figure 4.1, the radars scan an area of $N_c \leq N$ range bins (for a range unambiguous scenario $N_c = 1$ needs to be selected), each of them subdivided into L azimuth bins. The subscript (r, i) will be used to identify a specific range-azimuth bin.

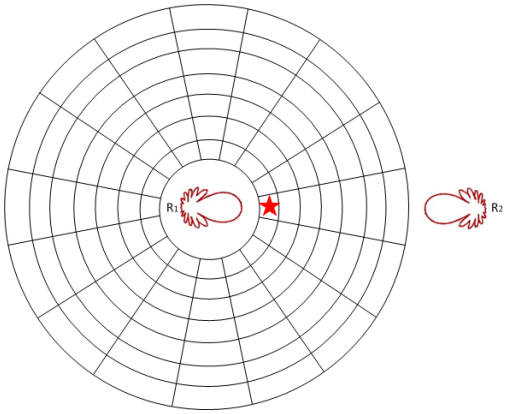

Figure 4.1: Geometry of the bistatic system. The radar at the center of the area under investigation is the reference radar, or Radar-1. The star identifies the target's position within the range-azimuth bins. The other radar identifies Radar-2.

4.1.1 Observations

The column-vector $\mathbf{x}_T = [\mathrm{x}_T(1), \mathrm{x}_T(2), \ldots \mathrm{x}_T(N)]^T \in \mathbb{C}^N$ encloses the signals scattered by the target and received by Radar-1 and can be written as:

$$\mathbf{x}_T = \alpha_{1,T}\mathbf{s}_1 \odot \mathbf{p}(\nu_{1,d_T}) + \alpha_{2,T}\mathbf{s}_2 \odot \mathbf{p}(\nu_{2,d_T}) + \mathbf{c} + \mathbf{n} \tag{4.1}$$

where $\alpha_{1,T}$ is the complex parameter that accounts for the propagation and backscattering effects of the channel Radar-1-Target-Radar-1 and $\alpha_{2,T}$ accounts for channel Radar-2-Target-Radar-1. Since only Radar-1 acts as receiver, the destination has been omitted from the notation. In the event of a formula of a more general nature, that equally holds for both radars, the subscript "rdr" will be used.

$$\mathbf{p}(\nu_{1,d_T}) = [1, \mathrm{e}^{j2\pi\nu_{1,d_T}}, \ldots \mathrm{e}^{j2\pi(N-1)\nu_{1,d_T}}]^T,$$

is the temporal steering vector accounting for the propagation effects from Radar-1, and:

$$\mathbf{p}(\nu_{2,d_T}) = [1, \mathrm{e}^{j2\pi\nu_{2,d_T}}, \dots \mathrm{e}^{j2\pi(N-1)\nu_{2,d_T}}]^T,$$

is the temporal steering vector accounting for the propagation effects from Radar-2. ν_{1,d_T} and ν_{2,d_T} are the normalized target Doppler frequencies seen by the two radars, $\mathbf{c}$ is the received clutter (hence at Radar-1) and $\mathbf{n}$ the received noise. The clutter vector $\mathbf{c}$ is modeled as the superposition of the returns coming from different uncorrelated scatterers within the various range-azimuth bins from both Radar-1 and Radar-2 and it can be written as: $\mathbf{c} = \mathbf{c}_1 + \mathbf{c}_2$, that is:

$$\begin{aligned} \mathbf{c} = &\sum_{r=0}^{N_c-1}\sum_{i=0}^{L-1} \alpha_{c1}(r,i)\mathbf{J}_r\mathbf{q}_1 \\ &+ \sum_{r=0}^{N_c-1}\sum_{i=0}^{L-1} \alpha_{c2}(r,i)\mathbf{J}_r\mathbf{q}_2, \end{aligned} \tag{4.2}$$

where $\mathbf{q}_1 = \mathbf{s}_1 \odot \mathbf{p}(\nu_{d_{1,(r,i)}})$, $\mathbf{q}_2 = \mathbf{s}_2 \odot \mathbf{p}(\nu_{d_{2,(r,i)}})$, α_{c1} is the reflectivity parameter associated with clutter as seen by Radar-1 and α_{c2} is the reflectivity parameter associated with clutter as seen by Radar-2. Also:

$$\mathbf{J}_r(l,m) = \begin{cases} 0 & \text{if } l-m \neq r \\ \\ 1 & \text{if } l-m = r \end{cases} \qquad (l,m) \in \{1, \dots N\} \tag{4.3}$$

denotes the time-shift matrix that accounts for range position of the bins with respect to Radar-1. A similar matrix $\mathbf{J}_{\tilde{r}}$ will be used to account for the range position with respect to Radar-2. $\mathbf{n}$ is a zero-mean white Gaussian noise and is therefore characterized by: $\mathbb{E}[\mathbf{n}] = 0$ and $\mathbb{E}[\mathbf{n}\mathbf{n}^H] = \sigma_n^2\mathbf{I}$, with σ_n^2 being its noise variance.

4.1.2 Statistical Characterization of the Clutter

The statistical characterization of the clutter vector $\mathbf{c}$ is analyzed hereafter. The scatterers are assumed to be uncorrelated. Each scatterer illuminated by Radar-1 is characterized by a variance equal to $\sigma^2_{c1,(r,i)} = \mathbb{E}[|\alpha_{c1,(r,i)}|^2]$, whereas Radar-2 sees a variance equal to $\sigma^2_{c2,(r,i)} = \mathbb{E}[|\alpha_{c2,(r,i)}|^2]$. The expected value of their complex amplitude is assumed to be zero $\mathbb{E}[\alpha_{c,\mathrm{rdr},(r,i)}] = 0$ and their normalized Doppler frequency is denoted as uniformly distributed around the mean doppler frequencies $\bar{\nu}_{d_{1,(r,i)}}$ and $\bar{\nu}_{d_{2,(r,i)}}$:

$$\nu_{d_{\mathrm{rdr},(r,i)}} \sim \mathcal{U}(\bar{\nu}_{d_{\mathrm{rdr},(r,i)}} - \frac{\epsilon_{\mathrm{rdr},(r,i)}}{2}, \bar{\nu}_{d_{\mathrm{rdr},(r,i)}} + \frac{\epsilon_{\mathrm{rdr},(r,i)}}{2})$$

where the subscript "rdr" identifies the radar under investigation (i.e. $rdr = 1, 2$), $\epsilon_{\mathrm{rdr},(r,i)}$ accounts for the uncertainty of the clutter Doppler. As a consequence, $\mathbb{E}[\mathbf{c}] = 0$ and:

$$\mathbf{\Psi}_c = \mathbb{E}[\mathbf{c}_1\mathbf{c}_1^H] + \mathbb{E}[\mathbf{c}_1\mathbf{c}_2^H] + \mathbb{E}[\mathbf{c}_2\mathbf{c}_1^H] + \mathbb{E}[\mathbf{c}_2\mathbf{c}_2^H] \tag{4.4}$$

The clutter statistics coming from a single radar can be expressed as:

$$\mathbb{E}[\mathbf{c}_1\mathbf{c}_1^H] = \sigma^2_{c1}\mathbf{J}_r\mathbf{\Gamma}(\mathbf{s}_1(r,i))\mathbf{J}_r^T$$

$$\mathbb{E}[\mathbf{c}_2\mathbf{c}_2^H] = \sigma^2_{c2}\mathbf{J}_{\tilde{r}}\mathbf{\Gamma}(\mathbf{s}_2(r,i))\mathbf{J}_{\tilde{r}}^T$$

where:

$$\mathbf{\Gamma}(\mathbf{s}_{\mathrm{rdr}}(r,i)) = \mathrm{diag}\{\mathbf{s}_{\mathrm{rdr}}\}\mathbf{\Phi}^{\bar{\nu}_{d_{c,\mathrm{rdr},(r,i)}}}_{\epsilon_{\mathrm{rdr},(r,i)}}\mathrm{diag}\{\mathbf{s}_{\mathrm{rdr}}\}^H \tag{4.5}$$

and:

$$\mathbf{\Phi}^{\bar{\nu}_{d_{\mathrm{rdr},(r,i)}}}_{\epsilon_{\mathrm{rdr},(r,i)}}(l,m) = \mathrm{e}^{j2\pi\bar{\nu}_{d_{\mathrm{rdr}}}(l-m)}\frac{\sin[\pi\epsilon_{\mathrm{rdr}}(l-m)]}{[\pi\epsilon_{\mathrm{rdr}}(l-m)]} \tag{4.6}$$

where (l, m) indicates a matrix element.

Unlike the case in [16], a bistatic radar has cross-correlation terms as discussed below:

$$\mathbb{E}[\mathbf{c}_1\mathbf{c}_2^H] = \alpha_{c1}\alpha_{c2}^*\mathbf{J}_r\mathbf{\Gamma}(\mathbf{s}_1(r,i),\mathbf{s}_2(r,i))\mathbf{J}_{\tilde{r}}^H \tag{4.7}$$

where:

$$\begin{aligned}\mathbf{\Gamma}(\mathbf{s}_1(r,i),\mathbf{s}_2(r,i)) &= \mathbb{E}[(\mathbf{s}_1 \odot \mathbf{p}(\nu_{1,(r,i)}))(\mathbf{s}_2 \odot \mathbf{p}(\nu_{2,(r,i)}))]^H \\ &= \mathrm{diag}\{\mathbf{s}_1\}\mathbb{E}[\mathbf{p}(\nu_{1,(r,i)})\mathbf{p}(\nu_{2,(r,i)})^H]\mathrm{diag}\{\mathbf{s}_2^H\} \\ &= \mathrm{diag}\{\mathbf{s}_1\}\mathbf{\Phi}_{\mathrm{cross},\epsilon_{(r,i)}}^{\bar{\nu}_{d_{(r,i)}}}\mathrm{diag}\{\mathbf{s}_2^H\}.\end{aligned} \tag{4.8}$$

Considering that:

$$\mathbf{p}(\nu_{1,(r,i)})\mathbf{p}(\nu_{2,(r,i)})^H = \begin{bmatrix} 1 \\ \mathrm{e}^{(j2\pi\nu_{1,(r,i)}(1))} \\ \vdots \\ \\ \mathrm{e}^{(j2\pi\nu_{1,(r,i)}(N-1))} \end{bmatrix} \begin{bmatrix} 1 & \mathrm{e}^{(-j2\pi\nu_{2,(r,i)}(1))} & \dots & \mathrm{e}^{(-j2\pi\nu_{2,(r,i)}(N-1))} \end{bmatrix}, \tag{4.9}$$

follows that:

$$\begin{aligned}\mathbf{\Phi}_{\mathrm{cross},\epsilon_{(r,i)}}^{\bar{\nu}_{d_{(r,i)}}}(l,m) &= \mathbb{E}[\mathrm{e}^{j2\pi(\nu_{1,(r,i)}+\theta_1)(l-1)}\mathrm{e}^{j2\pi(\nu_{2,(r,i)}+\theta_2)(m-1)}] \\ &= \mathrm{e}^{j2\pi\nu_{1,(r,i)}(l-1)}\mathrm{e}^{-j2\pi\nu_{2,(r,i)}(m-1)}\frac{\sin[\pi\epsilon_{(r,i)}(l-1)]}{[\pi\epsilon_{(r,i)}(l-1)]}\frac{\sin[\pi\epsilon_{(r,i)}(m-1)]}{[\pi\epsilon_{(r,i)}(m-1)]},\end{aligned} \tag{4.10}$$

where θ_1 and θ_2 are the Doppler integration variables. These cross-term statistics proved to be very close to zero and have therefore been ignored.

The final clutter statistics as a function of the transmitted signals result therefore:

$$\begin{aligned}\boldsymbol{\Psi}_c(\mathbf{s}_1,\mathbf{s}_2) &= \mathbb{E}[\mathbf{c}_1\mathbf{c}_1^H] + \mathbb{E}[\mathbf{c}_2\mathbf{c}_2^H] \\ &= \sum_{r=0}^{N_c-1}\sum_{i=0}^{L-1}(\sigma_{c,1}^2\mathbf{J}_r\boldsymbol{\Gamma}(\mathbf{s}_1(r,i))\mathbf{J}_r^T + \sigma_{c,2}^2\mathbf{J}_{\tilde{r}}\boldsymbol{\Gamma}(\mathbf{s}_2(r,i))\mathbf{J}_{\tilde{r}}^T)\end{aligned} \tag{4.11}$$

4.2 Problem Formulation

The analysis under discussion covers the design of two mutually orthogonal signals and corresponding receiver filter that maximize the SINR under some constraint on the shape of the codes.

Renaming for simplicity $\mathbf{q}_1 = [\mathbf{s}_1 \odot \mathbf{p}(\nu_{d_{1,T}})]$ and $\mathbf{q}_2 = [\mathbf{s}_2 \odot \mathbf{p}(\nu_{d_{2,T}})]$ and assuming that the received signal $\mathbf{x}$ is processed by a filter $\mathbf{w}$, the SINR at the output results:

$$\text{SINR} = \frac{|\alpha_{1,T}|^2|\mathbf{w}^H\mathbf{q}_1|^2 + |\alpha_{2,T}|^2|\mathbf{w}^H\mathbf{q}_2|^2}{\mathbf{w}^H\boldsymbol{\Psi}_c(\mathbf{s}_1,\mathbf{s}_2)\mathbf{w} + \sigma_n^2\|\mathbf{w}\|^2} \tag{4.12}$$

It is relevant to point out how the clutter energy depends both on the receiver filter $\mathbf{w}$ and the transmitted signals $\mathbf{s}_1$ and $\mathbf{s}_2$ through $\boldsymbol{\Psi}_c(\mathbf{s}_1,\mathbf{s}_2)$. This observation represents the main difference between a signal-dependent and a signal-independent environment where the output clutter energy is only a function of $\mathbf{w}$ [16].

The constraints on the codes can be subdivided into three categories:

- Mutual orthogonality: $\mathbf{s}_1^H\mathbf{s}_2 = 0$;
- Transmission of finite energy: $\|\mathbf{s}_{\text{rdr}}\|^2 = 1$;
- Similarity constraint: $\|\mathbf{s}_{\text{rdr}} - \mathbf{s}_{0,\text{rdr}}\|^2 \leq \delta$ where the parameter δ determines the similarity extent and $\mathbf{s}_{0,\text{rdr}}$ is an initial code which will be

chosen according to desired properties.

All of the aforementioned requirements and optimization choices lead to the following initial problem:

$$\begin{aligned} \max_{\mathbf{s},\mathbf{w}} \quad & \frac{|\alpha_{1,T}|^2|\mathbf{w}^H\mathbf{q}_1|^2+|\alpha_{2,T}|^2|\mathbf{w}^H\mathbf{q}_2|^2}{\mathbf{w}^H\mathbf{\Psi}_c(\mathbf{s}_1,\mathbf{s}_2)\mathbf{w}+\sigma_n^2\|\mathbf{w}\|^2} \\ \text{s.t.} \quad & \mathbf{s}_1^H\mathbf{s}_2 = 0 \\ & \|\mathbf{s}_1\|^2 = 1 \\ & \|\mathbf{s}_2\|^2 = 1 \\ & \|\mathbf{s}_1 - \mathbf{s}_{0,1}\|^2 \leq \delta \\ & \|\mathbf{s}_2 - \mathbf{s}_{0,2}\|^2 \leq \delta \end{aligned} \tag{4.13}$$

The above optimization problem is non-convex (the objective function is a non-convex function and $\|\mathbf{s}_{\text{rdr}}\|^2 = 1$ defines non-convex sets). The idea is to iteratively optimize the SINR. Specifically, starting from a receiver filter $\mathbf{w}^{(t-1)}$ at step $(t-1)$, where t indicates the iteration number, the code searches for the admissible radar codes $\mathbf{s}_1^{(t)}$ and $\mathbf{s}_2^{(t)}$ maximizing the SINR corresponding to the receiver filter $\mathbf{w}^{(t-1)}$. Whenever the $\mathbf{s}_{\text{rdr}}^{(n)}$ are found, the code searches for the adaptive filter $\mathbf{w}^{(t)}$ which maximizes the SINR corresponding to the radar codes $\mathbf{s}_{\text{rdr}}^{(t)}$, and so on, as presented in [16] for the case of monostatic radar. The outline of such optimization can be found in Table 4.1.

4.2.1 Receiver Filter Optimization

The first step consists of determining the receiver filter for the given pair of radar waveforms. The cost function in Equation (4.12) can be written as:

$$\frac{\mathbf{w}^{\text{H}}\mathbf{A}\mathbf{w}}{\mathbf{w}^{\text{H}}\mathbf{B}\mathbf{w}}, \tag{4.14}$$

Initialization:

- Select initial radar codes $\mathbf{s}_{0,\text{rdr}}$ with desired properties;
- Input range-azimuth parameters (N_c, L);
- Input target parameters ($\sigma^2_{1,T}$, $\sigma^2_{2,T}$, $\nu_{d_{1,T}}$ and $\nu_{d_{2,T}}$);
- Input clutter parameters (σ^2_{c1}, σ^2_{c2}, $\bar{\nu}_{d_1}$, $\bar{\nu}_{d_2}$ and ϵ_{rdr});
- Input the noise variance (σ^2_n);
- Estimate initial receiver filter $\mathbf{w}^{(0)}$ at step $t = 0$ by using initial waveforms $\mathbf{s}_{0,\text{rdr}}$;
- Estimate initial SINR by using $\mathbf{w}^{(0)}$ and $\mathbf{s}_{0,\text{rdr}}$;
- Initialize SINR$(t-1)$ and ζ appropriately;

while $|\text{SINR}(t-1) - \text{SINR}(t)| > \zeta$

- Waveform optimization (convex optimization technicques);
- Filter optimization (estimated with new, optimized waveform);
- Optimized SINR calculation.

end

The procedure is completed providing the output: $\mathbf{s}_{1,\text{final}}$, $\mathbf{s}_{2,\text{final}}$, $\mathbf{w}_{\text{final}}$.

Table 4.1: Outline of the optimization method from a simulation-oriented perspective. t indicates the iteration number.

where:

$$\mathbf{A} = |\alpha_{1,T}|^2 \mathbf{q}_1 \mathbf{q}_1^{\mathrm{H}} + |\alpha_{2,T}|^2 \mathbf{q}_2 \mathbf{q}_2^{\mathrm{H}},$$

and:

$$\mathbf{B} = \mathbf{\Psi}_c(\mathbf{s}_1, \mathbf{s}_2) + \sigma_n^2 \mathbf{I}.$$

The optimum receiver filter $\mathbf{w}$ can now be obtained as the generalized eigenvector corresponding to the largest generalized eigenvalue of the matrix pair $(\mathbf{A}, \mathbf{B})$.

4.2.2 Orthogonal Codes Optimization

The second step consists in the optimization of the radar codes. To start with, since the algorithm has now knowledge about $\mathbf{w}$ but not on the codes that need to be transmitted, the clutter statistics must be rewritten as a function of the optimized filter. Unifying, for convenience, the vectors and matrices of both radars the following equivalences can be obtained:

$$\mathbf{w}_{\mathrm{u}} = \begin{bmatrix} \sigma_{c1}\mathbf{w} & \sigma_{c2}\mathbf{w} \end{bmatrix}^T$$

$$\mathbf{s}_{\mathrm{u}} = \begin{bmatrix} \mathbf{s}_1 & \mathbf{s}_2 \end{bmatrix}^T$$

$$\mathbf{s}_{0,\mathrm{u}} = \begin{bmatrix} \mathbf{s}_{0,1} & \mathbf{s}_{0,2} \end{bmatrix}^T$$

$$\mathbf{J}_{r,\mathrm{u}} = \begin{bmatrix} \mathbf{J}_r & 0 \\ 0 & \mathbf{J}_{\tilde{r}} \end{bmatrix}$$

$$\mathbf{\Phi}^{\bar{\nu}_{d_{(r,i)}}}_{\epsilon_{(r,i),\mathrm{u}}} = \begin{bmatrix} \mathbf{\Phi}^{\bar{\nu}_{d_{1,(r,i)}}}_{\epsilon_{1,(r,i)}} & 0 \\ 0 & \mathbf{\Phi}^{\bar{\nu}_{d_{2,(r,i)}}}_{\epsilon_{2,(r,i)}} \end{bmatrix}$$

$$\mathbf{\Gamma}(\mathbf{s}_{\mathrm{u}}) = \mathrm{diag}(\mathbf{s}_{\mathrm{u}})\mathbf{\Phi}^{\bar{\nu}_{d_{(r,i)}}}_{\epsilon_{(r,i),\mathrm{u}}}\mathrm{diag}(\mathbf{s}_{\mathrm{u}})^H$$

With this notation, the clutter energy as a function of the transmitted code can be rewritten as:

$$\begin{aligned}\mathbf{w}_{\mathrm{u}}^H\mathbf{\Psi}_c(\mathbf{s}_{\mathrm{u}})\mathbf{w}_{\mathrm{u}} &= \sum_{r=0}^{N_c-1}\sum_{i=0}^{L-1}(\mathbf{w}_{\mathrm{u}}^H\mathbf{J}_{r,\mathrm{u}}\mathbf{\Gamma}(\mathbf{s}_{\mathrm{u}})\mathbf{J}_{r,\mathrm{u}}^T\mathbf{w}_{\mathrm{u}}) \\ &= \sum_{r=0}^{N_c-1}\sum_{i=0}^{L-1}(\mathbf{w}_{\mathrm{u}}^H\mathbf{J}_{r,\mathrm{u}}\mathrm{diag}(\mathbf{s}_{\mathrm{u}})\mathbf{\Phi}^{\bar{\nu}_{d_{(r,i)}}}_{\epsilon_{(r,i),\mathrm{u}}}\mathrm{diag}(\mathbf{s}_{\mathrm{u}})^H\mathbf{J}_{r,\mathrm{u}}^T\mathbf{w}_{\mathrm{u}}) \\ &= \sum_{r=0}^{N_c-1}\sum_{i=0}^{L-1}(\mathbf{s}_{\mathrm{u}}^T\mathrm{diag}\{\mathbf{J}_{-r,\mathrm{u}}\mathbf{w}_{\mathrm{u}}^*\}\mathbf{\Phi}^{\bar{\nu}_{d_{(r,i)}}}_{\epsilon_{(r,i),\mathrm{u}}}\mathrm{diag}\{\mathbf{J}_{-r,\mathrm{u}}\mathbf{w}_{\mathrm{u}}\}\mathbf{s}_{\mathrm{u}}^*)\end{aligned} \tag{4.15}$$

Naming now:

$$\mathbf{\Theta}_c(\mathbf{w}_{\mathrm{u}}) = \sum_{r=0}^{N_c-1}\sum_{i=0}^{L-1}(\mathrm{diag}\{\mathbf{J}_{-r,\mathrm{u}}\mathbf{w}_{\mathrm{u}}^*\}\mathbf{\Phi}^{\bar{\nu}_{d_{(r,i)}}}_{\epsilon_{(r,i),\mathrm{u}}}\mathrm{diag}\{\mathbf{J}_{-r,\mathrm{u}}\mathbf{w}_{\mathrm{u}}\})$$

the following equivalence can be obtained:

$$\mathbf{w}_{\mathrm{u}}^H\mathbf{\Psi}_c(\mathbf{s}_{\mathrm{u}})\mathbf{w}_{\mathrm{u}} = \mathbf{s}_{\mathrm{u}}^T\mathbf{\Theta}_c(\mathbf{w}_{\mathrm{u}})\mathbf{s}_{\mathrm{u}}^*$$

and by labeling:

$$\mathbf{r}_{\mathrm{u}} = \begin{bmatrix} \alpha_{1,T}(\mathbf{w}^* \odot \mathbf{p}(\nu_{d_{1,T}}) \\ \alpha_{2,T}(\mathbf{w}^* \odot \mathbf{p}(\nu_{d_{2,T}}) \end{bmatrix} \tag{4.16}$$

the initial optimization problem can be rewritten as:

$$\begin{aligned} \max_{\mathbf{s}_\mathrm{u}} \quad & \frac{|\mathbf{s}_\mathrm{u}^T \mathbf{r}_\mathrm{u}|^2}{\mathbf{s}_\mathrm{u}^T \boldsymbol{\Theta}_{c_1}(\mathbf{w}_\mathrm{u}^{(n-1)}) \mathbf{s}_\mathrm{u}^* + \sigma_n^2 \|\mathbf{w}_\mathrm{u}^{(n-1)}\|^2} \\ \text{s.t.} \quad & \mathbf{s}_1^H \mathbf{s}_2 = 0 \\ & \|\mathbf{s}_1\|^2 = 1 \\ & \|\mathbf{s}_2\|^2 = 1 \\ & \|\mathbf{s}_1 - \mathbf{s}_{0,1}\|^2 \leq \delta \\ & \|\mathbf{s}_2 - \mathbf{s}_{0,2}\|^2 \leq \delta \end{aligned} \tag{4.17}$$

This is a fractional quadratic problem and, in order to solve it, the guidelines in [16] and [49] should be used. Indicating with:

$$\mathbf{S} = \mathbf{r}_\mathrm{u}^* \mathbf{r}_\mathrm{u}^H$$

$$\mathbf{M} = \boldsymbol{\Theta}_{c_1}(\mathbf{w}_\mathrm{u}^{(t-1)}) + \sigma_n^2 \|\mathbf{w}_\mathrm{u}^{(t-1)}\|^2 \mathbf{I}$$

$$\mathbf{s}_1 = \begin{bmatrix} \mathbf{I}_N & \mathbf{0}_N \end{bmatrix} \begin{bmatrix} \mathbf{s}_1 \\ \mathbf{s}_2 \end{bmatrix} = \mathbf{m}_1 \mathbf{s}_\mathrm{u}$$

$$\mathbf{s}_2 = \begin{bmatrix} \mathbf{0}_N & \mathbf{I}_N \end{bmatrix} \begin{bmatrix} \mathbf{s}_1 \\ \mathbf{s}_2 \end{bmatrix} = \mathbf{m}_2 \mathbf{s}_\mathrm{u}$$

the optimization problem in Equation (4.17) can be therefore re-written as:

$$
\begin{aligned}
\max_{\mathbf{s}_\mathrm{u},p} \quad & \frac{\mathrm{tr}\left(\begin{bmatrix}\mathbf{S} & \mathbf{0}\\ \mathbf{0} & 0\end{bmatrix}\begin{bmatrix}\mathbf{s}_\mathrm{u}\mathbf{s}_\mathrm{u}^H & \mathbf{s}_\mathrm{u}p^*\\ \mathbf{s}_\mathrm{u}^H p & |p|^2\end{bmatrix}\right)}{\mathrm{tr}\left(\begin{bmatrix}\mathbf{M} & \mathbf{0}\\ \mathbf{0} & 0\end{bmatrix}\begin{bmatrix}\mathbf{s}_\mathrm{u}\mathbf{s}_\mathrm{u}^H & \mathbf{s}_\mathrm{u}p^*\\ \mathbf{s}_\mathrm{u}^H p & |p|^2\end{bmatrix}\right)} \\
\text{s.t.} \quad & \mathrm{tr}\left(\begin{bmatrix}\mathbf{m}_1^H\mathbf{m}_2 & \mathbf{0}\\ \mathbf{0} & 0\end{bmatrix}\begin{bmatrix}\mathbf{s}_\mathrm{u}\mathbf{s}_\mathrm{u}^H & \mathbf{s}_\mathrm{u}p^*\\ \mathbf{s}_\mathrm{u}^H p & |p|^2\end{bmatrix}\right) = 0, \\
& \mathrm{tr}\left(\begin{bmatrix}\mathbf{m}_1^H\mathbf{m}_1 & \mathbf{0}\\ \mathbf{0} & 0\end{bmatrix}\begin{bmatrix}\mathbf{s}_\mathrm{u}\mathbf{s}_\mathrm{u}^H & \mathbf{s}_\mathrm{u}p^*\\ \mathbf{s}_\mathrm{u}^H p & |p|^2\end{bmatrix}\right) = 1, \\
& \mathrm{tr}\left(\begin{bmatrix}\mathbf{m}_2^H\mathbf{m}_2 & \mathbf{0}\\ \mathbf{0} & 0\end{bmatrix}\begin{bmatrix}\mathbf{s}_\mathrm{u}\mathbf{s}_\mathrm{u}^H & \mathbf{s}_\mathrm{u}p^*\\ \mathbf{s}_\mathrm{u}^H p & |p|^2\end{bmatrix}\right) = 1, \\
& \mathrm{tr}\left(\begin{bmatrix}\mathbf{I} & -\mathbf{s}_{0,\mathrm{u}}\\ -\mathbf{s}_{0,\mathrm{u}}^H & \|\mathbf{s}_{0,\mathrm{u}}\|^2-\delta\end{bmatrix}\begin{bmatrix}\mathbf{s}_\mathrm{u}\mathbf{s}_\mathrm{u}^H & \mathbf{s}_\mathrm{u}p^*\\ \mathbf{s}_\mathrm{u}^H p & |p|^2\end{bmatrix}\right) \le 0, \\
& \mathrm{tr}\left(\begin{bmatrix}\mathbf{0} & \mathbf{0}\\ \mathbf{0} & 1\end{bmatrix}\begin{bmatrix}\mathbf{s}_\mathrm{u}\mathbf{s}_\mathrm{u}^H & \mathbf{s}_\mathrm{u}p^*\\ \mathbf{s}_\mathrm{u}^H p & |p|^2\end{bmatrix}\right) = 1, \\
& \mathbf{s}_\mathrm{u} \in \mathbb{C}^N \quad \text{and} \quad p \in \mathbb{C}.
\end{aligned}
\tag{4.18}
$$

By dropping the rank-one constraint the optimization problem (4.18) can be relaxed into the semidefinite programming (SDP) problem:

$$\begin{aligned} \max_{\mathbf{W}} \quad & \frac{\mathrm{tr}(\mathbf{Q}_{-1}\mathbf{W})}{\mathrm{tr}(\mathbf{Q}_0\mathbf{W})} \\ \text{s.t.} \quad & \mathrm{tr}(\mathbf{Q}_1\mathbf{W}) = 0 \\ & \mathrm{tr}(\mathbf{Q}_2\mathbf{W}) = 1 \\ & \mathrm{tr}(\mathbf{Q}_3\mathbf{W}) = 1 \\ & \mathrm{tr}(\mathbf{Q}_4\mathbf{W}) \leq 0 \\ & \mathrm{tr}(\mathbf{Q}_5\mathbf{W}) = 1 \\ & \mathbf{W} \succeq 0 \end{aligned} \tag{4.19}$$

where $\mathbf{W}$ and the $\mathbf{Q}_i$ matrices are defined as follows:

$$\mathbf{Q}_{-1} = \begin{bmatrix} \mathbf{S} & \mathbf{0} \\ \mathbf{0} & 0 \end{bmatrix}$$

$$\mathbf{Q}_0 = \begin{bmatrix} \mathbf{M} & \mathbf{0} \\ \mathbf{0} & 0 \end{bmatrix}$$

$$\mathbf{Q}_1 = \begin{bmatrix} \mathbf{m}_1^H \mathbf{m}_2 & \mathbf{0} \\ \mathbf{0} & 0 \end{bmatrix}$$

$$\mathbf{Q}_2 = \begin{bmatrix} \mathbf{m}_1^H \mathbf{m}_1 & \mathbf{0} \\ \mathbf{0} & 0 \end{bmatrix}$$

$$\mathbf{Q}_3 = \begin{bmatrix} \mathbf{m}_2^H \mathbf{m}_2 & \mathbf{0} \\ \mathbf{0} & 0 \end{bmatrix}$$

$$\mathbf{Q}_4 = \begin{bmatrix} \mathbf{I} & -\mathbf{s}_{0,\mathrm{u}} \\ -\mathbf{s}_{0,\mathrm{u}}^H & \|\mathbf{s}_{0,\mathrm{u}}\|^2 - \delta \end{bmatrix}$$

$$\mathbf{Q}_5 = \begin{bmatrix} \mathbf{0} & \mathbf{0} \\ \mathbf{0} & 1 \end{bmatrix}$$

As shown in [49] the fractional SDP problem (4.19) can be solved thanks to the Charnes-Cooper variable transformation. Thanks to this device, one can replace a linear fractional program with at most two straightforward linear programs that differ from each other by only a change of sign in the objective function and in the constraint, and thus achieve a global optimal solution of the linear fractional program by solving at most two linear programs. Defining now the transformed variable as $\mathbf{X} = u\mathbf{W}$ where $u \geq 0$ complies with $\mathrm{tr}(\mathbf{Q}_0 \mathrm{u}\mathbf{W}) = 1$. The following SDP problem can be derived:

$$\begin{aligned} \max_{\mathbf{X},u} \quad & \mathrm{tr}(\mathbf{Q}_{-1}\mathbf{X}) \\ \text{s.t.} \quad & \mathrm{tr}(\mathbf{Q}_0\mathbf{X}) = 1 \\ & \mathrm{tr}(\mathbf{Q}_1\mathbf{X}) = 0 \\ & \mathrm{tr}(\mathbf{Q}_2\mathbf{X}) = \mathrm{u} \\ & \mathrm{tr}(\mathbf{Q}_3\mathbf{X}) = \mathrm{u} \\ & \mathrm{tr}(\mathbf{Q}_4\mathbf{X}) \leq 0 \\ & \mathrm{tr}(\mathbf{Q}_5\mathbf{X}) = \mathrm{u} \\ & \mathbf{X} \succeq \mathbf{0}, u \geq 0 \end{aligned} \tag{4.20}$$

If $(\mathbf{X}^\star, \mathrm{u}^\star)$ solves (4.20), then $\mathbf{X}^\star/\mathrm{u}^\star$ solves (4.19). Once an optimal solution $\mathbf{X}^\star$ is obtained, its rank needs to be checked. If the rank of $\mathbf{X}^\star$ equals to one, the solution is a global optimal solution and it can be easily obtained

through the eigen-decomposition:

$$\mathbf{X}^\star = \mathbf{x}^\star(\mathbf{x}^\star)^H$$

where $\mathbf{x}^\star = \begin{bmatrix} \mathbf{x}^\star \\ \mathrm{p}^\star \end{bmatrix}$. The output results in $\mathbf{s}^\star = {}^{\mathrm{y}^\star}/_{\mathrm{p}^\star}$. If the rank of $\mathbf{X}^\star$ is higher than one, the randomization method needs to be applied in order to obtain a rank one solution [80]. In this case, the eigenvectors corresponding to significant eigenvalues of $\mathbf{X}^\star$ will be extracted and various linear combinations of these eigenvectors will be constructed using random combinations, and the best combination that maximizes the utility of (4.20) will be chosen.

4.3 Performance Analysis

In order to evaluate the performance of the proposed algorithm, a Matlab code was implemented. The initial signals $\mathbf{s}_{0,1}$ and $\mathbf{s}_{0,1}$ of length $N = 64$ are as developed in [1]. As it can be seen by referring back to Figure 1.2, these waveforms are characterized by very good auto-correlation and cross-correlation properties. This necessary combination of characteristics grants good range resolution while maintaining orthogonality, making these codes ideal for MIMO applications.

In the proposed scenario there is homogeneous range-azimuth clutter. The number of range rings that interfere with the range-azimuth bin of interest is $N_c = 7$ and the number of azimuth cells in each ring is $L = 50$. As for the parameters, the noise variance was set to $\sigma_n^2 = 0.1$, and the variance of the radar cross-section to $\sigma_1^2 = 0.18$ and $\sigma_2^2 = 0.20$. The mean Doppler frequencies are $\bar{\nu}_{d_{1,(r,i)}} = \bar{\nu}_{d_{1,(r,i)}} = 0.1$ and $\epsilon_{1,(r,i)} = \epsilon_{2,(r,i)} = 0.4$.
The exit for the iterative condition on the SINR was set to $\zeta = 10^{-3}$.

δ	$\overline{\text{SINR}}_{\text{start}}$(dB)	$\overline{\text{SINR}}_{\text{end}}$(dB)	SINR_{th}(dB)
0.2	3.9767	13.9188	13.8201
0.5	4.2019	20.0441	20.6110
1	4.8592	24.4945	25.0226

Table 4.2: Comparison between statistical characterization and modeled observations for $\delta = [0.2 \;\; 0.5 \;\; 1]$.

For solving the SDP problem, the CVX Software for Disciplined Convex Programming toolbox in [74] was used.

In order to evaluate the performance of the proposed analysis, a needed comparison between the statistical characterization and the modeled observations was carried out. Monte Carlo experiments were therefore implemented using 1000 random realizations of RCS, noise and Doppler frequencies, the obtained SINR was subsequently averaged and compared to the estimated one. This has been done for various values of δ. As shown in Table 4.2, the results prove the correctness of the model. The convergence of SINR against iteration number was also observed for different values of $\delta = \begin{bmatrix} 0.2 & 0.5 & 1 \end{bmatrix}$. By looking at Figure 4.2, it can be noted how to higher values of δ correspond bigger values of the achievable SINR. These gains are a consequence of the fact that bigger values of δ make the feasible set of the optimization problem become larger and larger [16]. Nevertheless, these increased gains are just potential values as in real conditions smaller SINR are to be expected due to an increasing divergence from the initial assumptions. As a matter of fact, by increasing δ a deterioration in both the auto-ambiguity and cross-ambiguity functions can be observed. This consequence can be appreciated by looking at Figures 4.3, 4.4 and 4.5. The ambiguity function is a very useful used tool that enables the estimation of the performance of a radar waveform's resolution. Due to the fact that the model

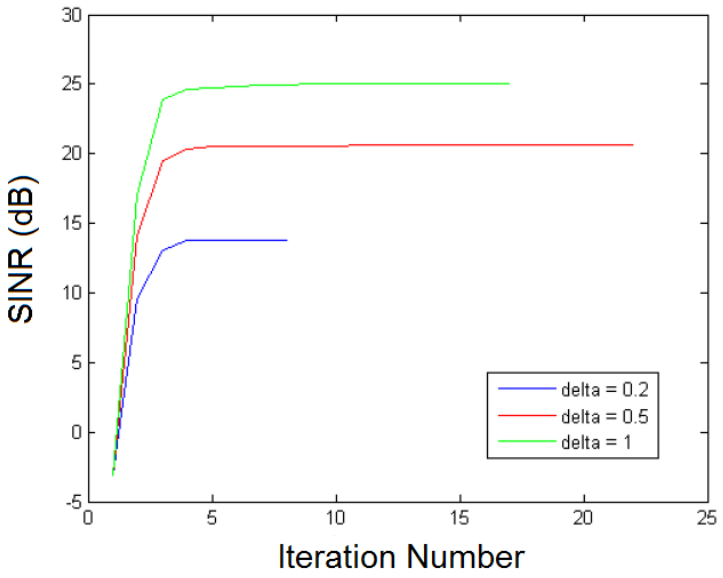

Figure 4.2: SINR evolution for $\delta = [0.2 \;\; 0.5 \;\; 1]$.

under discussion is of a bistatic nature, the AF has been split into two auto-ambiguity functions (AAF) for the evaluation of the resolution properties of $\mathbf{s}_1$ and $\mathbf{s}_2$ and a cross-ambiguity function (CAF) for the evaluation of their orthogonality features. Results show how for small values of δ, very narrow peaks of the AAF can be obtained, proving that excellent auto-correlation properties were maintained by the optimized waveform. Furthermore, a flat CAF was obtained, proving excellent rejection to interference between the two signals. As the value of δ increased, though, the features of the optimized waveform proved to be sub-optimal: very wide sidelobes in the AAF as well as a peak within the CAF, showed how the waveform optimized with $\delta = 1$ does not have ideal properties.

4.4 Conclusions

This chapter discussed a cognitive optimization framework for the design of transmit orthogonal signals and receiver filter in a signal-dependent clutter environment for a bistatic radar. Initially, a description of the signal-dependent clutter model was provided, followed by considerations on the cross-interference terms caused by the non-orthogonality between clutter terms originating from different radar signals. Consequently, the main optimization problem that maximizes the SINR under some constraints on the codes was proposed. The constraints were mutual orthogonality, transmission of finite energy and similarity to waveforms with desired characteristics. In order to solve this problem, an iterative algorithm that optimizes the transmitted waveform and the receiver filter was suggested. Simulation results showed how, by selecting parameters accurately, this optimization technique has the advantage of enhancing the SINR at the receiver filter while maintaining a narrow peak in the auto-ambiguity functions and a flat cross-ambiguity function.

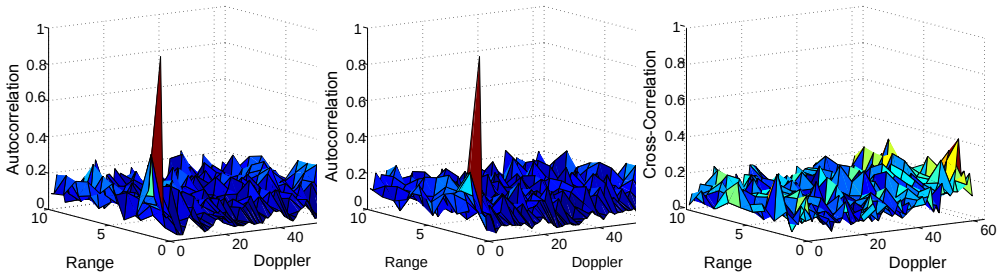

(a) AAF of signal s_1 (b) AAF of signal s_2 (c) CAF of s_1 and s_2

Figure 4.3: Auto-ambiguity and cross-ambiguity functions for the optimized waveform estimated with $\delta = 0.2$. As it can be noted, the very narrow peaks of the AAF prove that excellent auto-correlation properties were maintained by the optimized waveform. The flat CAF proved excellent rejection to interference between the two signals.

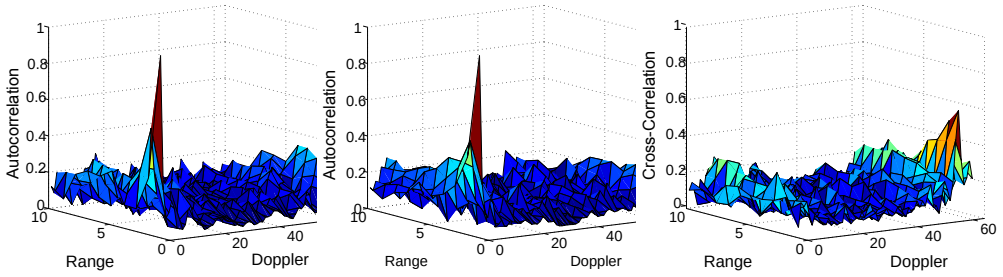

(a) AAF of signal s_1 (b) AAF of signal s_2 (c) CAF of s_1 and s_2

Figure 4.4: Auto-ambiguity and cross-ambiguity functions for the optimized waveform estimated with for $\delta = 0.5$. As it can be noted, the narrow peaks of the AAF prove that good auto-correlation properties were maintained by the optimized waveform. The fairly flat CAF proved acceptable rejection to interference between the two signals.

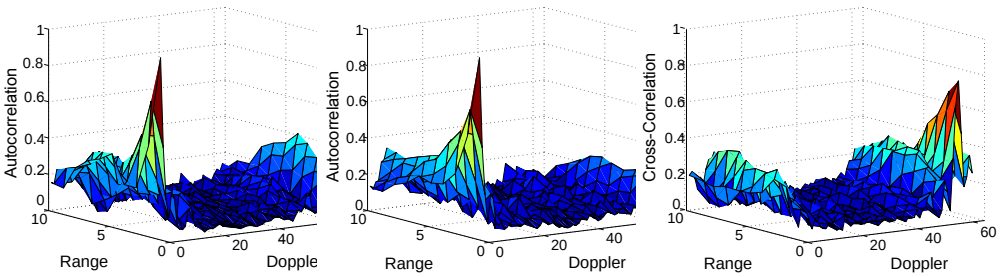

(a) AAF of signal s_1 (b) AAF of signal s_2 (c) CAF of s_1 and s_2

Figure 4.5: Auto-ambiguity and cross-ambiguity functions for the optimized waveform estimated with for $\delta = 1$. As it can be noted, the very wide sidelobes of the AAF show that for a big value of δ, the auto-correlation properties of the initial waveform were not maintained by the optimized waveform. The CAF also presents a peak, showing how $\delta = 1$ causes interference between the two signals.

Chapter 5

Waveform Optimization Techniques for Coordinated Networks

In the following chapter different waveform optimization techniques for coordinated cognitive networks will be presented. Three different optimization techniques have been developed. The first one aims at maximizing the accumulated target return signal power while keeping the total disturbance power to unity. This model is suitable for small networks with no specific target requirements. The other two optimization techniques are of a more sophisticated nature. The first one maximizes the signal power at a desired radar while keeping the SINR of all other radars at satisfactory level. This feature makes this algorithm suitable for applications where a radar finds itself in a particularly advantageous position and it can also be used to counteract blockage effects. The second technique optimizes all SINR equally and can be used for distributed surveillance in environments characterized by similar channels. This last model differs from the first

one since all SINRs are treated separately and the optimization technique is of a max-min nature. Also, these last two optimization methods have been extended to the case of M radars whereas the first one (although easily extendable) considers the basic case of two radars. This model was not included in the previous chapter because in this case both radars have receiving capabilities. All waveform optimization techniques hereby investigated are of an iterative nature and based on quadratically constrained quadratic program (QCQP) and semidefinite programming (SDP) convex optimization techniques. Thanks to the novelties introduced, the described work has been published in [81] and [82].

This chapter is organized as follows. Section 5.1 describes the basics of the considered model as well as the description of the receiver filter optimization and the generalities about the orthogonal codes optimization. Section 5.2 describes the waveform optimization designed for a two-radar system where both radars are equipped with receiving capabilities. This waveform optimization based on maximizing the accumulated radar returns is presented alongside with its performance analysis and some conclusions. In Section 5.3, waveform optimization techniques for a cognitive radar network are proposed. This work was developed for the general case of M transmitting and receiving radars. The section is further divided between a selective optimization technique, a max-min optimization technique, a performance analysis section and some concluding remarks. Finally, in Section 5.4, some conclusions on the topic of waveform optimization techniques for coordinated networks are drawn.

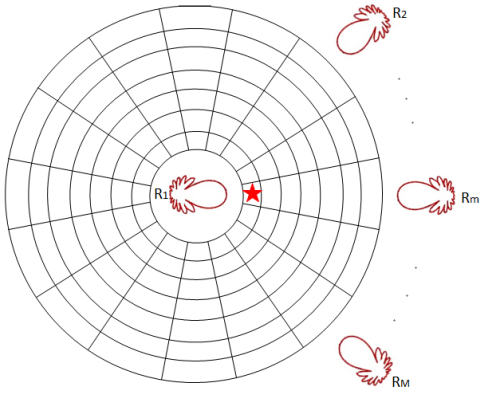

Figure 5.1: Geometry of the multistatic system. The radar at the center of the area under investigation is the reference radar. The star identifies the target's position within the range-azimuth bins. The other radars identify possible positions of other radars within the system.

5.1 System Model and Working Principles

This chapter discusses a radar network with centralized cognition. In this model the M radars transmit M mutually orthogonal signals. Thanks to optimized receiver filters, all radars can detect the propagated signals and send the acquired data to a processor. The processor performs the joint optimization algorithm, determines the most appropriate M waveforms for the subsequent transmissions of the radars and instructs them accordingly through a local backbone communication network.

The signal of length N transmitted by the generic Radar-i can be denoted as $\mathbf{s}_{(i)} = \begin{bmatrix} s_{(i)}(1) & s_{(i)}(2) & \dots & s_{(i)}(N) \end{bmatrix}^T$ with $i = 1, 2, \dots M$. In the considered model, depicted in Figure 5.1, the radars scan an area of N_c range bins, each of them subdivided into L azimuth bins. The index b_r is used to denote the range delay. The radar at the center of the area under investigation is the reference radar. The star identifies the target's position within the range-azimuth bins. This is assumed to be known. The other radars identify possible positions of other radars within the system. A Radar-i with $i = 1$

has been selected to act as a reference radar for the other radars towards the estimation of the position of the target. To account for the range position of the bins with respect to Radar-1, the time-shift matrix $\mathbf{J}_{j,i,b_r}$ described in [16], where Radar-j is the transmitting radar, Radar-i is the receiving radar and b_r is the relative range delay. Radar-1 has therefore a zero-shift with respect to the position of the target and the corresponding time-shift matrix is $\mathbf{J}_{(1,1,0)}$. On the other hand, the matrix $\mathbf{J}_{(j,i,b_r)}$ with $i \neq 1$ accounts for the delays of the signals originating from the other radars. The signal received by the generic Radar-i can be represented by the column-vector $\mathbf{x}_{(i)}$. This encloses the signals sent by every radar and subsequently scattered by the target as follows:

$$\mathbf{x}_{(i)} = \sum_{j=1}^{\mathrm{M}} \Big(\alpha_{T,(j,i)} \mathbf{J}_{(j,i,b_r)} \big(\mathbf{s}_{(j)} \odot \mathbf{p}(\nu_{T,(j,i)}) \big) \Big) + \mathbf{c}_{(i)} + \mathbf{n}, \tag{5.1}$$

where $\alpha_{T,(j,i)}$ is the complex parameter that accounts for the propagation and backscattering effects of the channel experienced by the waveform sent by Radar-j and received by Radar-i, $\mathbf{p}(\nu_{T,(j,i)}) = \begin{bmatrix} 1 & \mathrm{e}^{j2\pi\nu_{T,(j,i)}} & \dots & \mathrm{e}^{j2\pi(N-1)\nu_{T,(j,i)}} \end{bmatrix}^{\mathrm{T}}$ is the temporal Doppler steering vector as defined in [16] and $\nu_{T,(j,i)}$ is the normalized target Doppler frequency for the channel. The target parameter, as seen by each radar, will be characterized by the variance $\sigma^2_{T,(j,i)} = \mathbb{E}[|\alpha_{T,(j,i)}|^2]$ and mean $\mathbb{E}[\alpha_{T,(j,i)}] = 0$. This corresponds to the radar cross-section of the target. Similarly, for each illuminated clutter scatterer $\sigma^2_{c,(j,i,b_r)} = \mathbb{E}[|\alpha_{c,(j,i,b_r)}|^2]$ and $\mathbb{E}[\alpha_{c,(j,i,b_r)}] = 0$, where the subscript (j, i, b_r) marks the signal transmitted by Radar-j, scattered by the range-azimuth bin b_r and subsequently received at Radar-i. Also, the normalized Doppler frequency of the clutter is uniformly distributed between $\bar{\nu}_{c,(j,i,b_r)} - \epsilon$ and $\bar{\nu}_{c,(j,i,b_r)} + \epsilon$.

As in the previous chapter, the clutter is considered to be signal-dependent. The instantaneous received clutter component as seen by Radar-i is $\mathbf{c}_{(i)}$ and its covariance matrix (as defined in Subsection 4.1.2) is $\mathbf{\Psi}_{c,(i)} = \mathbb{E}[\mathbf{c}_{(i)}\mathbf{c}_{(i)}^{\mathrm{H}}]$. The noise $\mathbf{n}$ is considered to be a zero-mean white Gaussian noise characterized by $\mathbb{E}[\mathbf{n}] = \mathbf{0}$ and $\mathbb{E}[\mathbf{n}\mathbf{n}^{\mathrm{H}}] = \sigma_n^2\mathbf{I}$.

The proposed optimization is of an iterative nature where the receiver filter and the waveforms are designed alternatively by optimizing the SINR. The main structure is the same as the one described in the previous chapter and the reader can refer to Table 4.1 if needed. Starting from a given receiver filter $\mathbf{w}_{(i)}(t-1)$ at iteration $(t-1)$, the admissible radar codes $\mathbf{s}_{(i)}(t)$ that maximize the SINR subject to various constraints need to be estimated. When the waveforms are determined, the new adaptive receiver filter $\mathbf{w}_{(i)}(t)$ which maximizes the SINR corresponding to the waveforms $\mathbf{s}_{(i)}(t)$ can be estimated. A set of known waveforms with desired auto-correlation and cross-correlation properties will be utilized for initialization purposes.

5.1.1 Receive Filter Optimization

The first step consists of determining the receiver filter for a given set of radar waveforms. The SINR at Radar-i can be written as:

$$\begin{aligned}\mathrm{SINR}_{(i)} &= \frac{\left|\mathbf{w}_{(i)}^{\mathrm{H}}\sum_{j=1}^{\mathrm{M}}\Big(\sigma_{T,(j,i)}\mathbf{J}_{(j,i,b_r)}\big(\mathbf{s}_{(j)}\odot\mathbf{p}(\nu_{T,(j,i)})\big)\Big)\right|^2}{\mathbf{w}_{(i)}^{\mathrm{H}}\Big(\sum_{j=1}^{\mathrm{M}}\mathbf{\Psi}_{c,(j)}+\sigma_n^2\mathbf{I}\Big)\mathbf{w}_{(i)}} \\ &\triangleq \frac{\mathbf{w}_{(i)}^{\mathrm{H}}\mathbf{A}_{(i)}\mathbf{w}_{(i)}}{\mathbf{w}_{(i)}^{\mathrm{H}}\mathbf{B}_{(i)}\mathbf{w}_{(i)}}.\end{aligned} \tag{5.2}$$

The optimum receiver filter vectors $\mathbf{w}_{(i)}$ are obtained as the generalized eigenvector corresponding to the largest generalized eigenvalue of the matrix

pair $(\mathbf{A}_{(i)}, \mathbf{B}_{(i)})$.

5.1.2 Orthogonal Codes Optimization

The second step consists of optimizing the radar waveforms. The proposed algorithm requires the following constraints on the codes:

- All waveforms should be aimed at being mutually orthogonal or nearly orthogonal: $-\varrho \leq \mathbf{J}^{\mathrm{T}}_{(j,i,b_r)}\mathbf{s}^{\mathrm{H}}_{(i)}\mathbf{J}_{(j,i,b_r)}\mathbf{s}_{(j)} \leq \varrho$, where ϱ is a positive value very close to zero and $i \neq j$;

- All radars need to transmit finite energy (here assumed to be one): $\|\mathbf{s}_{(i)}\|^2 = 1$;

- In order to maintain good auto-correlation and cross-correlation properties, the estimated waveform $\mathbf{s}_{(i)}$ cannot diverge more than a specific amount from an initial waveform with desired features $\mathbf{s}_{0,(i)}$, i.e. $\|\mathbf{s}_{(i)} - \mathbf{s}_{0,(i)}\|^2 \leq \delta$.

The equations can now be reformulated in order to develop convex optimization techniques. The power of the desired signal component of the received signal at the i-th radar is written in terms of the transmitted waveforms as [82]:

$$\sum_{j=1}^{\mathrm{M}} \left| \mathbf{s}^{\mathrm{H}}_{(j)} \left(\sigma_{T,(j,i)} \mathbf{J}_{(j,i,b_r)} \left(\mathbf{w}_{(i)} \odot \mathbf{p}(\nu_{T,(j,i)}) \right) \right) \right|^2 = \mathrm{tr}(\mathbf{s}^{\mathrm{H}} \mathbf{R}_{(i)} \mathbf{s}), \tag{5.3}$$

where the received signal component is written as:

$\mathbf{R}_{(i)} = \mathrm{blkdiag}(\mathbf{R}_{(1,i)}, \mathbf{R}_{(2,i)}, \ldots, \mathbf{R}_{(M,i)})$,

where *blkdiag* is defined as the operator for block diagonalization, and where:

$\mathbf{R}_{(j,i)} = \mathbb{E}[\mathbf{r}_{(j,i)} \mathbf{r}^{\mathrm{H}}_{(j,i)}]$,

$\mathbf{r}_{(j,i)} = \alpha_{T,(j,i)} \mathbf{J}_{(j,i,b_r)} (\mathbf{w}_{(i)} \odot \mathbf{p}(\nu_{T,(j,i)}))$,

and:

$$\mathbf{s} = \begin{bmatrix} \mathbf{s}_{(1)}^{\mathrm{T}} & \dots & \mathbf{s}_{(i)}^{\mathrm{T}} & \dots & \mathbf{s}_{(M)}^{\mathrm{T}} \end{bmatrix}^{\mathrm{T}},$$

$$\mathbf{w} = \begin{bmatrix} \mathbf{w}_{(1)}^{\mathrm{T}} & \dots & \mathbf{w}_{(i)}^{\mathrm{T}} & \dots & \mathbf{w}_{(M)}^{\mathrm{T}} \end{bmatrix}^{\mathrm{T}}.$$

Similarly, the power of the clutter returns at the i-th radar can be calculated as:

$$\mathbf{w}_{(i)}^{\mathrm{H}} \Big(\sum_{j=1}^{\mathrm{M}} \mathbf{\Psi}_{c,(j,i)} \Big) \mathbf{w}_{(i)},$$

where, as previously mentioned, $\mathbf{\Psi}_{c,(j,i)}$ is the covariance matrix of the clutter. Extending the work in [16] to the case of multiple radars, the received interference power can also be written as:

$$\mathbf{w}_{(i)}^{\mathrm{H}} \Big(\sum_{j=1}^{\mathrm{M}} \mathbf{\Psi}_{c,(j,i)} \Big) \mathbf{w}_{(i)} = \mathbf{w}_{(i)}^{\mathrm{H}} (\mathbf{\Psi}_{c,(i)}) \mathbf{w}_{(i)} = \mathbf{s}^{\mathrm{H}} (\mathbf{\Theta}_{c,(i)}^{*}) \mathbf{s},$$

where:

$$\mathbf{\Theta}_{c,(i)} = \mathrm{blkdiag}(\mathbf{\Theta}_{c,(1,i)}, \mathbf{\Theta}_{c,(2,i)}, \dots, \mathbf{\Theta}_{c,(M,i)}).$$

It is important to note that $\mathbf{\Psi}_{c,(i)}$ is a function of the waveforms transmitted by all radars $\mathbf{s}$, and $\mathbf{\Theta}_{c,(i)}$ is a function of the receiver filter $\mathbf{w}_{(i)}$. Both notations will be used as appropriate for quantifying the interference at the receiver of the radar. The denominator of the $\mathrm{SINR}_{(i)}$ can therefore be rewritten as:

$$\mathrm{tr}\Big(\mathbf{s}^{\mathrm{H}} \Big(\mathbf{\Theta}_{c,(i)}^{*} + \frac{\sigma_n^2}{M} \|\mathbf{w}_{(i)}\|^2 \mathbf{I} \Big) \mathbf{s} \Big) = \mathrm{tr}\big(\mathbf{s}^{\mathrm{H}} \mathbf{Z}_{(i)} \mathbf{s} \big). \tag{5.4}$$

Subsequently, the optimization function as well as the constraints needed for the convex optimization problem can be derived. By following the guidelines provided for the single radar scenario in [16], the numerator and denominator

of $\mathrm{SINR}_{(i)}$ can be reorganized in the form $\mathrm{tr}(\mathbf{Q}_{\mathrm{nR,(i)}}\mathbf{X})$ and $\mathrm{tr}(\mathbf{Q}_{\mathrm{dR,(i)}}\mathbf{X})$, where:

$$\mathbf{Q}_{\mathrm{nR,(i)}} = \begin{bmatrix} \mathbf{R}_{(i)} & \mathbf{0} \\ \mathbf{0} & 0 \end{bmatrix},$$

$$\mathbf{Q}_{\mathrm{dR,(i)}} = \begin{bmatrix} \mathbf{Z}_{(i)} & \mathbf{0} \\ \mathbf{0} & 0 \end{bmatrix},$$

$$\mathbf{X} = \begin{bmatrix} \mathbf{s}\mathbf{s}^{\mathrm{H}} & \mathbf{s}u^{*} \\ \mathbf{s}^{\mathrm{H}}u & |u|^{2} \end{bmatrix},$$

where u is a variable needed for the homogenized QCQP optimization. The orthogonality constraint can be written as $\mathrm{tr}(\mathbf{Q}_{\mathrm{orth,(j,i)}}\mathbf{X}) \leq \varrho$ and $\mathrm{tr}(\mathbf{Q}_{\mathrm{orth,(j,i)}}\mathbf{X}) \geq -\varrho$, where:

$$\mathbf{Q}_{\mathrm{orth,(j,i)}} = \begin{bmatrix} \mathbf{m}_{(i)}^{\mathrm{T}}\mathbf{J}_{(j,i,b_r)}^{\mathrm{T}}\mathbf{J}_{(j,i,b_r)}\mathbf{m}_{(j)} & \mathbf{0} \\ \mathbf{0} & 0 \end{bmatrix},$$

$$\mathbf{m}_{(i)} = \begin{bmatrix} \mathbf{0}_N(1) & \dots & \mathbf{I}_N(i) & \dots & \mathbf{0}_N(k) & \dots & \mathbf{0}_N(M) \end{bmatrix},$$

where $\mathbf{m}_{(i)}$ is a vector matrix of size $NN \times M$ that contains all zeros for the exception of an $N \times N$ identity matrix at matrix position i, with $i = 1 \dots M$. The unit norm constraint at the i-th radar is written as:

$$\mathrm{tr}(\mathbf{Q}_{\mathrm{pw,(i)}}\mathbf{X}) = 1, \quad \text{where} \quad \mathbf{Q}_{\mathrm{pw,(i)}} = \begin{bmatrix} \mathbf{m}_{(i)}^{\mathrm{H}}\mathbf{m}_{(i)} & \mathbf{0} \\ \mathbf{0} & 0 \end{bmatrix}.$$

The constraint on the deviation of the waveform from an initial waveform can be written as $\mathrm{tr}(\mathbf{Q}_{\mathrm{init,(i)}}\mathbf{X}) \leq 0$, where:

$$\mathbf{Q}_{\mathrm{init,(i)}} = \begin{bmatrix} \mathbf{m}_{(i)}^{\mathrm{H}}\mathbf{m}_{(i)} & -\mathbf{m}_{(i)}^{\mathrm{H}}\mathbf{m}_{(i)}\mathbf{s}_0 \\ -\mathbf{s}_0^{\mathrm{H}}\mathbf{m}_{(i)}^{\mathrm{H}}\mathbf{m}_{(i)} & \mathbf{s}_0^{\mathrm{H}}\mathbf{m}_{(i)}^{\mathrm{H}}\mathbf{m}_{(i)}\mathbf{s}_0 - \delta \end{bmatrix}.$$

Furthermore, the Charnes-Cooper variable transformation will be used similarly to the work in [49]:

$$\mathbf{Q}_{\mathrm{CC}} = \begin{bmatrix} \mathbf{0} & \mathbf{0} \\ \mathbf{0} & 1 \end{bmatrix}.$$

From this starting point, different optimization problems can be formulated.

5.2 Waveform Optimization Techniques based on Accumulated Power Maximization

This method aims at maximizing the accumulated target return signal power. This model, although easily extendable, is suitable for small networks with no specific target requirements. Due to this reason, the following section considers the case of two radars.

At first, two known codes with desired auto-correlation and cross-correlation properties that grant good range resolution while maintaining orthogonality between the two radars needs to be considered for initialization purposes. Exploiting these codes, the receiver filters can be calculated using generalized eigenvalue decomposition. Thanks to the receiver filter,

the received signal strength can be estimated as well as the received interference plus noise power. The SINR values calculated in Formulas (5.5) and (5.6) allow the determination of the codes with convex optimization techniques [18].

$$\begin{aligned}\mathrm{SINR}_1 &= \frac{\sigma_{11,T}^2|\mathbf{w}_1(\mathbf{s}_1 \odot \mathbf{p}(\nu_{11,T}))|^2 + \sigma_{21,T}^2|\mathbf{w}_1(\mathbf{s}_2 \odot \mathbf{p}(\nu_{21,T}))|^2}{\mathbf{w}_1^{\mathrm{H}}\mathbf{\Phi}_{c_1}\mathbf{w}_1 + \sigma_n^2\|\mathbf{w}_1\|^2} \\ &= \frac{\mathbf{w}_1^{\mathrm{H}}\Big(\sigma_{11,T}^2|\mathbf{s}_1 \odot \mathbf{p}(\nu_{11,T})|^2 + \sigma_{21,T}^2|\mathbf{s}_2 \odot \mathbf{p}(\nu_{21,T})|^2\Big)\mathbf{w}_1}{\mathbf{w}_1^{\mathrm{H}}\Big(\mathbf{\Phi}_{c_1} + \sigma_n^2\Big)\mathbf{w}_1}\end{aligned} \tag{5.5}$$

and

$$\begin{aligned}\mathrm{SINR}_2 &= \frac{\sigma_{22,T}^2|\mathbf{w}_2(\mathbf{s}_2 \odot \mathbf{p}(\nu_{22,T}))|^2 + \sigma_{12,T}^2|\mathbf{w}_2(\mathbf{s}_1 \odot \mathbf{p}(\nu_{12,T}))|^2}{\mathbf{w}_2^{\mathrm{H}}\mathbf{\Phi}_{c_2}\mathbf{w}_2 + \sigma_n^2\|\mathbf{w}_2\|^2} \\ &= \frac{\mathbf{w}_2^{\mathrm{H}}\Big(\sigma_{22,T}^2|\mathbf{s}_2 \odot \mathbf{p}(\nu_{22,T})|^2 + \sigma_{12,T}^2|\mathbf{s}_1 \odot \mathbf{p}(\nu_{12,T})|^2\Big)\mathbf{w}_2}{\mathbf{w}_2^{\mathrm{H}}\Big(\mathbf{\Phi}_{c_2} + \sigma_n^2\Big)\mathbf{w}_2}\end{aligned} \tag{5.6}$$

5.2.1 Orthogonal Codes Optimization

The optimization of the orthogonal codes is based on the maximization of the accumulated target return signal powers while keeping the disturbance power at both the radar receivers to unity.

$$\begin{aligned}\max \quad & \mathbf{S}_{\mathrm{pw},1} + \mathbf{S}_{\mathrm{pw},2} \\ \text{s.t.} \quad & \mathbf{IN}_{\mathrm{pw},1} + \mathbf{IN}_{\mathrm{pw},2} = 1 \\ & \mathbf{s}_1^{\mathrm{H}}\mathbf{J}_{\tilde{r}}\mathbf{s}_2 = 0 \\ & \|\mathbf{s}_1\|^2 = 1 \\ & \|\mathbf{s}_2\|^2 = 1 \\ & \|\mathbf{s}_1 - \mathbf{s}_{0,1}\|^2 \leq \delta \\ & \|\mathbf{s}_2 - \mathbf{s}_{0,2}\|^2 \leq \delta\end{aligned} \tag{5.7}$$

where the accumulated signal power at Radar-1 and Radar-2 is:

$$\begin{aligned}\mathbf{S}_{\text{pw},1} + \mathbf{S}_{\text{pw},2} =& \mathbf{s}_1^{\text{T}}(\alpha_{11}|\mathbf{w}_1^* \odot \mathbf{p}_{11}|^2)\mathbf{s}_1 + \mathbf{s}_2^{\text{T}}(\alpha_{21}|\mathbf{w}_1^* \odot \mathbf{p}_{21}|^2)\mathbf{s}_2 + \\ & \mathbf{s}_2^{\text{T}}(\alpha_{22}|\mathbf{w}_2^* \odot \mathbf{p}_{22}|^2)\mathbf{s}_2 + \mathbf{s}_1^{\text{T}}(\alpha_{12}|\mathbf{w}_2^* \odot \mathbf{p}_{12}|^2)\mathbf{s}_1\end{aligned} \tag{5.8}$$

and the sum of clutter and noise power at both receivers is:

$$\mathbf{IN}_{\text{pw},1} + \mathbf{IN}_{\text{pw},2} = \mathbf{s}_1^{\text{T}}\boldsymbol{\Theta}_{c,11}\mathbf{s}_1 + \mathbf{s}_2^{\text{T}}\boldsymbol{\Theta}_{c,21}\mathbf{s}_2 + \mathbf{s}_2^{\text{T}}\boldsymbol{\Theta}_{c,22}\mathbf{s}_2 + \mathbf{s}_1^{\text{T}}\boldsymbol{\Theta}_{c,12}\mathbf{s}_1 + 2\sigma_n^2 \tag{5.9}$$

where $\boldsymbol{\Theta}_{c,ij}$ accounts for the disturbance occurred due to clutter in the transmission of the waveform from radar j to radar i [8]. The optimization in (5.7) can be solved using SDP with rank relaxation.

5.2.2 Performance Analysis

In order to evaluate the performance of the proposed algorithm, a simulation has been carried out with the parameters as outlined in Table 5.1. The initial waveforms $\mathbf{s}_{0,1}$ and $\mathbf{s}_{0,2}$ are again fractional Fourier waveforms as developed in [83] and are characterized by very good auto-correlation and cross-correlation properties. These features allow good range resolution while maintaining orthogonality between the two radar waveforms. For solving the SDP problem, the CVX Matlab Software for Disciplined Convex Programming [74] has been used.

More specifically, the simulation tested the SINR evolution for both radars for different values of δ ($\delta = [0.1\ 0.25\ 0.5]$). Once the optimization was complete, the auto-ambiguity and cross-ambiguity functions were plotted.

As it can be seen in Figure 5.2, despite some minor oscillations due to the combined optimization of the two radars, the SINR converges. Simil-

Variable	Description	Value
N_c	Range Bins	7
L	Azimuth Bins	50
σ_n^2	Noise Variance	0.1
$\sigma_{11,T}^2$	Target RCS from R1 to R1	1.0671
$\sigma_{21,T}^2$	Target RCS from R2 to R1	1.1630
$\sigma_{22,T}^2$	Target RCS from R2 to R2	1.0717
$\sigma_{12,T}^2$	Target RCS from R1 to R2	0.8793
$\sigma_{11,c}^2$	Clutter RCS from R1 to R1	0.2227
$\sigma_{21,c}^2$	Clutter RCS from R2 to R1	0.2417
$\sigma_{22,c}^2$	Clutter RCS from R2 to R2	0.1856
$\sigma_{12,c}^2$	Clutter RCS from R1 to R2	0.1944
$\nu_{11,T}$	Target Doppler from R1 to R1	0.4467
$\nu_{21,T}$	Target Doppler from R2 to R1	0.3669
$\nu_{22,T}$	Target Doppler from R2 to R2	0.3993
$\nu_{12,T}$	Target Doppler from R1 to R2	0.3652
$\bar{\nu}_c$	Mean Clutter Doppler	0.01
ϵ	Clutter Doppler Uncertainty	0.4
ξ	Cycle Entering Condition	10^{-3}
N	Signal Length	64

Table 5.1: Simulation parameters for performance analysis for accumulated power maximization techniques.

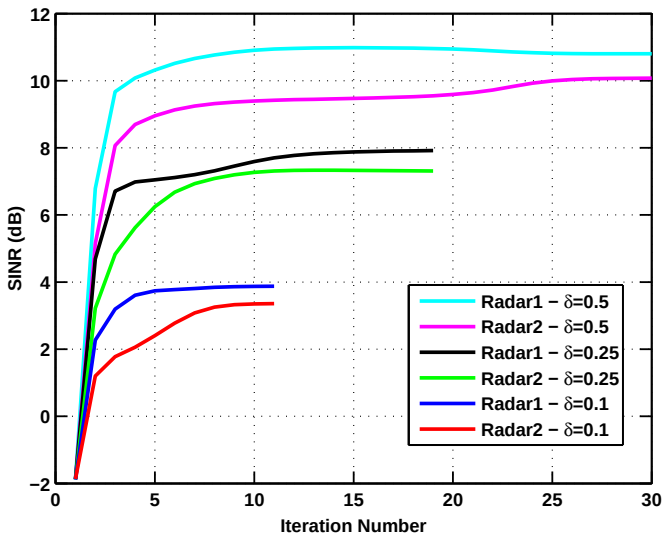

Figure 5.2: Performance analysis for accumulated power maximization techniques: SINR evolution of both radars for $\delta = [0.1 \;\; 0.25 \;\; 0.5]$.

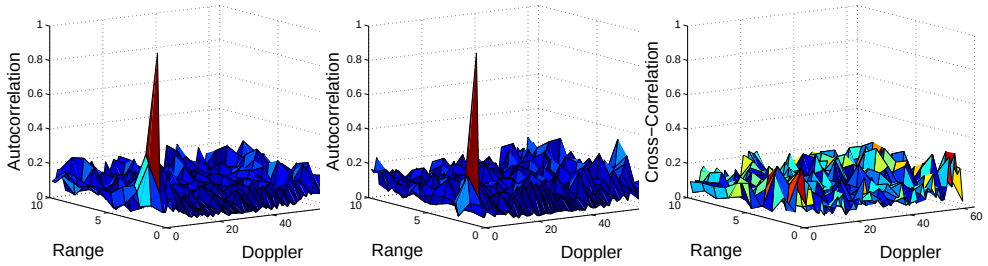

(a) AAF of s_1 (b) AAF of s_2 (c) CAF of s_1, s_2

Figure 5.3: Performance analysis for accumulated power maximization techniques: auto-ambiguity and cross-ambiguity functions for $\delta = 0.1$. The small δ value does not allow the waveforms to diverge from the initial waveform with ideal autocorrelation and cross-correlation properties. The estimated waveforms present very narrow autocorrelation peaks, proving their resolution in both range (τ) and Doppler (ν) domains. Their cross-correlation function shows no significant interference between the two waveforms.

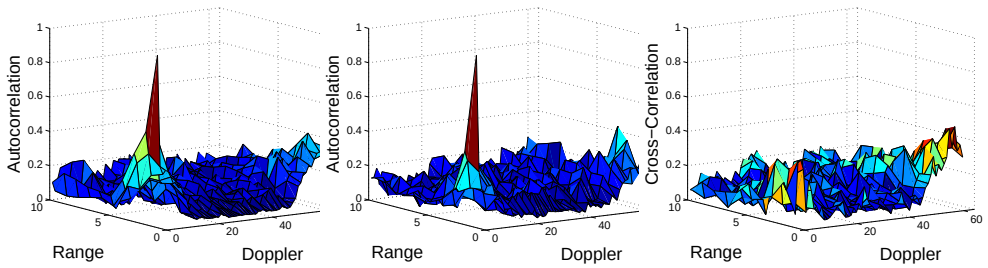

(a) AAF of s_1 (b) AAF of s_2 (c) CAF of s_1, s_2

Figure 5.4: Performance analysis for accumulated power maximization techniques: auto-ambiguity and cross-ambiguity functions for $\delta = 0.25$. The moderate δ value does not allow the waveforms to excessively diverge from the initial waveform with ideal autocorrelation and cross-correlation properties. The estimated waveforms still present narrow autocorrelation peaks. Their cross-correlation function shows only partial interference between the two waveforms.

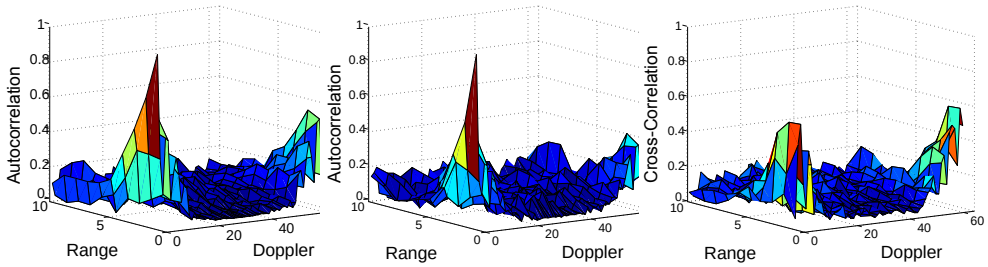

(a) AAF of s_1 (b) AAF of s_2 (c) CAF of s_1, s_2

Figure 5.5: Performance analysis for accumulated power maximization techniques: auto-ambiguity and cross-ambiguity functions for $\delta = 0.5$. The high δ value allows the waveforms to significantly diverge from the initial waveform with ideal autocorrelation and cross-correlation properties. The estimated waveforms do not present narrow autocorrelation peaks and their cross-correlation function shows interference between the two waveforms.

arly to the previous chapter, higher values of δ provide better SINR results. These gains are a consequence of the fact that bigger values of δ increase the feasibility set of the problem. Unlike the previous case, both radar have receiving capabilities and therefore in Figure 5.2 two SINR values can be seen for *each* value of δ. It needs to be reminded that, despite the apparently better results, bigger values of δ imply an increasing divergence from the initial assumptions, making these values only potential results rather than SINR that can be expected in reality. This fact can be well appreciated by looking at the deterioration in both the auto-ambiguity and cross-ambiguity functions in Figures 5.3, 5.4 and 5.5. It is clear from these results that the optimization goal is to enhance the SINR of the radars while keeping the δ value to an acceptable level.

5.2.3 Conclusions

This method provided satisfactory results in terms of SINR improvement for the joint optimization of both radars. Being rather generic, it does not allow freedom for specific choices such as imposing desired SINR values. However, due to its simple nature, this method requires less iterations than the subsequently discussed methods, making it efficient in terms of run time.

5.3 Waveform Optimization Techniques for a Cognitive Radar Network

The two waveform optimization methods described in this section are more sophisticated than the one described in Section 5.2. First of all, they can be applied to any number of radars and secondly, since they have specific

SINR requirements, the optimizations also have an "inner loop" so that the SINR_{min} can be iteratively optimized until it reaches the SINR_{target}. This aspect makes these methods ideal for systems with specific requirements or complicated environments but less applicable to systems with more stringent time efficiency requests.

5.3.1 Selective Optimization

Suppose that the goal SINR for all radars except Radar-i is SINR_{goal}. It is unlikely to achieve this value at the first iteration, as the initial waveforms and the receiver filters are not optimized enough to meet the goal. As the SINRs of the radars are expected to improve at every iteration, the algorithm should start by setting a small goal SINR, namely SINR_{min}, for the first iteration. As the iterations of the inner loop progress, this minimum goal is to be increased by a small constant amount Δ_{step} until the problem is infeasible or SINR_{min} reaches SINR_{goal}. The outline of this iterative optimization is described in Table 5.2. At each iteration, the waveforms are obtained using the following optimization problem:

$$
\begin{aligned}
\max_{\mathbf{X}} \quad & \text{tr}(\mathbf{Q}_{\text{nR,(i)}}\mathbf{X}) \\
\text{s.t.} \quad & \text{tr}(\mathbf{Q}_{\text{dR,(i)}}\mathbf{X}) = 1 \\
& \text{tr}(\mathbf{Q}_{\text{nR,(j)}}\mathbf{X}) - \text{SINR}_{\text{min}}\text{tr}(\mathbf{Q}_{\text{dR,(j)}}\mathbf{X}) \geq 0 \quad \forall j, \;\; j \neq i \\
& \text{tr}(\mathbf{Q}_{\text{orth,(j,i)}}\mathbf{X}) \geq -\varrho \text{u} \quad \forall i, j, \;\; j \neq i \\
& \text{tr}(\mathbf{Q}_{\text{orth,(j,i)}}\mathbf{X}) \leq \varrho \text{u} \quad \forall i, j, \;\; j \neq i \\
& \text{tr}(\mathbf{Q}_{\text{pw,(i)}}\mathbf{X}) = \text{u} \quad \forall i \\
& \text{tr}(\mathbf{Q}_{\text{init,(i)}}\mathbf{X}) \leq 0 \quad \forall i \\
& \text{tr}(\mathbf{Q}_{\text{CC}}\mathbf{X}) = \text{u} \\
& \mathbf{X} \succeq \mathbf{0}, \text{u} \geq 0
\end{aligned}
\tag{5.10}
$$

Initialization:

- Parameter Initialization:
  - $\text{SINR}_{iteration} = 0$;
  - *step* is set;
  - SINR_{goal} is set;
- Known waveform $\mathbf{s}(0)$ with desired features.

while $|\text{SINR}_1(t-1) - \text{SINR}_1(t)| > \zeta$

- Filter Optimization: as described in (5.2);
- Waveform Optimization: $\text{SINR}_{min} = \text{SINR}_{iteration}$;

  while ($feasible$ & $\text{SINR}_{min} \leq \text{SINR}_{goal}$)

  perform *cvx* with $\text{SINR}_{min} = \text{SINR}_{iteration}$ as described in (5.10);

  if $feasible = 0$
  $\mathbf{s} = \mathbf{s}(t-1)$
  else
  $\text{SINR}_{iteration} = \text{SINR}_{iteration} + step.$
  end

  end

  $\text{SINR}_{iteration} = \text{SINR}_{iteration} - step.$

end

Table 5.2: Outline of the optimization method from a simulation-oriented perspective. *feasible* is a parameter that is set to one as long as the SDP provides defined numerical results and t is the iteration number.

Once the waveforms are obtained in this inner loop iteration process, the code goes back to the outer loop and the receiver filter is optimized as described in Section 5.1.1, the SINR_{min} is increased of the value Δ_{step} and the optimization in (5.10) is repeated until feasible. It needs to be noted that a problem that becomes infeasible in the inner loop for a specific SINR_{min} might provide again valid results after the filter optimization is performed in the outer loop. The specific steps involved in the optimization are summarized as follows:

1. Initialize the minimum SINR that the Radar-j need to achieve: $\text{SINR}_{min} = 0$;

2. **while** (the SDP provides defined numerical results *and* $\text{SINR}_{min} \leq \text{SINR}_{goal}$):

   2.1) Solve the SDP problem in (5.10) with the current value of SINR_{min};

   2.2) Check if the variables assumed undefined numerical results:

   - If YES: Reassign to the waveform the same value it had at the previous cycle;
   - If NO: Increase the value of SINR_{min} of a desired constant Δ_{step} and go back to step 2.

5.3.2 Max-Min Optimization

The second optimization technique is based on iteratively increasing the value of SINR_{min} at all radars until the problem becomes unfeasible:

$$\begin{aligned}
\min \quad & \mathrm{z} \\
\text{s.t.} \quad & \mathrm{tr}(\mathbf{Q}_{\mathrm{nR,(i)}}\mathbf{X}) - \mathrm{SINR}_{\mathrm{min}}\mathrm{tr}(\mathbf{Q}_{\mathrm{dR,(i)}}\mathbf{X}) \geq 0 \quad \forall i \\
& \mathrm{tr}(\mathbf{Q}_{\mathrm{orth,(i,j)}}\mathbf{X}) \geq -\varrho \mathrm{u} \quad \forall i,j, \quad j \neq i \\
& \mathrm{tr}(\mathbf{Q}_{\mathrm{orth,(i,j)}}\mathbf{X}) \leq \varrho \mathrm{u} \quad \forall i,j, \quad j \neq i \\
& \mathrm{tr}(\mathbf{Q}_{\mathrm{pw,(i)}}\mathbf{X}) = \mathrm{u} \quad \forall i \\
& \mathrm{tr}(\mathbf{Q}_{\mathrm{init,(i)}}\mathbf{X}) \leq 0 \quad \forall i \\
& \mathrm{tr}(\mathbf{Q}_{\mathrm{CC}}\mathbf{X}) = \mathrm{u} \\
& \mathbf{X} \succeq \mathbf{0}, \mathrm{u} \geq 0, \mathrm{z} \geq 0
\end{aligned} \tag{5.11}$$

The only difference between the optimizations in (5.10) and (5.11) is that instead of maximizing the SINR of Radar-i, all radar SINRs are maximized equally. Otherwise, the optimization procedure remains as described for (5.10): a number of iterations in both the inner and outer loops is required so that the transmitted waveforms and receiver filters are optimized together by a controlled increase of SINR_{min}. Due to the strong similarities in the method, the process will not be further specified and the reader should refer to Table 5.2 and to the step-by-step description in the previous Section 5.3.1.

5.3.3 Performance Analysis

To evaluate the performance of the proposed algorithms, both optimization techniques have been tested for the case of two radars ($M = 2$). The initial waveforms $\mathbf{s}_{0,1}$ and $\mathbf{s}_{0,2}$ are fractional Fourier waveforms of length $N = 64$ as developed in [83]. These initial waveforms provide very good

auto-correlation and cross-correlation properties (refer back to Figure 1.2) granting therefore good range resolution while maintaining orthogonality between the two radar waveforms. The number of range rings that interfere with the range-azimuth bin of interest is $N_c = 7$. The number of azimuth cells in each ring is $L = 50$. As for the parameters of the target, these are generated randomly for each simulation and generated in line with the RCS clutter models in [16]. The various radar cross-sections generated during this simulation are $\sigma^2_{11,T} = 1.0671$, $\sigma^2_{21,T} = 1.1630$, $\sigma^2_{22,T} = 1.0717$ and $\sigma^2_{12,T} = 0.8793$. The target doppler values are set to $\nu_{11,T} = 0.4467$, $\nu_{21,T} = 0.3669$, $\nu_{22,T} = 0.3993$ and $\nu_{12,T} = 0.3652$. The clutter power in each bin is $\sigma^2_{11,c} = 0.2227$, $\sigma^2_{21,c} = 0.2417$, $\sigma^2_{22,c} = 0.1856$, $\sigma^2_{12,c} = 0.1944$. The noise variance was set to $\sigma^2_n = 0.1$, the mean doppler frequency to $\bar{\nu}_c = 0.01$ and its uncertainty to $\epsilon = 0.4$. Finally, the maximum deviation to the initial waveform was set to $\delta = 0.1$ and the orthogonality threshold to $\varrho = 0.05$. For solving the SDP problem, the CVX Matlab Software for Disciplined Convex Programming [74] was again used. In the simulation, both the selective optimization as well as the max-min optimization are tested. In both cases the SINR_{min} is increased iteratively by a step of value $\Delta_{step} = 0.1$.

Initially, the selective optimization has been tested. Radar-1 was selected as privileged radar (i.e. the one for which the SINR will be maximized as objective function of the optimization problem). Radar-2 needs to achieve a specific SINR goal. In order to prove the validity of the algorithm, the achievable SINR_1 value at Radar-1 for a set of goal SINR at Radar-2 ranging from 1dB to 5dB has been estimated. More specifically, the SINR_2 achieved at the end of the Δ_{step}-incrementing process has been plotted against the SINR_1 obtained at the end of the iterative process. As seen in Figure 5.6, a lower goal SINR_2 can push up the achievable values of SINR_1 whereas a high

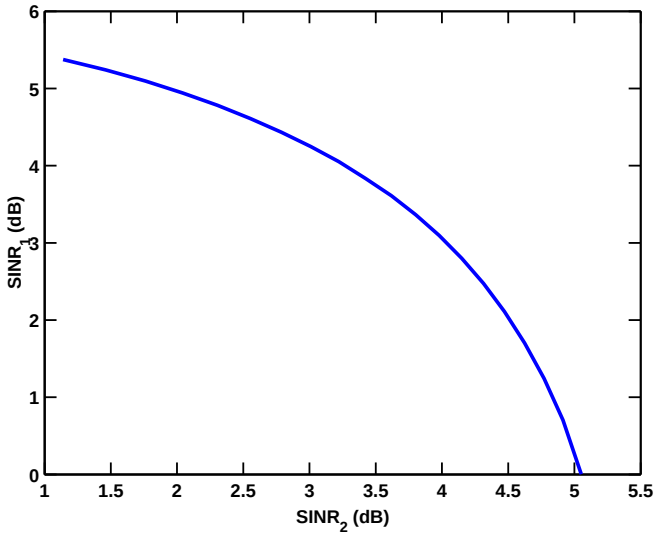

Figure 5.6: Selective optimization: achievable $SINR_1$ versus minimum $SINR_2$. As it can be seen, a lower goal $SINR_2$ can push up the achievable values of $SINR_1$ whereas a high goal $SINR_2$ will exhaust all the degrees of freedom for Radar-1 to optimize its SINR. This proves the effectiveness of the algorithm in allowing a specific radar to obtain desired SINR values.

goal $SINR_2$ will exhaust all the degrees of freedom for Radar-1 to optimize its SINR. This proves the effectiveness of the algorithm in allowing a specific radar to obtain desired SINR values.

In order to test the max-min optimization, the SINR evolution during the iterations of the optimization process for both radars has been estimated and plotted. As seen in Figure 5.7, the initial SINR before the iteration starts is -1.87dB. This corresponds to the SINR achieved with the initial waveform and the corresponding optimum receiver filter. However, as the iteration progresses, the SINR is increased to 3.15dB. This SINR value corresponds to the optimum waveform and receiver filter. In the first optimization scheme, Radar-1 achieves an SINR of 5.37dB for an SINR value of 1.14dB for Radar-2. In the max-min optimization case, the SINR values are almost equal, i.e. 3.07dB and 3.15dB, as requested by the optimization. Despite this significant SINR increase, by comparing the AAF and CAF

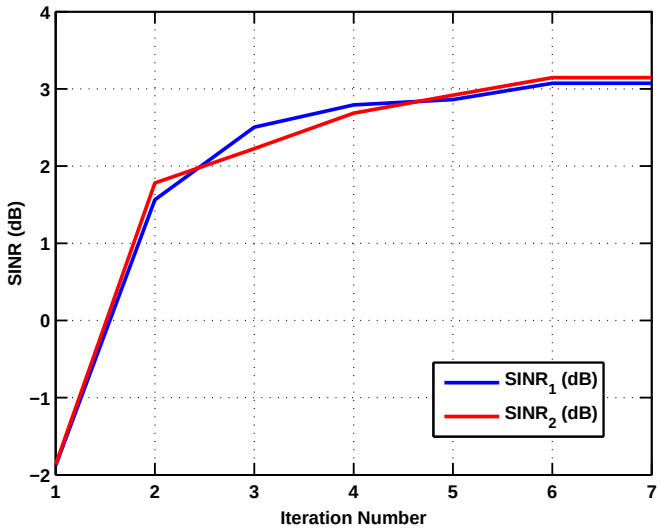

Figure 5.7: Max-min optimization: SINR evolution of both Radar-1 and Radar-2. As it can be seen, the initial SINR (i.e. before the optimizing iterations) is -1.87dB. This corresponds to the SINR achieved with the initial waveform and the corresponding optimum receiver filter. However, as the iteration progresses, the SINR is increased (step by step) to 3.15dB. This SINR value corresponds to the optimum waveform and receiver filter. In the max-min optimization, as by design specifications, the SINR values are almost equal for the two radars, i.e. 3.07dB and 3.15dB.

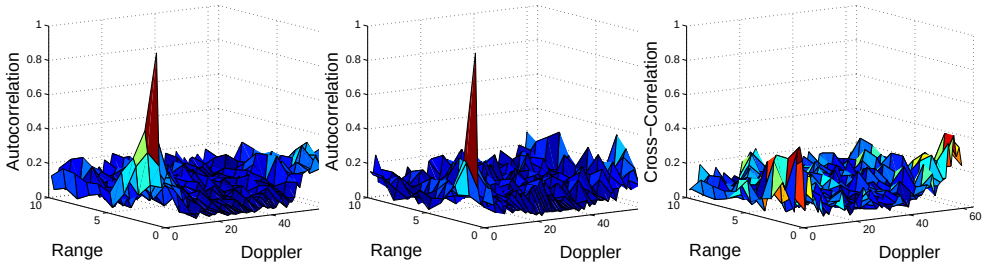

(a) AAF of s_1 (b) AAF of s_2 (c) CAF of s_1, s_2

Figure 5.8: Auto-ambiguity function (AAF) and cross-ambiguity function (CAF) after max-min optimization techniques. The estimated waveforms perform better in the environment under investigation and provide a 5dB SINR increase with respect to the initial waveforms. As it can be seen in the figures, the estimated waveforms still present narrow autocorrelation peaks, proving their resolution in both range (τ) and Doppler (ν) domains. Furthermore, their cross-correlation function shows limited interference between the two waveforms.

of the initial waveforms (please refer back to Figure 1.2 if needed) and the AAF and CAF of the optimized waveforms in Figure 5.8, it can be noted how the auto-correlation and cross-correlation functions still maintain the desired characteristics.

These results show how an adaptable optimization process can be designed. This flexibility, used in combination with the knowledge of the environment inherent of cognitive radars can provide great advantages: radars with bad channels could be set to very low goal SINR values so that the optimization process could focus on better channels whereas radars in uniform environments could be optimized equally.

5.3.4 Conclusions

In this section two waveform design methods have been proposed. The first one optimizes the signal strength at a desired radar while keeping the SINR of the remaining radars at an acceptable level. The second one optimizes

the SINR of all radars equally. The derived formulations of the signal's strength as well as the interference and noise power for the case of multiple radars with both transmission and reception capabilities proved to be effective in a simulated environment. The developed methods allow great flexibility in terms of SINR maximization as they can be utilized both for application that require uniformity and for those that need to maximize the signal strength at a specific radar. These methods, that exploit features of both cognition and MIMO radars, have great potential for applications in complex environments.

5.4 Conclusions

This chapter discussed different waveform optimization techniques for cognitive radar networks. The three proposed methods have peculiarities that make them ideal for different scenarios and therefore constitute a rather comprehensive framework for cognitive radar techniques.

In Section 5.2 a basic method aimed at maximizing the accumulated target return signal power was introduced. This method is applicable to small networks with no specific target requirements. Simulation results proved how this method is effective in terms of SINR improvement and number of iterations. On the other hand, it does not allow any design freedom (i.e. target SINR requirements).

In Section 5.3 two different optimization techniques have been proposed. Both optimizations can be applied to any number of radars and allow the user to impose desired SINR requirements. These methods are ideal for systems with specific targets or complicated environments but, due to the fact that they require an additional inner loop, they are less applicable to

systems with more stringent time efficiency requests. More specifically, the first algorithm optimizes the signal strength at a desired radar while keeping the SINR of the remaining radars at an acceptable level. The second one optimizes the SINR of all radars equally. Both proved to be effective in terms of SINR improvement.

Chapter 6

Robust Optimization Techniques

In this chapter, various robust optimization techniques for coordinated cognitive radar networks are presented. In a traditional adaptive array setting, the interference plus noise covariance matrix is not known a priori and needs to be estimated thanks to a training signal. Estimation of the covariance matrix would normally require that the signal component reflected on a target is absent during the estimation of the statistical parameters of the interference and noise. If this was not the case, the system would incur in a signal cancelation phenomenon which would lead to severely degraded performance. Additionally, mismatches may occur because of a limited number of data snapshots that are used to estimate the covariance matrix, environmental nonstationarities (such as rapid motion of the interferers), signal location errors, antenna motion and/or vibration and so on. As a result, such techniques can become severely degraded in scenarios when the exploited assumptions on the environment, antenna array and/or sources are wrong or inaccurate [84]. In the case of cognitive radars, it is also possible to

estimate the covariance matrix thanks to a priori information such as previous radar experiences or access to land cover databases. Nevertheless, errors in the available information will result in significant optimization errors. As a consequence, it is of primary importance to ensure that the waveform optimization techniques described in Chapter 5 are robust against uncertainty on the covariance matrix or on other parameters.

In this work three different robust optimization techniques will be proposed. The first two techniques employ traditional worst-case optimization and probabilistic (stochastic) optimization, respectively. Both methods are used for robust radar waveform design in the presence of uncertainty on the clutter-plus-noise covariance matrix. The third technique considers a novel approach where uncertainty is assumed directly on the radar cross-section and the Doppler of the clutter rather than on the clutter-plus-noise covariance matrix. The latter is solved using Taylor approximations and stochastic optimization. This work was published in [85].

The present chapter is organized as follows. At first an introduction on the topic of robust and stochastic optimization techniques is presented. In Section 6.2, the mathematics for the worst-case performance optimization techniques is presented, followed by the description in Section 6.3 of the equations necessary for stochastic optimization techniques. Section 6.4 introduces a novel approach for clutter-specific stochastic optimization for the case of signal-dependent clutter. The final two sections provide the simulation results of the three methods and some comparison between the different techniques, followed by concluding remarks.

6.1 Introduction

In cognitive radars second order statistics are assumed to be known thanks to external databases or previous experiences. Methods for the estimation of the required covariance matrices through training sequences are also available (an example could be the work in [86]). In practical scenarios, though, these values may not be correct and the performance degradation may become even more pronounced because the optimization techniques are based on the assumption of an accurate knowledge of the array response to the desired signal. Moreover, these methods often use quite restrictive assumptions on the environment and interferences, for example they assume that the received array data are stationary and/or that the interferers can be described using a low-rank model.

The sequential filter-waveform design optimization described in the model in the optimization problem in (5.10) defined in Section 5.3.1 assumes perfect knowledge of the second order statistics of both the signal-dependent clutter and the additive noise. This scenario is not always practically feasible or realistic, especially in a non-stationary case where the interfering sources move rapidly and the system may not be able to adapt fast enough to compensate for this motion. It is therefore important to take into account the mismatch between actual and presumed values of the covariance matrix.

In order to tackle the problem of optimization affected by parameter uncertainty, two main approaches can be undertaken. The first one is robust or worst-case optimization and the second one is stochastic optimization. In the first technique the uncertainty model is deterministic and set-based whereas in the latter case the uncertainty has a probabilistic description. Both robust methods were applied to the selective optimization described in

Section 5.3.1.

6.2 Worst-Case Optimization Techniques

In this section a worst-case robust optimization technique that assumes uncertainty in the clutter plus noise covariance matrix is outlined. In a worst-case robust optimization model the decision maker constructs a solution that is feasible for any realization of the uncertainty in a given set. This formulation is inherently that of a max-min problem and is the most rigorous approach to account for the mismatch [87].

This work is based on the optimization of the SINR at Radar-i whilst satisfying a specific SINR_{goal} for all Radar-j with $j \neq i$. However, in the presence of an error on the estimate of the clutter plus noise covariance matrix, it will not always be possible to achieve the desired SINR_{goal} due to the mismatch between the real covariance matrix and the assumed covariance matrix for the clutter plus noise. In order to describe the robust approach, the estimate of the covariance matrix $\mathbf{Q}_{dR,(j)}$ in the optimization problem in (5.10) is assumed to have an error as follows:

$$\tilde{\mathbf{Z}}_{(i)} = \mathbf{Z}_{(i)} + \Delta_{\beta},$$

where, with reference to Equation (5.4), $\mathbf{Z}_{(i)}$ is the presumed interference plus noise covariance matrix and $\tilde{\mathbf{Z}}_{(i)}$ denotes its actual value. The subscript β in the error matrix Δ_{β} indicates that the mismatch between the expected and received covariance matrix is bounded through the constant value β in the Frobenius norm:

$$||\Delta_{\beta}||_{\mathcal{F}} \leq \beta.$$

The denominator of SINR_i can be rewritten as:

$$\text{tr}\big(\mathbf{s}^{\text{H}}(\mathbf{Z}_{(i)} + \Delta_\beta)\mathbf{s}\big). \tag{6.1}$$

The robust worst-case optimization problem is consequently formulated as:

$$\max_{\mathbf{s}} \max_{||\Delta_\beta||_{\mathcal{F}} \leq \beta} \text{tr}\big(\mathbf{s}^{\text{H}}(\mathbf{Z}_{(i)} + \Delta_\beta)\mathbf{s}\big). \tag{6.2}$$

This can be modified in the following well-known equivalent formulation thanks to the Lagrangian multipliers method [84], [50]:

$$\max_{\mathbf{s}} \text{tr}\big(\mathbf{s}^{\text{H}}(\mathbf{Z}_{(i)} + \beta\mathbf{I})\mathbf{s}\big). \tag{6.3}$$

The final robust waveform optimization problem can be expressed as the one in (5.10) but modifying the constraint on the Radar-j as:

$$\text{tr}(\mathbf{Q}_{\text{nR,(j)}}\mathbf{X}) - \text{SINR}_{\text{min}}\text{tr}(\tilde{\mathbf{Q}}_{\text{dR,(j)}}\mathbf{X}) \geq 0 \quad \forall j, \;\; j \neq i, \tag{6.4}$$

where $\tilde{\mathbf{Q}}_{\text{dR,i}} = \begin{bmatrix} \mathbf{Z}_{(i)} + \beta\mathbf{I} & \mathbf{0} \\ \mathbf{0} & 0 \end{bmatrix}$.

The final robust waveform optimization problem can be expressed as the convex optimization problem (5.10) by modifying the constraint on the Radar-j

as:

$$\begin{aligned}
\max_{\mathbf{X}} \quad & \mathrm{tr}(\mathbf{Q}_{\mathrm{nR,i}}\mathbf{X}) \\
\text{s.t.} \quad & \mathrm{tr}(\mathbf{Q}_{\mathrm{dR,i}}\mathbf{X}) = 1 \\
& \mathrm{tr}(\mathbf{Q}_{\mathrm{nR,j}}\mathbf{X}) - \mathrm{SINR}_{\min}\mathrm{tr}(\tilde{\mathbf{Q}}_{\mathrm{dR,j}}\mathbf{X}) \geq 0 \quad \forall j, \ \ j \neq i \\
& \mathrm{tr}(\mathbf{Q}_{\mathrm{orth,ij}}\mathbf{X}) \geq -\varrho \mathrm{u} \quad \forall i, j, \ \ j \neq i \\
& \mathrm{tr}(\mathbf{Q}_{\mathrm{orth,ij}}\mathbf{X}) \leq \varrho \mathrm{u} \quad \forall i, j, \ \ j \neq i \\
& \mathrm{tr}(\mathbf{Q}_{\mathrm{pw,i}}\mathbf{X}) = \mathrm{u} \quad \forall i \\
& \mathrm{tr}(\mathbf{Q}_{\mathrm{init,i}}\mathbf{X}) \leq 0 \quad \forall i \\
& \mathrm{tr}(\mathbf{Q}_{\mathrm{CC}}\mathbf{X}) = \mathrm{u} \\
& \mathbf{X} \succeq \mathbf{0}, \mathrm{u} \geq 0
\end{aligned} \tag{6.5}$$

where $\tilde{\mathbf{Q}}_{\mathrm{dR,i}} = \begin{bmatrix} \tilde{\mathbf{Z}}_i & \mathbf{0} \\ \mathbf{0} & 0 \end{bmatrix}$.
The iterative optimization process is the same as described in Chapter 5 and, more specifically, in Table 5.2.

6.3 Stochastic Optimization Techniques

The problem associated with worst-case optimization techniques is that they result in overly-conservative methods as they aim at satisfying the SINR for worst-case errors. For this reason, most of the time the achieved SINR is much greater than the required SINR. By utilizing statistical knowledge of the error of the covariance matrix, it is possible to achieve robustness against the uncertainty with a certain outage probability [53]. As the RCS and Doppler values change randomly, it is more efficient to exploit the statistical nature of these errors.

The SINR constraints in the optimization be reformulated as:

$$P_{(j)} = \Pr\left(\frac{\mathrm{tr}\big(\mathbf{s}^{\mathrm{H}}\mathbf{R}_{(j)}\mathbf{s}\big)}{\mathrm{tr}\big(\mathbf{s}^{\mathrm{H}}\big(\mathbf{Z}_{(j)} + \mathbf{E}_{(j)}\big)\mathbf{s}\big)} \geq \mathrm{SINR}_{goal} \right), \tag{6.6}$$

with $P_{(j)} \geq p_{(j)}$, $j \neq i$. Similarly to Section 6.2, uncertainty should be considered only at those radars with specific SINR requirements. $P_{(j)}$ defines the probability that the jth user achieves the required SINR_{goal} and $p_{(j)}$ is a preselected threshold value. In (6.6), $\Pr(\cdot)$ identifies the probability operator and $\mathbf{E}_{(j)}$ is the error matrix. $\mathbf{E}_{(j)}$ is a block diagonal matrix (as is $\mathbf{Z}_{(j)}$) where each of the inner matrices has been modeled as a Hermitian matrix whose elements are taken from the distribution $\mathcal{CN}(0, \sigma^2_{e_{(j)}})$, where $\mathcal{CN}(\mu, \sigma^2)$ identifies a complex normal distribution characterized by a mean μ and a variance σ^2. Naming $\mathbf{S} = \mathbf{s}\mathbf{s}^{\mathrm{H}}$, the variance of $\mathrm{tr}(\mathbf{E}_{(j)}\mathbf{S})$ can be therefore calculated as:

$$\begin{aligned} \mathbb{E}\{\mathrm{tr}(\mathbf{E}_{(j)}\mathbf{S})\mathrm{tr}(\mathbf{E}_{(j)}\mathbf{S})^*\} &= \sum_{q=0}^{\text{M-1}} \sum_{l=1}^{\text{N}} \sum_{m=1}^{\text{N}} \sigma^2_{e_{(j)}} \mathbf{S}^2_{l+qM,m+qM} \\ &= \sigma^2_{e_{(j)}}[\mathrm{tr}(\mathbf{S}_1\mathbf{S}_1^{\mathrm{H}}) + \cdots + \mathrm{tr}(\mathbf{S}_M\mathbf{S}_M^{\mathrm{H}})] \\ &= M\sigma^2_{e_{(j)}}, \end{aligned} \tag{6.7}$$

where (l, m) identifies the matrix cell. (6.6) can be reformulated as:

$$P_{(j)} = \Pr\Big(\mathrm{tr}\big((\mathbf{Z}_{(j)} + \mathbf{E}_{(j)})\mathbf{S}\big) \leq \gamma_{(j)}\Big), \tag{6.8}$$

where:

$$\gamma_{(j)} = \frac{\mathrm{tr}(\mathbf{R}_{(j)}\mathbf{S})}{\mathrm{SINR}_{goal}}, \quad \text{and} \quad \mathbf{S} = \mathbf{s}\mathbf{s}^{\mathrm{H}}.$$

It is now possible to define the random variable $y_{(j)} = \mathrm{tr}\big((\mathbf{Z}_{(j)} + \mathbf{E}_{(j)})\mathbf{S}\big)$. This is a real variable because both $\mathbf{Z}_{(j)} + \mathbf{E}_{(j)}$ and $\mathbf{S}$ are Hermitian and, as

by Lemma 1 in [53], is assumed to have the probability distribution $y_{(j)} \sim \mathcal{N}\big(\mathrm{tr}(\mathbf{Z}_{(j)}\mathbf{S}), M\sigma^2_{e_{(j)}}\big)$. The probability of achieving the required SINR_{goal} is therefore calculated as:

$$P_{(j)} = \int_{-\infty}^{\gamma_{(j)}} \frac{1}{\sqrt{2\pi}\sigma_{e_{(j)}}\sqrt{M}} \exp\bigg(-\frac{(y_{(j)}-\mu_{(j)})^2}{2\sigma^2_{e_{(j)}}M}\bigg)\mathrm{d}y, \tag{6.9}$$

where $\mu_{(j)} = \mathrm{tr}(\mathbf{Z}_{(j)}\mathbf{S})$. Using the error function $\mathrm{erf}(\cdot)$ solution of the Gaussian integral, (6.9) can be rewritten as:

$$P_{(j)} = \frac{1}{2} + \frac{1}{2}\mathrm{erf}\bigg(\frac{\gamma_{(j)}-\mu_{(j)}}{\sqrt{2}\sigma_{e_{(j)}}\sqrt{M}}\bigg) \geq p_{(j)}, \tag{6.10}$$

hence,

$$\gamma_{(j)} - \mu_{(j)} \geq \mathrm{erf}^{-1}(2p_{(j)}-1)\sqrt{2}\sigma_{e_{(j)}}\sqrt{M}.$$

Equivalently:

$$\frac{\mathrm{tr}(\mathbf{R}_{(j)}\mathbf{S})}{\mathrm{SINR}_{min}} - \mathrm{tr}(\mathbf{Z}_{(j)}\mathbf{S}) \geq \delta_{e_{(j)}}, \tag{6.11}$$

where

$$\delta_{e_{(j)}} = \mathrm{erf}^{-1}(2p_{(j)}-1)\sqrt{2}\sigma_{e_{(j)}}\sqrt{M}, \tag{6.12}$$

and $||\mathbf{S}|| = ||\mathbf{s}\mathbf{s}^{\mathrm{H}}|| = \mathrm{tr}(\mathbf{s}\mathbf{s}^{\mathrm{H}}) = M$ since $\mathbf{s}$ is a vector containing the M radar waveforms. Writing the condition for stochastic robustness so that it is more convenient in light of the SDP formulation:

$$\mathrm{tr}(\mathbf{R}_{(j)}\mathbf{S}) - \mathrm{SINR}_{min}\mathrm{tr}\bigg(\Big(\mathbf{Z}_{(j)} + \frac{\delta_{e_{(j)}}}{\mathrm{tr}(\mathbf{S})}\Big)\mathbf{S}\bigg) \geq 0,$$

leads to the convex optimization problem constraint:

$$\mathrm{tr}(\mathbf{Q}_{\mathrm{nR,(j)}}\mathbf{X}) - \mathrm{SINR}_{\mathrm{min}}\mathrm{tr}(\tilde{\mathbf{Q}}_{\mathrm{dR,(j)}}\mathbf{X}) \geq 0 \quad \forall j, \;\; j \neq i, \tag{6.13}$$

where $\tilde{\mathbf{Q}}_{\mathrm{dR,(j)}} = \begin{bmatrix} \mathbf{Z}_{(j)} + \frac{\delta_{e_{(j)}}}{\mathrm{tr}(\mathbf{S})}\mathbf{I} & \mathbf{0} \\ \mathbf{0} & 0 \end{bmatrix}$, and δ_{e_j} is as described in Equation 6.12. Therefore the final robust waveform optimization problem in convex form is again:

$$
\begin{aligned}
\max_{\mathbf{X},u} \quad & \mathrm{tr}(\mathbf{Q}_{\mathrm{nR,(i)}}\mathbf{X}) \\
\text{s.t.} \quad & \mathrm{tr}(\mathbf{Q}_{\mathrm{dR,(i)}}\mathbf{X}) = 1 \\
& \mathrm{tr}(\mathbf{Q}_{\mathrm{nR,(j)}}\mathbf{X}) - \mathrm{SINR}_{\min}\mathrm{tr}(\tilde{\mathbf{Q}}_{\mathrm{dR,(j)}}\mathbf{X}) \geq 0 \quad \forall j, \;\; j \neq i \\
& \mathrm{tr}(\mathbf{Q}_{\mathrm{orth,(i,j)}}\mathbf{X}) \geq -\varrho \mathrm{u} \quad \forall i,j, \;\; j \neq i \\
& \mathrm{tr}(\mathbf{Q}_{\mathrm{orth,(i,j)}}\mathbf{X}) \leq \varrho \mathrm{u} \quad \forall i,j, \;\; j \neq i \\
& \mathrm{tr}(\mathbf{Q}_{\mathrm{pw,(i)}}\mathbf{X}) = \mathrm{u} \quad \forall i \\
& \mathrm{tr}(\mathbf{Q}_{\mathrm{init,(i)}}\mathbf{X}) \leq 0 \quad \forall i \\
& \mathrm{tr}(\mathbf{Q}_{\mathrm{CC}}\mathbf{X}) = \mathrm{u} \\
& \mathbf{X} \succeq \mathbf{0}, \mathrm{u} \geq 0
\end{aligned}
\tag{6.14}
$$

The iterative optimization process is the same as described in Chapter 5 and, more specifically, in Table 5.2.

6.4 Clutter-Specific Stochastic Optimization

The methods described so far are applicable to uncertainties introduced directly to the clutter-plus-noise covariance matrix, hence they are very generic and over-conservative. In most cases, the covariance matrix will be constructed using the estimates of the underlying parameters of the clutter such as radar cross-section and Doppler. Hence, in order to prove the validity of the previous models as well as to investigate new optimization techniques aimed at guaranteeing enhanced accuracy, a clutter parameter-specific stochastic optimization is proposed. The clutter covariance matrix is a function of the

RCS and Doppler of the clutter. Hence in the presence of uncertainty, this can be expressed for radar i as:

$$\begin{aligned}\mathbf{\Theta}_{c,\mathrm{rob},(i)} = &\sum_{j=1}^{\mathrm{M}}\sum_{b=0}^{\mathrm{B}}\Big((\sigma^2_{c,(j,i,b)} + \varepsilon_{RCS,(j,i,b)})\times \\ &\mathrm{diag}\{\mathbf{J}^{\mathrm{T}}_{(j,i,b_r)}\mathbf{w}^*_{(i)}\}\mathbf{\Phi}_{\epsilon,\mathrm{rob},(j,i,b)}\mathrm{diag}\{\mathbf{J}^{\mathrm{T}}_{(j,i,b_r)}\mathbf{w}_{(i)}\}\Big),\end{aligned} \tag{6.15}$$

with $i = 1, 2, \ldots M$ and where the matrix accounting for the Doppler shift is:

$$\mathbf{\Phi}_{\epsilon,\mathrm{rob},(j,i,b)}(l,m) = \mathrm{e}^{j2\pi\bar{\nu}_{(j,i,b)}(l-m)}\frac{\sin[\pi(\epsilon_{(j,i,b)} + \varepsilon_{\nu,(j,i,b)})(l-m)]}{[\pi(\epsilon_{(j,i,b)} + \varepsilon_{\nu,(j,i,b)})(l-m)]}, \tag{6.16}$$

and:

- $\varepsilon_{RCS,(j,i,b)} \sim \mathcal{CN}(0, \sigma^2_{\varepsilon_{RCS,(j,i,b)}})$ defines the statistics of the uncertainty on the radar cross-section;
- $\varepsilon_{\nu,(j,i,b)} \sim \mathcal{CN}(0, \sigma^2_{\varepsilon_{\nu,(j,i,b)}})$ provides the statistics associated to the uncertainty on the Doppler interval.

For notational convenience the subscript (i) will be hereafter omitted. The reader will therefore need to keep in mind that all of the following equations refer to a receiving/transmitting radar (i) even if not directly specified.
In order to develop robust optimization techniques, the elements of the matrix $\mathbf{\Phi}_{\epsilon,\mathrm{rob}}$ have been expanded using Taylor series as a function of the error

$$\begin{aligned}\tilde{\mathbf{\Theta}}_{c,rob,(i)} =& \sum_{j=1}^{\mathrm{M}}\sum_{b=1}^{\mathrm{B}} \sigma^2_{c,(j,i,b)}\mathrm{diag}\{\mathbf{J}^{\mathrm{T}}_{(j,i,b_r)}\mathbf{w}^*_{(i)}\}\mathbf{\Phi}_{\epsilon,(j,i,b)}\mathrm{diag}\{\mathbf{J}^{\mathrm{T}}_{(j,i,b_r)}\mathbf{w}_{(i)}\} + \\ & \sum_{j=1}^{\mathrm{M}}\sum_{b=1}^{\mathrm{B}} \varepsilon_{RCS,(j,i,b)}\mathrm{diag}\{\mathbf{J}^{\mathrm{T}}_{(j,i,b_r)}\mathbf{w}^*_{(i)}\}\mathbf{\Phi}_{\epsilon,(j,i,b)}\mathrm{diag}\{\mathbf{J}^{\mathrm{T}}_{(j,i,b_r)}\mathbf{w}_{(i)}\} + \\ & \sum_{j=1}^{\mathrm{M}}\sum_{b=1}^{\mathrm{B}} \sigma^2_{c,(j,i,b)}\mathrm{diag}\{\mathbf{J}^{\mathrm{T}}_{(j,i,b_r)}\mathbf{w}^*_{(i)}\}\mathbf{\Phi}_{\varepsilon_\nu,(j,i,b)}\mathrm{diag}\{\mathbf{J}^{\mathrm{T}}_{(j,i,b_r)}\mathbf{w}_{(i)}\} + \\ & \sum_{j=1}^{\mathrm{M}}\sum_{b=1}^{\mathrm{B}} \varepsilon_{RCS,(j,i,b)}\mathrm{diag}\{\mathbf{J}^{\mathrm{T}}_{(j,i,b_r)}\mathbf{w}^*_{(i)}\}\mathbf{\Phi}_{\varepsilon_\nu,(j,i,b)}\mathrm{diag}\{\mathbf{J}^{\mathrm{T}}_{(j,i,b_r)}\mathbf{w}_{(i)}\} \\ & \sum_{j=1}^{\mathrm{M}}\sum_{b=1}^{\mathrm{B}} \sigma^2_{c,(j,i,b)}\mathrm{diag}\{\mathbf{J}^{\mathrm{T}}_{(j,i,b_r)}\mathbf{w}^*_{(i)}\}\mathbf{\Phi}_{o2,(j,i,b)}\mathrm{diag}\{\mathbf{J}^{\mathrm{T}}_{(j,i,b_r)}\mathbf{w}_{(i)}\} + \\ & \sum_{j=1}^{\mathrm{M}}\sum_{b=1}^{\mathrm{B}} \varepsilon_{RCS,(j,i,b)}\mathrm{diag}\{\mathbf{J}^{\mathrm{T}}_{(j,i,b_r)}\mathbf{w}^*_{(i)}\}\mathbf{\Phi}_{o2,(j,i,b)}\mathrm{diag}\{\mathbf{J}^{\mathrm{T}}_{(j,i,b_r)}\mathbf{w}_{(i)}\} \\ =& \mathbf{\Theta}_{c,(i)} + \mathbf{\Theta}_{\varepsilon_{RCS},(i)} + \mathbf{\Theta}_{\varepsilon_\nu,(i)} + \mathbf{\Theta}_{\varepsilon_{RCS}\varepsilon_\nu,(i)} + \mathbf{\Theta}_{o2,(i)} + \mathbf{\Theta}_{\varepsilon_{RCS}o2,(i)} \\ & \text{for} \quad i = \{1, 2, \ldots M\}\end{aligned} \tag{6.18}$$

term ε_ν. This results in the following expression:

$$\begin{aligned}\tilde{\mathbf{\Phi}}_{\epsilon,\mathrm{rob}}(l,m) =& \mathrm{e}^{j2\pi\bar{\nu}(l-m)}\left(\frac{\sin[\pi\epsilon(l-m)]}{[\pi\epsilon(l-m)]} + \right. \\ & \frac{1}{\epsilon}\left(\cos[\pi\epsilon(l-m)] - \frac{\sin[\pi\epsilon(l-m)]}{[\pi\epsilon(l-m)]}\right)\varepsilon_\nu + \\ & \left.\frac{1}{\epsilon^2}\left(\frac{2-(\pi\epsilon(l-m))^2}{2}\frac{\sin[\pi\epsilon(l-m)]}{[\pi\epsilon(l-m)]} - \cos[\pi\epsilon(l-m)]\right)\varepsilon_\nu^2\right),\end{aligned} \tag{6.17}$$

where (l, m) identifies the position of the element within the matrix. Substituting Equation (6.17) into Equation (6.15) leads to Equation (6.18). This can also be written in the form:

$$\tilde{\mathbf{\Theta}}_{c,rob} = \mathbf{\Theta}_c + \mathbf{\Theta}_{\varepsilon_{RCS}} + \mathbf{\Theta}_{\varepsilon_\nu} + \mathbf{\Theta}_{\varepsilon_{RCS}\varepsilon_\nu} + \mathbf{\Theta}_{o2} + \mathbf{\Theta}_{\varepsilon_{RCS}o2}.$$

Some necessary remarks on Equation (6.18):

- The notation ˜ identifies the difference between the original matrix $\mathbf{\Theta}_{c,rob}$ and the Taylor series-approximated matrix $\tilde{\mathbf{\Theta}}_{c,rob}$;
- $\mathbf{\Theta}_c$ is the error-free clutter covariance matrix;
- $\mathbf{\Theta}_{\varepsilon_{RCS}}$ is the covariance matrix carrying the uncertainty on the radar cross-section of the clutter;
- $\mathbf{\Theta}_{\varepsilon_\nu}$ is the covariance matrix carrying the uncertainty on the Doppler of the clutter;
- the expected value of $\mathbf{\Theta}_{\varepsilon_{RCS}\varepsilon_\nu}$ can be assumed to be zero since it contains a multiplication between the two errors which are very small and uncorrelated;
- the terms $\mathbf{\Theta}_c$ and $\mathbf{\Theta}_{o2}$ will contribute to the mean of $\tilde{\mathbf{\Theta}}_{c,rob}$;
- the terms $\mathbf{\Theta}_{\varepsilon_{RCS}}$ and $\mathbf{\Theta}_{\varepsilon_\nu}$ will contribute to the variance of $\tilde{\mathbf{\Theta}}_{c,rob}$;
- the term $\mathbf{\Theta}_{\varepsilon_{RCS}o2}$ will contribute with a mean value to the variance of $\mathbf{\Theta}_{\varepsilon_{RCS}}$.

In other words, the new clutter covariance matrix can be re-written as the error-free clutter covariance matrix plus a series of signal-dependant error matrices. The denominator of the SINR can be therefore written as:

$$y = \mathrm{tr}\big((\mathbf{Z} + \mathbf{\Theta}^*_{\varepsilon_{RCS}} + \mathbf{\Theta}^*_{\varepsilon_\nu} + \mathbf{\Theta}^*_{\varepsilon_{RCS}o2} + \mathbf{\Theta}^*_{o2})\mathbf{S}\big),$$

where $\mathbf{Z} = \mathbf{\Theta}^*_c + \sigma_n^2\mathbf{I}$ (please refer to Equation (5.4)). The statistics of y are derived hereafter.

The expected value of y is:

$$\begin{aligned}\mu = \mathbb{E}\{y\} =& \mathbb{E}\{\mathrm{tr}\big((\mathbf{Z} + \mathbf{\Theta}^*_{\varepsilon_{RCS}} + \mathbf{\Theta}^*_{\varepsilon_\nu} + \mathbf{\Theta}^*_{\varepsilon_{RCS}o2} + \mathbf{\Theta}^*_{o2})\mathbf{S}\big)\} \\ =& \mathbb{E}\{\mathrm{tr}\big((\mathbf{Z} + \mathbf{\Theta}^*_{o2})\mathbf{S}\big)\} \\ =& \mathrm{tr}(\mathbf{ZS}) + \mathrm{tr}(\tilde{\mathbf{\Theta}}^*_{o2}\mathbf{S}),\end{aligned} \tag{6.19}$$

where:

$$\tilde{\mathbf{\Theta}}_{o2} = \sum_{j=1}^{\mathrm{M}} \sum_{b=1}^{\mathrm{B}} \sigma^2_{c,(j,b_r)} \mathrm{diag}\{\mathbf{J}^{\mathrm{T}}_{(j,b_r)}\mathbf{w}^*\} \tilde{\mathbf{\Phi}}_{o2,(j,b_r)} \mathrm{diag}\{\mathbf{J}^{\mathrm{T}}_{(j,b_r)}\mathbf{w}\}, \tag{6.20}$$

where, omitting for notational convenience the subscript (j, b_r):

$$\begin{aligned}\tilde{\mathbf{\Phi}}_{o2}(l,m) &= \mathbb{E}\{\mathbf{\Phi}_{o2}(l,m)\} \\ &= \mathbb{E}\left\{\frac{1}{\epsilon^2}\left(\frac{2-(\pi\epsilon(l-m))^2}{2}\frac{\sin[\pi\epsilon(l-m)]}{[\pi\epsilon(l-m)]} - \cos[\pi\epsilon(l-m)]\right)\varepsilon^2_\nu\right\} \\ &= \frac{1}{\epsilon^2}\left(\frac{2-(\pi\epsilon(l-m))^2}{2}\frac{\sin[\pi\epsilon(l-m)]}{[\pi\epsilon(l-m)]} - \cos[\pi\epsilon(l-m)]\right)\sigma^2_{\varepsilon_\nu}.\end{aligned} \tag{6.21}$$

In the above, the mean of $\mathbf{\Theta}_{\varepsilon_{RCS}}$, $\mathbf{\Theta}_{\varepsilon_\nu}$ and $\mathbf{\Theta}_{\varepsilon_{RCS}o2}$ goes to zero and $\mathbb{E}\{\varepsilon^2_\nu\} = \sigma^2_{\varepsilon_\nu}$ as consequence of the Gaussian variables being distributed with $\varepsilon_{RCS,(j,i,b)} \sim \mathcal{CN}(0, \sigma^2_{\varepsilon_{RCS,(j,i,b)}})$ and $\varepsilon_{\nu,(j,i,b)} \sim \mathcal{CN}(0, \sigma^2_{\varepsilon_{\nu,(j,i,b)}})$. The second order statistics of y can be calculated as:

$$\begin{aligned}\mathbb{E}\{y^2\} &= \mathbb{E}\Big\{\Big(\mathrm{tr}\big((\mathbf{Z} + \mathbf{\Theta}^*_{\varepsilon_{RCS}} + \mathbf{\Theta}^*_{\varepsilon_\nu} + \mathbf{\Theta}^*_{\varepsilon_{RCS}o2} + \mathbf{\Theta}^*_{o2})\mathbf{S}\big) - \mu\Big)^2\Big\} \\ &= \mathbb{E}\Big\{\Big(\mathrm{tr}\big((\mathbf{\Theta}^*_{\varepsilon_{RCS}} + \mathbf{\Theta}^*_{\varepsilon_\nu} + \mathbf{\Theta}^*_{\varepsilon_{RCS}o2})\mathbf{S}\big)\Big)^2\Big\}.\end{aligned} \tag{6.22}$$

The statistics of the matrix elements of $\mathbf{\Theta}_{\varepsilon_{RCS}}$ and $\mathbf{\Theta}_{\varepsilon_\nu}$ can be derived as follows:

$$\mathbf{\Theta}_{\varepsilon_{RCS}}(l,m) \sim \mathcal{CN}\Big(0, \mathbf{A}^2_{\varepsilon_{RCS}}(l,m)\sigma^2_{\varepsilon_{RCS}}\Big),$$

$$\mathbf{\Theta}_{\varepsilon_\nu}(l,m) \sim \mathcal{CN}\Big(0, \mathbf{A}^2_{\varepsilon_\nu}(l,m)\sigma^2_{\varepsilon_\nu}\Big),$$

where:

$$\mathbf{A}_{\varepsilon_{RCS}} = \sum_{j=1}^{\mathrm{M}}\sum_{b=1}^{\mathrm{B}} \mathrm{diag}\{\mathbf{J}^{\mathrm{T}}_{(j,b_r)}\mathbf{w}^*\}\mathbf{\Phi}_{\epsilon,(j,b)}\mathrm{diag}\{\mathbf{J}^{\mathrm{T}}_{(j,b_r)}\mathbf{w}\},$$

$$\mathbf{A}_{\varepsilon_\nu} = \sum_{j=1}^{\mathrm{M}}\sum_{b=1}^{\mathrm{B}} \sigma^2_{c,(j,b_r)}\mathrm{diag}\{\mathbf{J}^{\mathrm{T}}_{(j,b_r)}\mathbf{w}^*\}\mathbf{K}\ \mathrm{diag}\{\mathbf{J}^{\mathrm{T}}_{(j,b_r)}\mathbf{w}_{(i)}\},$$

and:

$$\mathbf{K}(l,m) = \mathrm{e}^{j2\pi\bar{\nu}(l-m)} \cdot \frac{1}{\epsilon}\bigg(\cos[\pi\epsilon(l-m)] - \frac{\sin[\pi\epsilon(l-m)]}{[\pi\epsilon(l-m)]}\bigg).$$

Also,

$$\begin{aligned}
&\mathbb{E}\{\mathrm{tr}((\mathbf{\Theta}^*_{\varepsilon_{RCS}} + \mathbf{\Theta}^*_{\varepsilon_{RCS}o2})\mathbf{S})\mathrm{tr}((\mathbf{\Theta}_{\varepsilon^*_{RCS}} + \mathbf{\Theta}^*_{\varepsilon_{RCS}o2})\mathbf{S})^*\} = \\
&= \mathbb{E}\{\mathrm{tr}(\varepsilon_{RCS}\mathbf{A}^*_{\varepsilon_{RCS}}\mathbf{S})\mathrm{tr}(\varepsilon_{RCS}\mathbf{A}^*_{\varepsilon_{RCS}}\mathbf{S})^* + \mathrm{tr}(\varepsilon_{RCS}\mathbf{A}^*_{o2}\mathbf{S})\mathrm{tr}(\varepsilon_{RCS}\mathbf{A}^*_{o2}\mathbf{S})^*\} \\
&= \sigma^2_{\varepsilon_{RCS}}\sum_{j=1}^{\mathrm{M}}\sum_{b=1}^{\mathrm{B}} \mathrm{tr}\Big(\mathrm{diag}\{\mathbf{J}^{\mathrm{T}}_{(j,b_r)}\mathbf{w}^*\}(\mathbf{\Phi}_{\varepsilon,(j,b_r)} + \tilde{\mathbf{\Phi}}_{o2}) \times \mathrm{diag}\{\mathbf{J}^{\mathrm{T}}_{(j,b_r)}\mathbf{w}\}\mathbf{S}\Big)^2 \\
&= \sigma^2_{\varepsilon_{RCS}}\|\mathbf{v}_{RCS}\|^2,
\end{aligned} \tag{6.23}$$

where $\mathbf{v}_{RCS}$ is a vector of dimension $MB \times 1$ containing in each element the value $\mathrm{tr}\Big(\mathrm{diag}\{\mathbf{J}^{\mathrm{T}}_{(j,b_r)}\mathbf{w}^*\}(\mathbf{\Phi}_{\varepsilon,(j,b)} + \tilde{\mathbf{\Phi}}_{o2})\mathrm{diag}\{\mathbf{J}^{\mathrm{T}}_{(j,b_r)}\mathbf{w}\}\mathbf{S}\Big)^2$ for a specific radar j and range-azimuth bin b and

$$\mathbf{A}_{o2} = \sum_{j=1}^{\mathrm{M}}\sum_{b=1}^{\mathrm{B}} \mathrm{diag}\{\mathbf{J}^{\mathrm{T}}_{(j,b_r)}\mathbf{w}^*\}\tilde{\mathbf{\Phi}}_{o2}\mathrm{diag}\{\mathbf{J}^{\mathrm{T}}_{(j,b_r)}\mathbf{w}\}.$$

It needs to be noted that in Equation (6.23) the cross products between $\mathbf{\Theta}_{\varepsilon_{RCS}}$ and $\mathbf{\Theta}_{\varepsilon_{RCS}o2}$ go to zero as they present the multiplication $\sigma^2_{\varepsilon_{RCS}} \times \sigma^2_{\varepsilon_\nu}$ which can be approximated to zero. Furthermore, given the fact that the

two errors are uncorrelated, the expected value would also be zero. The variance of the uncertainty related to the Doppler can be calculated in the same way:

$$\begin{aligned}\mathbb{E}\{\mathrm{tr}(\boldsymbol{\Theta}^*_{\varepsilon_\nu}\mathbf{S})\mathrm{tr}(\boldsymbol{\Theta}^*_{\varepsilon_\nu}\mathbf{S})^*\} &= \mathbb{E}\{\mathrm{tr}(\varepsilon_\nu\mathbf{A}^*_{\varepsilon_\nu}\mathbf{S})\mathrm{tr}(\varepsilon_\nu\mathbf{A}^*_{\varepsilon_\nu}\mathbf{S})^*\} \\ &= \sigma^2_{\varepsilon_\nu}\sum_{j=1}^{\mathrm{M}}\sum_{b=1}^{\mathrm{B}}\mathrm{tr}\Big(\mathrm{diag}\{\mathbf{J}^{\mathrm{T}}_{(j,b_r)}\mathbf{w}^*\}\mathbf{K}_{(j,b)}\mathrm{diag}\{\mathbf{J}^{\mathrm{T}}_{(j,b_r)}\mathbf{w}\}\mathbf{S}\Big)^2 \\ &= \sigma^2_{\varepsilon_\nu}\|\mathbf{v}_\nu\|^2,\end{aligned} \tag{6.24}$$

where $\mathbf{v}_\nu$ is a vector of dimension $MB \times 1$ containing in each element the value $\mathrm{tr}\Big(\mathrm{diag}\{\mathbf{J}^{\mathrm{T}}_{(j,b_r)}\mathbf{w}^*\}\mathbf{K}_{(j,b)}\mathrm{diag}\{\mathbf{J}^{\mathrm{T}}_{(j,b_r)}\mathbf{w}\}\mathbf{S}\Big)^2$ for a specific radar j and range-azimuth bin b_r. In this model the variance depends on the signal as well as other parameters specifically related to the scenario under investigation. The variance of y is written as:

$$\begin{aligned}\mathbb{E}\{y^2\} &= \sigma^2_{\varepsilon_{RCS}}\|\mathbf{v}_{RCS}\|^2 + \sigma^2_{\varepsilon_\nu}\|\mathbf{v}_\nu\|^2 \\ &= \|[\sigma_{\varepsilon_{RCS}}\mathbf{v}_{RCS}; \sigma_{\varepsilon_\nu}\mathbf{v}_\nu]\|^2.\end{aligned} \tag{6.25}$$

Similarly to the case described in Subsection 6.3:

$$P = \int_{-\infty}^{\gamma}\frac{1}{\sqrt{2\pi}\|\mathbf{v}_\varepsilon\|}\exp\Big(-\frac{(y-\mu)^2}{2\|\mathbf{v}_\varepsilon\|^2}\Big)\mathrm{d}y, \tag{6.26}$$

where $\mathbf{v}_\varepsilon = [\sigma_{\varepsilon_{RCS}}\mathbf{v}_{RCS}; \sigma_{\varepsilon_\nu}\mathbf{v}_\nu]$. This leads to the second order cone programming (SOCP) convex constraint:

$$\frac{\mathrm{tr}(\mathbf{R}_{(j)}\mathbf{S})}{\mathrm{SINR}_{min}} - \mathrm{tr}\big((\mathbf{Z}_{(j)} + \tilde{\boldsymbol{\Theta}}^*_{(j),o2})\mathbf{S}\big) \geq \delta_{p_{(j)}}\|\mathbf{v}_\varepsilon\|, \tag{6.27}$$

where $\delta_{p_{(j)}} = \mathrm{erf}^{-1}(2p_{(j)} - 1)\sqrt{2}$.

6.5 Performance Analysis

In order to evaluate the performance of the proposed algorithms, Monte Carlo simulations for the case of $M = 2$ radars have been performed. Monte Carlo simulations use random sampling and statistical modeling to estimate mathematical functions and mimic the operations of complex systems [88]. It is therefore a valuable tool to test the validity of the statistical model at hand.

The SINR of the first radar is maximized while requiring the second radar to achieve a desired SINR_{goal}. The SINR achieved by the optimization for the second radar is investigated for both the robust and non-robust cases. The initial waveforms $\mathbf{s}_{0,1}$ and $\mathbf{s}_{0,2}$ are again fractional Fourier waveforms of length $N = 64$ as developed in [83]. These waveforms provide very good auto-correlation and cross-correlation properties (refer to Figure 1.2), granting therefore good range resolution while maintaining orthogonality between the two radar waveforms. The scatterers are located in $N_c = 4$ range rings. The number of azimuth cells in each ring is $L = 8$. As for the parameters of the target, the various radar cross-sections are set randomly to $\sigma^2_{11,T} = 0.5823$, $\sigma^2_{21,T} = 0.6036$, $\sigma^2_{22,T} = 0.5935$ and $\sigma^2_{12,T} = 0.6203$. The target Doppler values are set randomly to $\nu_{11,T} = 0.0141$, $\nu_{21,T} = 0.0237$, $\nu_{22,T} = 0.0249$ and $\nu_{12,T} = 0.0044$. The clutter power as seen by the radars is $\sigma^2_{11,c} = \sigma^2_{21,c} = \sigma^2_{22,c} = \sigma^2_{12,c} = 1$. The noise variance is set to $\sigma^2_n = 0.25$ and the Doppler frequency is uniformly distributed around its mean value of $\bar{\nu}_c = 0.0267$ with a spread of $\epsilon = 0.02$. Finally, the maximum acceptable deviation to the initial waveform is set to $\delta = 0.1$ and the orthogonality threshold to $\varrho = 0.05$. For solving the SDP problem, CVX Matlab Software for Disciplined Convex Programming [74] toolbox has been used. The

waveform optimization was solved as described in the optimization problem in (5.10) and for thorough description of the optimization method the reader can refer to Chapter 5 and Table 5.2. For all simulations the parameters used were $\Delta_{step} = 0.1$, $\text{SINR}_{iteration} = 0$ at the initialization stage and $\text{SINR}_{goal} = 2\text{dB}$. SINR_{goal} refers to Radar-2 since SINR_1 will be maximized in the objective function of the SDP. The number of Monte Carlo experiments for the simulation results is 10000.

6.5.1 Performance Analysis of Worst-Case Optimization Techniques

In order to test the algorithm for worst-case optimization techniques, the Frobenius norm bound of the error matrix was set to $\beta = 0.18$. This β value corresponds to the 1% of the Frobenius norm of the error-free covariance matrix of the clutter.

As it can be seen in Figure 6.1, the required SINR_{goal} of 2dB was over satisfied with robust optimization techniques but the non-robust case achieved the required SINR of 2dB only half of the times. As expected, the results are over-conservative for the worst-case optimization techniques since the achieved SINR is always higher than the required one by a considerable margin.

The SINR achieved by Radar-1, i.e. the radar whose SINR is maximized, was equal to $\text{SINR}_{1,max} = 3.73\text{dB}$ on average.

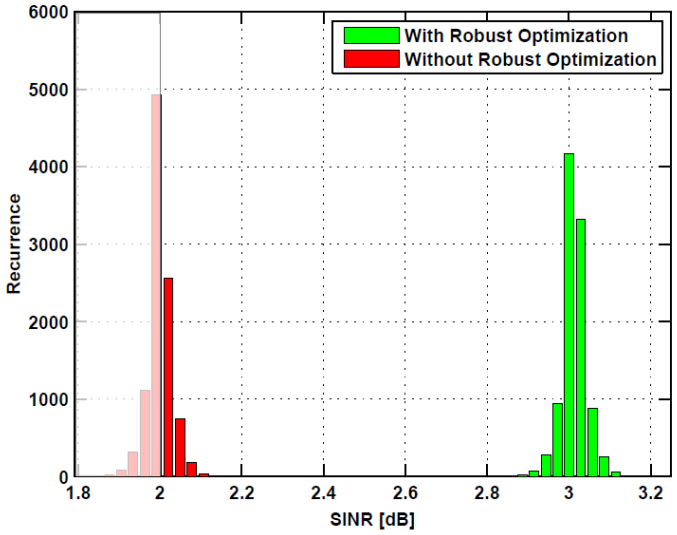

Figure 6.1: Worst-case robust optimization. The required SINR_{goal} of 2dB is achieved every time with robust optimization techniques. The SINR_{goal} is not always achieved for the non-robust case, with the transparent area marking values below 2dB. As expected, the results are over-conservative for the worst-case optimization techniques, i.e. >> 2dB.

6.5.2 Performance Analysis of Stochastic Optimization Techniques

In order to test the stochastic optimization techniques, the standard deviation of the error was set to $\sigma_{e_j} = 0.01$. The value was selected so that $\sqrt{M}\sigma_{e_j}$ is 4% of the mean of $\text{tr}(\mathbf{Z}_{(j)}\mathbf{S})$ (please refer to the probability distribution of $y_{(j)}$ in Subsection 6.3). This has been tested for an SINR achievement rate of 70%, 80% and 90%.

As it can be seen in Figures 6.2, 6.3 and 6.4 respectively, the robust algorithm provides the desired SINR with the desired percentage. On the other hand, the non-robust algorithm was able to achieve the desired SINR of 2dB only about half of the times. The specific values have been provided in Table 6.1.

The average SINR achieved by Radar-1 was equal to $\text{SINR}_{1,max} =$

Desired percentage	70%	80%	90%
Obtained percentage *with* stochastic optimization techniques	70.2	79.8	89.5
Obtained percentage *without* stochastic optimization techniques	50.5	49.7	49.6

Table 6.1: Stochastic optimization results. Comparison between the achievable percentage of a desired SINR_{goal} with stochastic waveform optimization techniques and non-robust waveform optimization techniques.

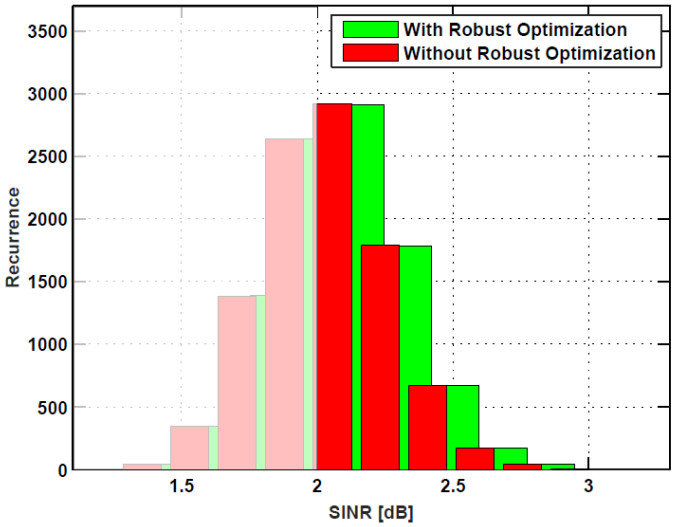

Figure 6.2: Stochastic optimization, SINR of at least 2dB to be achieved 70% of the time. Required SINR_{goal} achieved 70.2% of times with stochastic optimization. Required SINR_{goal} achieved 50.5% without robust optimization. The values not achieving the target are displayed with transparent colours.

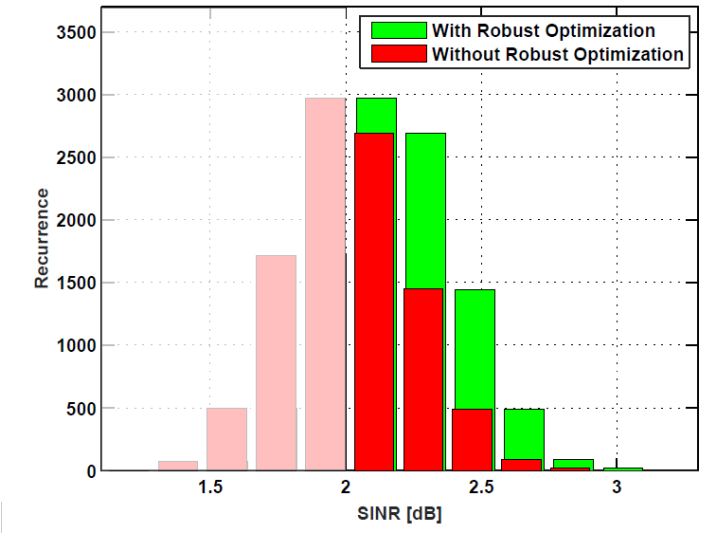

Figure 6.3: Stochastic optimization, SINR of at least 2dB to be achieved 80% of the time. Required SINR_{goal} achieved 79.8% of times with stochastic optimization. Required SINR_{goal} achieved 49.7% without robust optimization. The values not achieving the target are displayed with transparent colours.

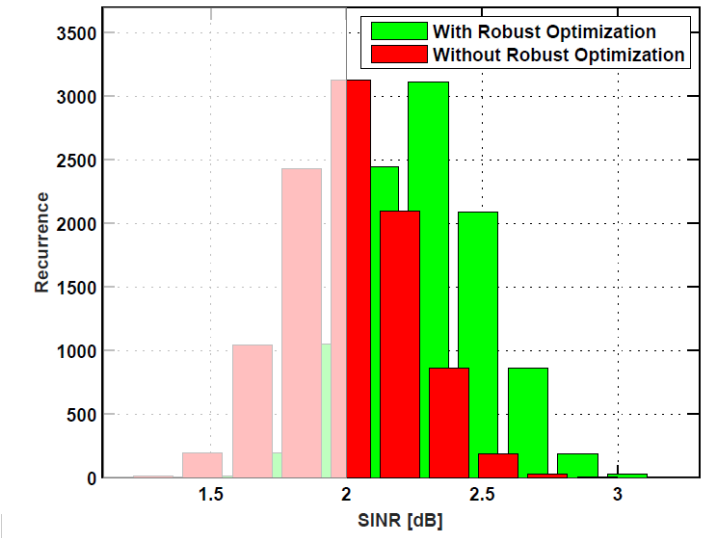

Figure 6.4: Stochastic optimization, SINR of at least 2dB to be achieved 90% of the time. Required SINR_{goal} achieved 89.5% of times with stochastic optimization. Required SINR_{goal} achieved 49.6% without robust optimization. The values not achieving the target are displayed with transparent colours.

3.76dB.

6.5.3 Performance Analysis of Clutter-Specific Stochastic Optimization

In order to test the clutter-specific stochastic optimization, the standard deviation of the error of the RCS of the clutter was set to 20% of the RCS of the clutter, i.e. $\sigma^2_{\varepsilon_{RCS}} = (\frac{\sigma^2_{c,(j,i,b)}}{5})^2$. Similarly, the variation of the error on the Doppler was set to $\sigma^2_{\varepsilon_\nu} = (\frac{\epsilon}{5})^2$ i.e. 20% of ϵ.

The results obtained through the Monte Carlo simulations for clutter-specific stochastic optimization have been provided in the second row of Table 6.2 as well as in the green histograms in Figures 6.5, 6.6 and 6.7. As it can be seen, by using the proposed optimization method, there generally is a very good match between the desired and the obtained SINR percentages. However, a 2.5% mismatch occurs for the 90% case. This is a consequence of the Taylor series approximation of the covariance matrix. Nonetheless, during this Monte Carlo simulation, the value of 1.99dB was achieved 90% of the time, showing how this mismatch is actually negligible.

It needs to be noted that uncertainty could have also been considered on the average of the Doppler $\bar{\nu}_c$. The methodology proposed in this work is still applicable to this case. However, incorporating error to the average Doppler in Equation (6.16) will lead to additional terms in the covariance matrix in Equation (6.18). For clarity of the description of the algorithm, the present work considers uncertainty only on the Doppler spread.

The above results were also compared with non-robust optimization and with the ordinary stochastic method described in Subsection 6.3.

In order to compare the parameter-specific uncertainty with the

stochastic method that considers the uncertainty directly on the covariance matrix of the clutter, the same level of uncertainty needs to be used in both optimizations. To estimate the variance σ_e^2 while making sure to maintain an equivalent level of uncertainty, the following method was employed. Errors were introduced directly to the clutter parameters as in Equation (6.15) and the difference between the true covariance matrix and the error-free covariance matrix was computed as:

$$\tilde{\mathbf{E}} = \mathbf{\Theta}_{c,rob} - \mathbf{\Theta}_c, \tag{6.28}$$

where $\mathbf{\Theta}_{c,rob}$ and $\mathbf{\Theta}_c$ are defined in Equation (6.18). Once $\tilde{\mathbf{E}}$ is obtained, $\mathbb{E}\{|\text{tr}(\tilde{\mathbf{E}}\mathbf{S}|^2\}$ is computed using the 10000 Monte Carlo runs, and the equivalent variance of the error σ_e^2 for the ordinary optimization is obtained using Equation (6.7) as $\frac{\mathbb{E}\{|\text{tr}(\tilde{\mathbf{E}}\mathbf{S}|^2\}}{M}$. It should be noted that $\tilde{\mathbf{E}}$ is a function of the receiver filter $\mathbf{w}_{(i)}$ and the percentage of SINR achievement rate. Hence the equivalent error terms for the final value of $\mathbf{w}_{(i)}$ were computed as obtained by the proposed stochastic optimizations for each percentage 70%, 80% and 90%. The variance σ_e^2 thus obtained was then used for the ordinary stochastic optimization.

The results obtained for non-robust optimization, ordinary stochastic optimization and clutter-specific optimization for the case of when the error is applied directly to the radar cross-section and the Doppler spread, are depicted in Figures 6.5, 6.6 and 6.7 and summed up in Table 6.2. As it can be seen, there is a significant difference between the desired and obtained SINR_{goal} for the case of ordinary stochastic optimization i.e. obtained by assuming that the error is directly applied to the clutter plus noise covariance matrix. The reason is that the assumption of errors applied directly to the

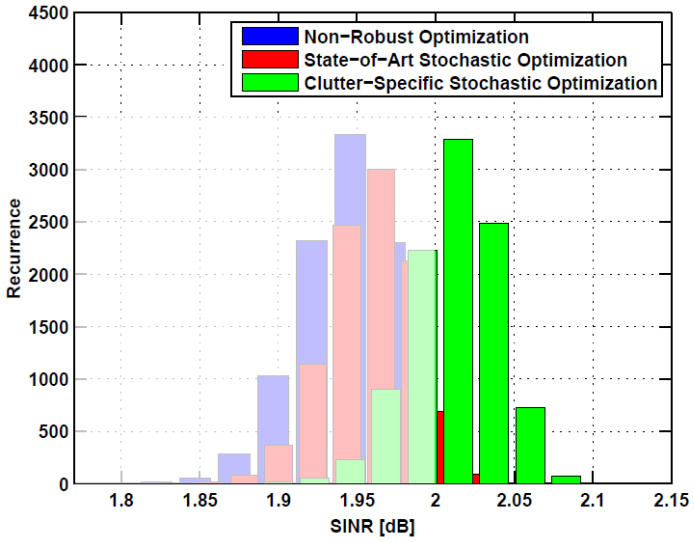

Figure 6.5: The SINR goal of 2dB was required to be achieved 70% of the time. Comparison between non-robust optimization, ordinary stochastic optimization and the clutter-specific optimization proposed in this work. The required SINR_{goal} of 2 dB was achieved 69.8% of times with clutter-specific stochastic optimization. The required SINR_{goal} was achieved 6.6% of the time with the more generic stochastic optimization method and 1.3% with non-robust optimization. The values not achieving the target are displayed with transparent colours.

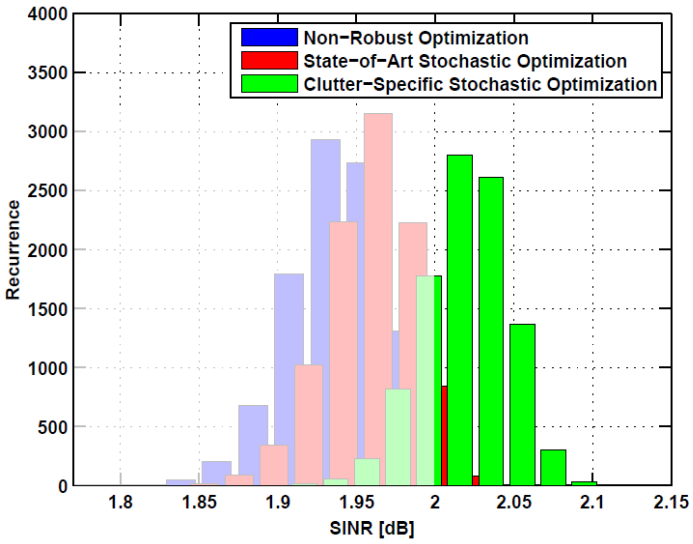

Figure 6.6: The SINR goal of 2dB was required to be achieved 80% of the time. Comparison between non-robust optimization, ordinary stochastic optimization and the clutter-specific optimization proposed in this work. The required SINR_{goal} of 2 dB was achieved 79.4% of times with clutter-specific stochastic optimization. The required SINR_{goal} was achieved 7.0% of the time with the more generic stochastic optimization method and 0.7% with non-robust optimization. The values not achieving the target are displayed with transparent colours.

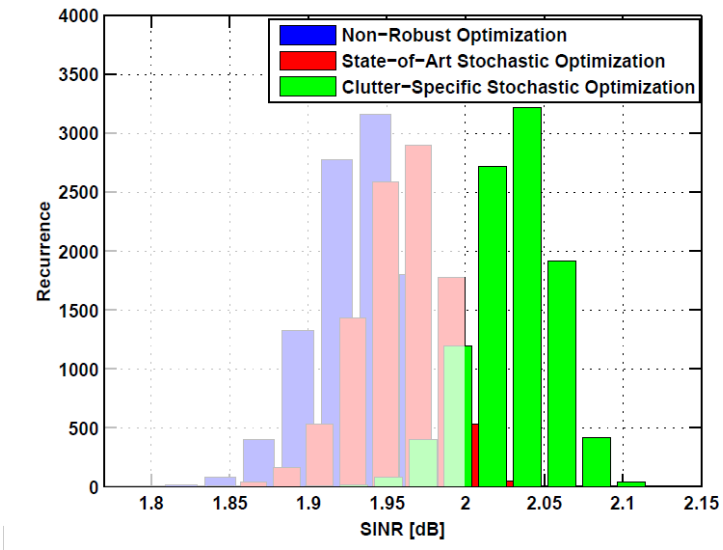

Figure 6.7: The SINR goal of 2dB was required to be achieved 90% of the time. Comparison between non-robust optimization, ordinary stochastic optimization and the clutter-specific optimization proposed in this work. The required SINR_{goal} of 2 dB was achieved 87.5% of times with clutter-specific stochastic optimization. The required SINR_{goal} was achieved 6.5% of the time with the more generic stochastic optimization method and 0.4% with non-robust optimization. The values not achieving the target are displayed with transparent colours.

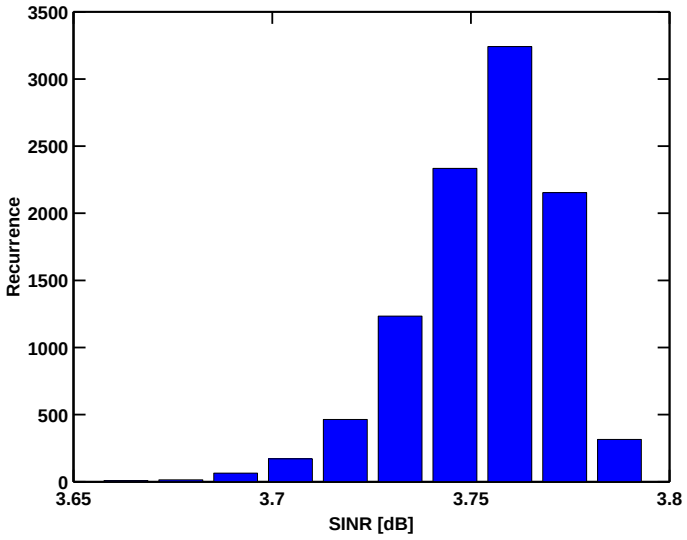

Figure 6.8: Achieved SINR of Radar-1 obtained through clutter specific optimization technique for different realization of the clutter parameters.

covariance matrix is not sufficiently accurate to describe the structure of the error. As a matter of fact, there is almost no difference between the results obtained with non-robust optimization and with ordinary stochastic optimization, proving how this model is an over-simplification when considering signal-dependent clutter. It should be noted that only Radar-2 is required to achieve a specific SINR. But for Radar-1, the aim was to maximize its achievable SINR. Hence robust formulation is applicable to only Radar-2. However, since this work assumes various realizations of the clutter parameters, the SINR achieved by Radar-1 varied slightly but with a mean value of 3.78dB, as shown in Figure 6.8. It needs to be noted that, in principle, the proposed techniques are applicable to more than two radars. However, in practice, the performance in the presence of more than two radars will be very limited in the presence of severely cluttered environment. For example, in our simulation model, the variance of the RCS of the target was selected randomly around the value of 0.6 whereas the variance of the RCS of the

Desired percentage	70%	80%	90%
Obtained percentage with clutter-specific stochastic optimization techniques	69.8	79.4	87.5
Obtained percentage with ordinary stochastic optimization techniques	6.6	7.0	6.5
Obtained percentage with non-robust optimization techniques	1.3	0.7	0.4

Table 6.2: Results for signal-dependent clutter i.e. for error applied directly to the RCS and Doppler of the clutter. Comparison between the achievable percentage of the desired SINR_{goal} by using the proposed optimization that assumes uncertainty on the clutter parameters directly (row 2), the ordinary stochastic optimization (row 3) and non-robust optimization (row 4).

clutter was set to 1. Also, each radar receives signal components from only two distinct paths (one from each radar), and the clutter returns for each radar were modeled by considering $N_c \times L = 32$ range-azimuth bins. In addition, due to the fact that the waveforms cannot be perfectly orthogonal at various time lacks, adding more than two radars will add more interference to the already severely cluttered environment, leading to unrealistically small SINR_{goal} values. Furthermore, adding more radars will increase the computational burden. In addition to these challenges, efficient methods for obtaining realistic estimates of the uncertainty of the clutter parameters is also an important research direction.

6.6 Conclusions

The development of robust optimization techniques is of fundamental importance to enhance the SINR in the presence of uncertainty of the environment. In this chapter the problem of robust waveform design for multistatic cognitive radars in a signal-dependent clutter environment was de-

scribed. Assuming uncertainty on the clutter statistics, this work proposed worst-case robust optimization and stochastic robust optimization methods. While non-robust optimization methods are unable to achieve the required SINR_{goal}, the worst-case robust optimization is always able to achieve this goal SINR, however, this method is over-conservative as it aims to achieve the desired SINR for the worst-case clutter statistics. The stochastic robust optimization is able to achieve the goal SINR with a specified outage probability in the presence of uncertainty on the clutter covariance matrix. Finally, the proposed algorithm that assumes uncertainty directly on the clutter parameter is able to achieve the desired probability of SINR_{goal} with a small margin error due to Taylor series approximation. However, this method is able to outperform the ordinary stochastic robust optimization method significantly due to possible preservation of the structure of the error matrix.

Chapter 7

Robust Matched-Illumination for Through-the-Wall Radar

This chapter discusses robust matched-illumination techniques for a through-the-wall radar. This chapter sets itself apart from the previous ones since it does not regard waveform optimization techniques specifically. Furthermore, the mathematical framework on which it is based differs from the previous chapters. More specifically, this chapter discusses a monostatic radar in a correlated clutter scenario rather than a multistatic radar in signal-dependent clutter. The work discussed in this chapter was inspired by [28]. This chapter fits well within the narrative of this thesis since it discusses robust optimization techniques for cognitive radars. More specifically, the first of the two proposed techniques optimizes the target return (i.e. the vector originated from the convolution between the transmitted signal and the combined wall-target response) and the second technique optimizes the receiver filter.

The work in [28] discusses matched-illumination waveform design for a multistatic through-the-wall radar system where the target is assumed to

be stationary and with a known impulse-response. As mentioned, cognitive techniques such as matched-illumination techniques, rely on a priori knowledge. It is well known, though, that it is difficult to obtain exact a priori information and that uncertainties in the parameters might severely degrade the SINR. In order to create reliable systems that are able to tolerate estimation errors, robust optimization techniques need to be implemented.

The novelty introduced in this chapter is to investigate robust optimization techniques usually known for beamforming, to the through-the-wall radar application, where the uncertainty is placed on the knowledge of the combined target-wall impulse response.

This chapter is organized as follows. In Section 7.1 the general through-the-wall problem is presented. In Section 7.2, robust optimization techniques are discussed. More specifically, the section starts with a short overview on robust beamforming optimization techniques, propaedeutic for a thorough understanding of the proposed techniques. Subsequently, Sub-Section 7.2.1 develops a mathematical model for uncertainty ellipsoid-based optimization and Sub-Section 7.2.2 presents norm-bound vector optimization techniques. Finally, Section 7.3 presents the performance analysis of the proposed techniques and is followed by conclusions.

7.1 Through-the-Wall Radar Problem formulation

For the case of through-the-wall radar systems, the target return can be calculated as the convolution between the transmitted signal $s(t)$ of length N and the combined target-wall impulse response $q(t)$ of duration N_q samples. In matrix form, this can be written as $\mathbf{z} = \mathbf{Qs}$, where $\mathbf{z}$ is the received

target return vector, $\mathbf{Q}$ is the combined wall-target convolution matrix of size $N_z \times N$ with $N_z = N + N_q - 1$, and $\mathbf{s}$ is the transmitted signal vector. More specifically:

$$\underset{N_z\times 1}{\begin{bmatrix} z_1 \\ z_2 \\ \vdots \\ z_{N_z} \end{bmatrix}} = \underset{(N_q+N-1)\times N}{\begin{bmatrix} q_1 & 0 & 0 & \dots & 0 \\ q_2 & q_1 & 0 & \dots & 0 \\ \vdots & \vdots & \vdots & \ddots & \vdots \\ q_{N_q} & q_{N_q-1} & \dots & \dots & q_1 \\ 0 & q_{N_q} & \dots & \dots & q_2 \\ \vdots & & & & \vdots \\ 0 & 0 & \dots & \dots & q_{N_q} \end{bmatrix}} \underset{N\times 1}{\begin{bmatrix} s_1 \\ s_2 \\ \vdots \\ s_N \end{bmatrix}} \tag{7.1}$$

As a result, the received signal vector can be written as $\mathbf{r} = \mathbf{z} + \mathbf{c} + \mathbf{n}$, where $\mathbf{c}$ is the correlated clutter return and $\mathbf{n}$ is the additive noise vector.

After the detection problem in [28] and [89], the receiver filter is calculated as the matched filter:

$$\mathbf{b}_{match} = (\mathbf{\Psi}_c + \sigma_n^2 \mathbf{I})^{-1} \mathbf{z}, \tag{7.2}$$

where $\mathbf{\Psi}_c$ is the covariance matrix of the clutter, σ_n^2 is the noise variance and $\mathbf{I}$ is an identity matrix that has the same dimension as $\mathbf{\Psi}_c$. The received signal is then calculated as $\mathbf{y} = \mathbf{b}_{match}^{\mathrm{H}} \mathbf{r}$, which leads to the SINR:

$$\mathrm{SINR} = \frac{\mathbf{b}_{match}^{\mathrm{H}} \mathbf{z}\mathbf{z}^{\mathrm{H}} \mathbf{b}_{match}}{\mathbf{b}_{match}^{\mathrm{H}} (\mathbf{\Psi}_c + \sigma_n^2 \mathbf{I}) \mathbf{b}_{match}}. \tag{7.3}$$

The objective of the matched-illumination waveform design is to determine the transmitted signal vector $\mathbf{s}$ that maximizes the signal to interference plus noise ratio at the output of the matched filter. The waveform design

problem can be formulated as the maximization over $\mathbf{z}$ (because z is a linear transformation of s) of the cost function in Equation (7.3) [28]. By substituting the value of $\mathbf{b}_{match}$ from Equation (7.2) into Equation (7.3), the optimization can be rewritten as:

$$\max_{\mathbf{z}} \mathbf{z}^{\mathrm{H}}(\mathbf{\Psi}_c + \sigma_n^2\mathbf{I})^{-1}\mathbf{z}, \tag{7.4}$$

or, equivalently:

$$\max_{\mathbf{s}} \mathbf{s}^{\mathrm{H}}\mathbf{Q}^{\mathrm{H}}(\mathbf{\Psi}_c + \sigma_n^2\mathbf{I})^{-1}\mathbf{Q}\mathbf{s}. \tag{7.5}$$

The optimal waveform can be estimated as the eigenvector associated with the largest eigenvalue of the matrix $\mathbf{\Omega} = \mathbf{Q}^{\mathrm{H}}(\mathbf{\Psi}_c + \sigma_n^2\mathbf{I})^{-1}\mathbf{Q}$.

7.2 Robust Optimization Techniques

The matched-illumination work in [28] assumes to have perfect knowledge of the combined wall-target convolution matrix $\mathbf{Q}$ and on the clutter-plus-noise covariance matrix $\mathbf{\Psi}_c + \sigma_n^2\mathbf{I}$. In practical scenarios though, neither of these (particularly $\mathbf{Q}$) is easy to obtain, nor there is any guarantee that its knowledge will be accurate. Estimation errors will lead to incorrect results. This work therefore introduces two different robust optimization techniques that assume uncertainty on the combined wall-target impulse response $\mathbf{q}$. As a consequence, uncertainty on the convolution matrix $\mathbf{Q}$ is also considered as well as on the received signal component $\mathbf{z}$. Both optimization techniques were inspired by robust adaptive beamforming optimizations.

In a traditional beamforming problem, there is an array of N_{beam} sensors receiving signals arriving from K directions. Let $\mathbf{a}(\theta_0)$ denote the response of the array to a plane wave of unit amplitude arriving from direction θ_0

and that a source $\mathbf{s}(t)$ is impinging upon the array from angle θ_0 [90]. The vector array output is then:

$$\mathbf{y}(t) = \mathbf{a}(\theta_0)\mathbf{s}(t) + \mathbf{c}(t) + \mathbf{n}(t), \tag{7.6}$$

where $\mathbf{c}(t)$ is the sum of all signals impinging on the array that do not carry information of interest. The combined sampled beamformer output is then given by:

$$r_{beam}(k) = \mathbf{w}^{\mathrm{H}}\mathbf{y}(k) = \mathbf{w}^{\mathrm{H}}\mathbf{a}(\theta_0)\mathbf{s}(k) + \mathbf{w}^{\mathrm{H}}(\mathbf{c}(k) + \mathbf{n}(k)), \tag{7.7}$$

where $\mathbf{w}$ is a vector of weights [90]. The goal is to make the gain of the received signal component equal to one $\mathbf{w}^{\mathrm{H}}\mathbf{a}(\theta_0) = 1$ and the clutter plus noise $\mathbf{w}^{\mathrm{H}}(\mathbf{c}(k) + \mathbf{n}(k))$ as small as possible. Naming $\mathbf{R}_{c+n} = \mathbb{E}\{(\mathbf{c}(k) + \mathbf{n}(k))(\mathbf{c}(k)+\mathbf{n}(k))^{\mathrm{H}}\}$ the clutter-plus-noise covariance matrix, the traditional beamforming problem can be written as:

$$\begin{aligned} \min_{\mathbf{w}} \quad & \mathbf{w}^{\mathrm{H}}\,\mathbf{R}_{c+n}\,\mathbf{w} \\ \text{s.t.} \quad & \mathbf{w}^{\mathrm{H}}\mathbf{a}(\theta) = 1. \end{aligned} \tag{7.8}$$

In practical applications, $\mathbf{R}_{c+n}$ is replaced by the sample covariance matrix [57].

The solution to the optimization problem can be found thanks to the Lagrangian multiplier:

$$\mathcal{L}(\mathbf{w}, \lambda) = \mathbf{w}^{\mathrm{H}}\mathbf{R}_{c+n}\mathbf{w} + \lambda(\mathbf{w}^{\mathrm{H}}\mathbf{a}(\theta) - 1), \tag{7.9}$$

where λ is the Lagrange multiplier. Calculating the partial derivative of $\mathcal{L}(\mathbf{w}, \lambda)$ with respect to $\mathbf{w}^{\mathrm{H}}$, the following result can be obtained:

$$\mathbf{w} = \frac{\mathbf{R}_{c+n}^{-1}\mathbf{a}(\theta)}{\mathbf{a}^{\mathrm{H}}(\theta)\mathbf{R}_{c+n}^{-1}\mathbf{a}(\theta)}, \tag{7.10}$$

where $\alpha = 1/\mathbf{a}^{\mathrm{H}}(\theta)\mathbf{R}_{c+n}^{-1}\mathbf{a}(\theta)$ can be considered a normalization constant, leading to the result $\mathbf{w} = \alpha\mathbf{R}_{c+n}^{-1}\mathbf{a}(\theta)$. Aiming to show the analogy between the MVDR optimization problem and the one at hand, this excursus will now go back to the discussion of the through-the-wall radar problem.

The optimization problem obtained by maximizing the cost function in (7.3) can be reformulated as minimizing the power of the interference plus noise (denominator) subject to the signal component being equal to one (numerator):

$$\begin{aligned} \min_{\mathbf{b}} \quad & \mathbf{b}^{\mathrm{H}}(\mathbf{\Psi}_c + \sigma_n^2\mathbf{I})\mathbf{b} \\ \text{s.t.} \quad & \mathbf{b}^{\mathrm{H}}\mathbf{z} = 1. \end{aligned} \tag{7.11}$$

Remembering how, in practical applications, the clutter plus noise covariance matrix can be replaced by the sample covariance matrix, the above problem can be reformulated as:

$$\begin{aligned} \min_{\mathbf{b}} \quad & \mathbf{b}^{\mathrm{H}}\,\hat{\mathbf{R}}\,\mathbf{b} \\ \text{s.t.} \quad & \mathbf{b}^{\mathrm{H}}\mathbf{z} = 1, \end{aligned} \tag{7.12}$$

where the sample covariance matrix can be calculated as [58]:

$$\hat{\mathbf{R}} = \frac{1}{N_s}\sum_{n_s=1}^{N_s}\mathbf{y}(n_s)\mathbf{y}^{\mathrm{H}}(n_s), \tag{7.13}$$

where N_s is the number of training snapshots. Once in this form, the connection between the optimization problem in (7.12) and the minimum variance

distortionless response (MVDR) or Capon beamformer (7.8) is apparent. The receiver filter can therefore be calculated as [58]:

$$\mathbf{b} = \hat{\mathbf{R}}^{-1}\mathbf{z}, \tag{7.14}$$

where the normalization constant $1/\mathbf{z}^{\mathrm{H}}\hat{\mathbf{R}}^{-1}\mathbf{z}$ has been omitted as it doesn't affect the SINR value (appearing at both numerator and denominator).

7.2.1 Uncertainty Ellipsoid Optimization

One possible way to make the problem robust by considering uncertainty on the signature of the wall-target response, is to assume that $\mathbf{z}$ belongs to the following uncertainty ellipsoid:

$$[\mathbf{z} - \bar{\mathbf{z}}]^{\mathrm{H}}\mathbf{C}^{-1}[\mathbf{z} - \bar{\mathbf{z}}] \leq 1, \tag{7.15}$$

where $\bar{\mathbf{z}}$ and $\mathbf{C}$ (a positive semidefinite matrix) are given. Furthermore, for the purpose of this problem, it can be assumed that $\mathbf{C} = \varepsilon_1\mathbf{I}$.
By following the directions in [57], solving a covariance fitting problem, the optimization problem in (7.12) can now be reformulated as:

$$\begin{aligned} \max_{\sigma^2,\mathbf{z}} \quad & \sigma^2 \\ \text{s.t.} \quad & \hat{\mathbf{R}} - \sigma^2\mathbf{z}\mathbf{z}^{\mathrm{H}} \geq 0 \\ & [\mathbf{z} - \bar{\mathbf{z}}]^{\mathrm{H}}\mathbf{C}^{-1}[\mathbf{z} - \bar{\mathbf{z}}] \leq 1, \end{aligned} \tag{7.16}$$

where σ^2 is the power of the received signal component. Finally, the above problem can be reformulated in matrix form thanks to the Schur Comple-

ment (refer to next paragraph) [57]:

$$\begin{aligned} \min_{\rho,\mathbf{z}} \quad & \rho \\ \text{s.t.} \quad & \begin{bmatrix} \hat{\mathbf{R}} & \mathbf{z} \\ \mathbf{z}^{\mathrm{H}} & \rho \end{bmatrix} \geq 0 \\ & \begin{bmatrix} \mathbf{C} & (\mathbf{z}-\bar{\mathbf{z}}) \\ (\mathbf{z}-\bar{\mathbf{z}})^{\mathrm{H}} & 1 \end{bmatrix} \geq 0, \end{aligned} \tag{7.17}$$

where $\rho = {}^{1}/_{\sigma^2}$. The constraints in the optimization problem (7.17) are now in the form of linear matrix inequalities, hence this is a semidefinite programming problem that can be solved with convex optimization techniques. The optimized value $\mathbf{z}_{opt}$, obtained by solving the above optimization problem, can then be substituted in Equation (7.14), to calculate the new filter $\mathbf{b}_{opt}$ and then the new SINR value as:

$$\mathrm{SINR}_{opt} = \frac{|\mathbf{b}_{opt}^{\mathrm{H}}\mathbf{z}|^2}{\mathbf{b}_{opt}^{\mathrm{H}}(\boldsymbol{\Psi}_c + \sigma_n^2\mathbf{I})\mathbf{b}_{opt}}. \tag{7.18}$$

7.2.1.1 The Schur Complement

The Schur Complement is a way to solve an $n \times n$ system of linear equations by row reduction. Consider the linear system $\mathbf{Mz} = 0$ with a non-singular leading principal submatrix. Partition M as:

$$\begin{bmatrix} \mathbf{A} & \mathbf{B} \\ \mathbf{C} & \mathbf{D} \end{bmatrix} \tag{7.19}$$

suppose A is non-singular and partition $\mathbf{z}$ as $\begin{bmatrix}\mathbf{x}\\ \mathbf{y}\end{bmatrix}$. The linear system $\mathbf{Mz} = 0$ is now equal to the pair of linear systems:

$$\begin{cases} \mathbf{Ax} + \mathbf{By} = 0 \\ \mathbf{Cx} + \mathbf{Dy} = 0 \end{cases} \tag{7.20}$$

By multiplying the first row of the system by $-\mathbf{CA}^{-1}$ and adding the result to the second row of the system, the following equation can be obtained:

$$-\mathbf{Cx} - \mathbf{CA}^{-1}\mathbf{By} + \mathbf{Cx} + \mathbf{Dy} = (\mathbf{D} - \mathbf{CA}^{-1}\mathbf{B})\mathbf{y} = 0 \tag{7.21}$$

The matrix $(\mathbf{D} - \mathbf{CA}^{-1}\mathbf{B})$ is called the Schur complement of $\mathbf{M}$ relative to $\mathbf{A}$ [91].

7.2.2 Norm-Bound Vector Optimization

Another way to derive robust techniques for the through the wall radar detection, is to assume that the distortions on the combined wall-target impulse response vector $\mathbf{z}$ can be bounded by some constant ε_2 [58]. In case of mismatch between the estimated $\mathbf{z}$ and the real one, a new vector can be defined as:

$$\bar{\mathbf{z}} = \mathbf{z} + \mathbf{\Delta}, \tag{7.22}$$

where $\mathbf{\Delta}$ is an unknown complex vector which describes the effect of the vector distortions. Also, it is assumed that $\mathbf{\Delta}$ is bound by some known constant $\varepsilon_2 > 0$:

$$\|\mathbf{\Delta}\| \leq \varepsilon_2. \tag{7.23}$$

$\bar{\mathbf{z}}$ is one of the possible realizations within the set of all possible real vectors:

$$A(\varepsilon_2) \triangleq \{\mathbf{c} \mid \mathbf{c} = \mathbf{z} + \mathbf{e}, \quad \|\mathbf{e}\| \leq \varepsilon_2\}. \tag{7.24}$$

As a matter of fact, $\bar{\mathbf{z}}$ is the vector within $A(\varepsilon_2)$ for the case of $\mathbf{e} = \boldsymbol{\Delta}$. Then, following the directions in [58], the optimization problem (7.12) can be re-written as:

$$\begin{aligned} \min_{\mathbf{b}} \quad & \mathbf{b}^{\mathrm{H}}\hat{\mathbf{R}}\mathbf{b} \\ \text{s.t.} \quad & |\mathbf{b}^{\mathrm{H}}\mathbf{c}| \geq 1 \quad \forall \quad \mathbf{c} \in A(\varepsilon_2). \end{aligned} \tag{7.25}$$

The constraint in (7.25) can be rewritten by following the instructions in [58] as:

$$|\mathbf{b}^{\mathrm{H}}\mathbf{z} + \mathbf{b}^{\mathrm{H}}\mathbf{e}| \geq 1. \tag{7.26}$$

Or, equivalently [58]:

$$\begin{aligned} & \mathbf{b}^{\mathrm{H}}\mathbf{z} \geq \varepsilon_2\|\mathbf{b}\| + 1 \\ & \mathrm{Im}\{\mathbf{b}^{\mathrm{H}}\mathbf{z}\} = 0, \end{aligned} \tag{7.27}$$

leading to the following optimization problem:

$$\begin{aligned} \min_{\tau,\mathbf{b}} \quad & \tau \\ \text{s.t.} \quad & \|\mathbf{U}\mathbf{b}\| \leq \tau \\ & \mathbf{b}^{\mathrm{H}}\mathbf{z} \geq \varepsilon_2\|\mathbf{b}\| + 1 \\ & \mathrm{Im}\{\mathbf{b}^{\mathrm{H}}\mathbf{z}\} = 0, \end{aligned} \tag{7.28}$$

where $\mathbf{U}$ is the Cholesky factorization of $\hat{\mathbf{R}}$. Every covariance matrix is positive semidefinite, and every positive definite matrix can be factored as $\mathbf{U}^{\mathrm{H}}\mathbf{U}$ where $\mathbf{U}$ is called the Cholesky factor of $\hat{\mathbf{R}}$ and it is an upper triangular matrix with positive diagonal elements. It is then true that:

$$\mathbf{b}^{\mathrm{H}}\hat{\mathbf{R}}\mathbf{b} = \|\mathbf{U}\mathbf{b}\|^2.$$

The optimization problem in (7.28) is a second order cone programming and can be solved with convex optimization techniques.

7.3 Performance Analysis of Robust Optimization Techniques for a Multistatic Through-the-Wall Radar System

To estimate the performance of the proposed robust optimization techniques, Matlab simulations have been performed. $\mathbf{q}$ was modeled as a complex random vector of length $N_q = 8$ with an amplitude of $\sigma_q = 1$ and the vector $\mathbf{c}$ as correlated clutter with a radar cross-section of $\sigma_c = 0.7$. A noise variance of $\sigma_n^2 = 0.1$ was selected and the signal length was set to $N = 10$. The uncertainty on $\mathbf{z}$ was bound by different values of ε_2. More specifically, an error equivalent to 10% of $\mathbf{q}$ was considered to obtain the results in Figures 7.1 and 7.2; and a variable error (ranging from 0% to 100% of $\mathbf{q}$) was considered to generate Figure 7.2 and 7.4.
The optimal waveform $\mathbf{s}$ was initially calculated by following the guidelines in [28] and estimated $\hat{\mathbf{R}}$ by averaging $N_s = 10000$ snapshots. For solving the SDP problem, CVX Matlab Software for Disciplined Convex Programming [74] has been used.

The simulations for the uncertainty ellipsoid optimization discussed in Sub-Section 7.2.1 were initially performed. The results for 10000 realizations of $\bar{\mathbf{z}}$ obtained with a 10% error on the estimation of $\mathbf{q}$, can be found in Figure 7.1. As it can be seen, utilizing robust optimization techniques the SINR could be improved by 1.25dB (over 15%). Furthermore, as it can be seen in Figure 7.2, this improvement becomes more and more significant as

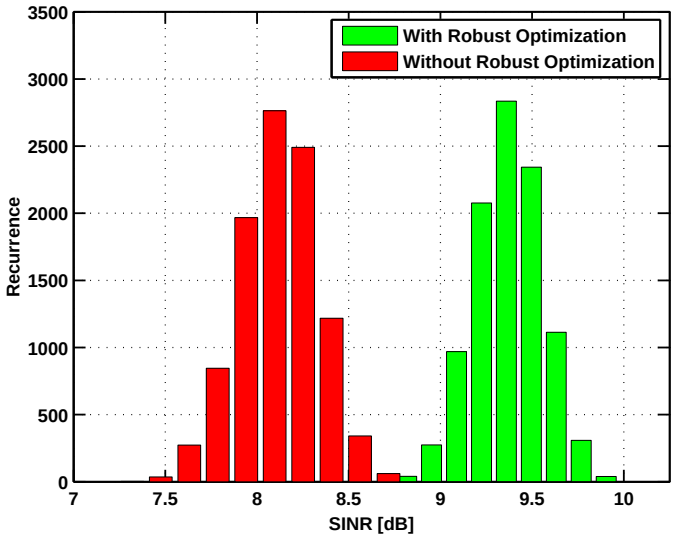

Figure 7.1: Simulation results for Robust Uncertainty Ellipsoid Optimization. The histograms show how, for a 10% error in the estimation of $\mathbf{q}$, robust optimization techniques can improve the SINR by 1.25dB.

error percentage is increased. This is a logical consequence: the bigger the error in the estimation of $\mathbf{q}$, the more it is necessary to implement robust optimization techniques. This improvement is compared against the optimal SINR obtained with no estimation errors on $\mathbf{q}$ (blue line in the figure).

Similarly were also performed the simulations for the norm-bound vector optimization discussed in sub-section 7.2.2. As it can be seen in both Figures 7.3 and 7.4, the performance for the two optimization techniques is identical.

7.4 Conclusion

In this chapter the problem of robust optimization techniques for through-the-wall radars relying on matched-illumination techniques has been considered. Assuming uncertainty on the combined target-wall impulse response and assuming the clutter covariance matrix is unknown a-priori, two robust

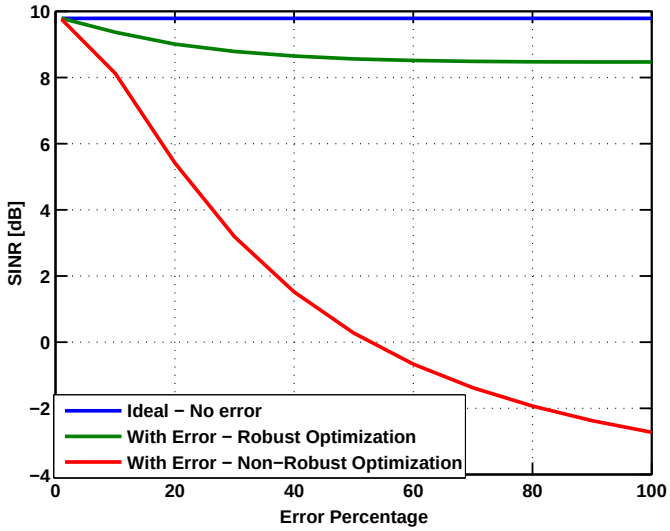

Figure 7.2: Simulation results for robust uncertainty ellipsoid optimization as the error percentage is increased. The plot shows how the bigger the error in the estimation of $\mathbf{q}$, the more it is necessary to implement robust optimization techniques. For instance, estimation errors in the order of 80% can be improved by almost 11dB by implementing robust optimization techniques. The blue line identifies the optimal SINR obtained with no estimation errors on $\mathbf{q}$.

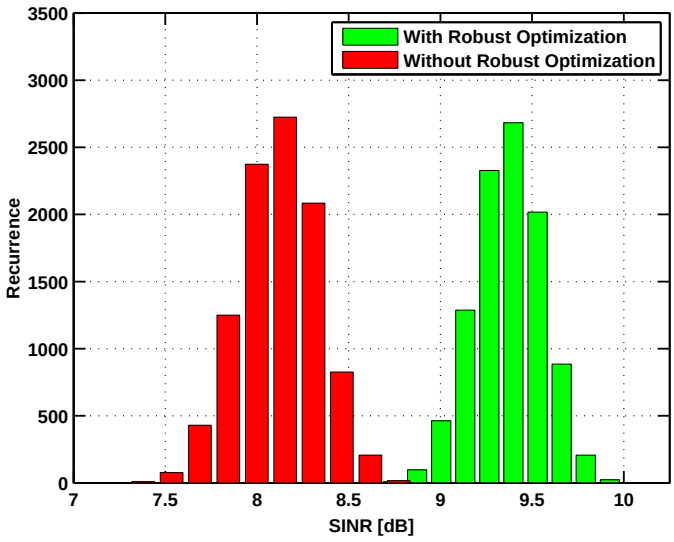

Figure 7.3: Simulation results for norm-bound vector optimization. The histograms show how, for a 10% error in the estimation of $\mathbf{q}$, robust optimization techniques can improve the SINR by 1.25dB.

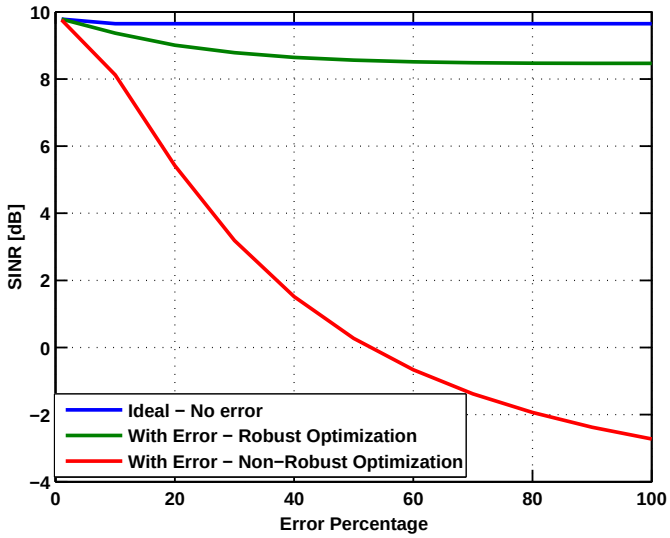

Figure 7.4: Simulation results for norm-bound vector optimization as the error percentage is increased. The plot shows how the bigger the error in the estimation of $\mathbf{q}$, the more it is necessary to implement robust optimization techniques. As in the previous case, estimation errors in the order of 80% can be improved by almost 11dB by implementing robust optimization techniques. The blue line identifies the optimal SINR obtained with no estimation errors on $\mathbf{q}$.

optimization techniques have been proposed. These were developed by noticing the similarities between the MVDR problem and the one at hand. The first was based on an uncertainty ellipsoid model and the second on norm-bound uncertainty. By performing simulations, the validity of both models was demonstrated in terms of SINR improvement. Furthermore, this work showed how it is increasingly necessary to implement robust methods as the uncertainty on the knowledge of the parameters increases.

Chapter 8

Conclusions

In this thesis several mathematical optimization techniques for cognitive radar systems have been presented. The ensemble of chapters provided a series of convex optimizations aimed at increasing the SINR of different radar systems while designing waveforms with desired auto and cross-correlation properties. All considered systems had signal-dependent clutter but differentiated themselves according to size and target requirements. Furthermore, this work included robust optimization techniques. This aspect proved to be of fundamental importance when dealing with cognitive radars and possible errors in prior knowledge of the environment. Also, in order to provide the reader with a further option to implement cognition, the last chapter introduced robust matched-illumination techniques. All discussed optimizations proved effective in terms of improved SINR and waveform characterized by desired features (i.e. narrow beams in the auto-ambiguity function and flat cross-ambiguity functions).

The thesis started with an introductory chapter providing a general overview on radars, waveform analysis, minimum variance distortionless response

(MVDR) beamformers, cognitive radars and convex optimization techniques.

A literature survey was provided in Chapter 2. The main findings were as follows. The sense-learn-adapt approach of cognitive radars makes them an invaluable tool for effective target detection and tracking in complex environments. Waveform design is a key aspect of any signal processing optimization for radar applications. Signals that feature excellent auto and cross-correlation properties are of particular importance in MIMO systems. Furthermore, due to the fact that cognitive radars strongly rely on previous knowledge, it is of paramount importance to implement robust optimization techniques. However, unlike the case of robust beamforming techniques, still not many works have been carried out on cognitive radars, specifically regarding robust optimization techniques. Hence, the focus of this thesis has been on robust optimizations techniques.

In Chapter 3, some important convex optimization definitions and problems were outlined. These were relevant mathematical tools towards a full understanding of the problems and equations developed in the subsequent chapters. Furthermore, thanks to their computational efficiency and the availability of free toolboxes, they are of a great importance towards solving many engineering problems.

In Chapter 4, the model of a bistatic cognitive radar was introduced by developing a known monostatic model within the literature. This system model is the foundational building block of the models introduced in the subsequent chapters. It provided a progressive description of the discussed research and was propaedeutic towards a thorough understanding of the thesis. This chapter also introduced a cognitive optimization framework for the iterative design of orthogonal signals and receiver filter in a highly reverberating environment. The optimization problem was formulated in convex

form. The aim was to maximize the SINR at the receiving radar under some constraints on the waveforms. These were mutual orthogonality, transmission of finite energy and similarity to an initial waveform with optimal auto and cross-correlation properties. Simulation results showed how, by selecting parameters in an accurate way, this optimization technique proved to be a valuable tool to enhance the SINR at the receiver filter output while maintaining a narrow peak in the auto-ambiguity functions and a flat cross-ambiguity function.

In Chapter 5, different waveform optimization techniques for cognitive radar networks have been presented. The three proposed methods complemented each other and are suitable for different environments and systems. The first method is applicable to small networks with no specific target requirements and is aimed at maximizing the accumulated target returns of all radars. Simulation results proved how this method is effective in terms of SINR improvement and number of iterations. On the other hand, it does not allow any design freedom (i.e. target SINR requirements). The other two optimization techniques can be applied to any number of radars and allow the user to impose specific SINR requirements. These methods were designed for systems with specific targets or uneven environments. However, due to the fact that they require an additional inner loop, they are less applicable to systems with more stringent time efficiency requests. More specifically, the first of the two algorithms was based on the optimization of the signal strength at a desired radar while keeping the SINR of the remaining radars at an acceptable level. The second one was based on the optimization of the SINR of all radars equally. Both proved to be effective in terms of SINR improvement.

In Chapter 6, different robust waveform design techniques were presen-

ted for multistatic cognitive radars. Assuming uncertainty on the clutter statistics, the work proposed worst-case robust optimization and stochastic robust optimization methods. While non-robust optimization methods were unable to achieve the required SINR_{goal}, the worst-case robust optimization was always able to achieve the goal SINR. However, worst-case methods proved over-conservative. Stochastic robust optimization techniques were also developed and able to achieve the goal SINR with a specified outage probability in the presence of uncertainty on the clutter covariance matrix. Furthermore, an algorithm that assumed uncertainty directly on the clutter parameter was able to achieve the desired probability of SINR_{goal} with a small margin error due to Taylor series approximation. This method was able to outperform the ordinary stochastic robust optimization method significantly due to possible preservation of the structure of the error matrix for the case of signal-dependent clutter.

Finally, in Chapter 7, the problem of robust optimization techniques for through-the-wall radars relying on matched-illumination techniques was discussed. Assuming uncertainty on the combined target-wall impulse response and assuming the clutter covariance matrix to be unknown a-priori, two robust optimization techniques were proposed. These were developed by noticing the similarities between the minimum variance distortionless response (MVDR) problem and the one at hand. The first was based on an uncertainty ellipsoid model and the second on norm-bound uncertainty. By performing simulations, the validity of both the models was proved in terms of SINR improvement. Furthermore, it was shown how it is increasingly necessary to implement robust techniques as the uncertainty on the knowledge of the parameters increases.

8.0.1 Future Work

The works presented in this thesis can be extended towards the following areas of research.

All of the optimization techniques proposed for cognitive radar networks can be extended to distributed optimization techniques (as opposed to utilizing a centralized controller). In this scenario, the individual radars as well as the central base station are all cognitive. However, distributed optimization techniques have the ability to avoid extensive feedback to a centralized processor and will be able to react to changes in the environment faster than a centralized scheme. A second option for further developments is to impose the desired features of the waveform directly in the optimization problem rather than relying on a previously known waveform. The problem could therefore be reformulated as the maximization of the cost function (i.e. the SINR) subject to minimizing both the range-Doppler sidelobes and cross-correlation peaks in the auto-ambiguity and cross-ambiguity functions.

For the matched illumination work, the proposed model could be extended to multiple radars. Additionally, an iterative method optimizing the transmitted waveform and the receiver filter until convergence to optimized SINR values, could be designed.

Bibliography

[1] C. Clemente, C. Ilioudis, D. Gaglione, K. Thompson, S. Weiss, I. Proudler, and J. J. Soraghan, "Reuse of fractional waveform libraries for MIMO radar and electronic countermeasures ," in *2014 6th International Symposium on Communications, Control and Signal Processing (ISCCSP)*, 2014, pp. 505–508.

[2] S. Haykin, "Cognitive Radar: A Way of the Future," *IEEE Signal Processing Magazine*, vol. 23, no. 1, pp. 30–40, 2006.

[3] S. Kingsley and S. Quegan, *Understanding Radar Systems*. SciTech Publishing Inc., 1999.

[4] E. Knott, J. F. Schaeffer, and M. T. Tuley, *Radar Cross Section*, 2nd ed. SciTech Publishing Inc., 15 July 2004.

[5] N. Levanon and E. Mozeson, *Radar Signals*. Wiley, 2004.

[6] A. Filip and D. Shutin, "Ambiguity function analysis for ofdm-based ldacs passive multistatic radar," *IEEE Trans. Aerosp. Elec. Syst.*, vol. Early Access, pp. 1–1, 2017.

[7] L. Wu, P. Babu, and D. P. Palomar, "Transmit waveform/receive filter design for mimo radar with multiple waveform constraints," *IEEE Trans. Sig. Proc.*, vol. 66, no. 6, pp. 1526 – 1540, 2018.

[8] A. Aubry, A. De Maio, B. Jiang, and S. Zhang, "Ambiguity Function Shaping for Cognitive Radar via Complex Quartic Optimization," *IEEE Transactions on Signal Processing*, vol. 61, no. 22, pp. 5603–5619, 2013.

[9] L. Wu, P. Babu, and D. P. Palomar, "Cognitive radar-based sequence design via sinr maximization," *IEEE Trans. Sig. Proc.*, vol. 65, no. 3, pp. 779 – 793, 2017.

[10] S. Haykin, *Adaptive Filter Theory*, 4th ed. Prentice Hall, 2002.

[11] Y. Li, S. A. Vorobyov, and A. Hassanien, "Robust beamforming for jammers suppression in MIMO radar," in *2014 IEEE Radar Conference*, 2014, pp. 0629–0634.

[12] D. J. Rabideau, "Mimo radar waveforms and cancellation ratio," *IEEE Trans. Aerosp. Elect. Syst.*, vol. 48, no. 2, pp. 1167 – 1178, 2012.

[13] U. K. Majumder, M. R. Bell, and M. Rangaswamy, "A novel approach for designing diversity radar waveforms that are orthogonal on both transmit and receive," in *2013 IEEE Radar Conference (RadarCon13)*, 2013, pp. 1–6.

[14] J. R. Guerci, R. M. Guerci, J. S. Bergin, and M. C. Wicks, "CoFAR: Cognitive Fully Adaptive Radar," in *2014 IEEE Radar Conference*, 2014, pp. 984–989.

[15] X. Li, Z. Hu, R. C. Qiu, Z. Wu, J. P. Browning, and M. C. Wicks, "Demonstration of Cognitive Radar for Target Localization Under Interference," *IEEE Transactions on Aerospace and Electronic Systems*, vol. 50, no. 4, pp. 2440–2455, 2014.

[16] A. Aubry, A. Demaio, A. Farina, and M. Wicks, "Knowledge-Aided (Potentially Cognitive) Transmit Signal and Receive Filter Design in Signal-Dependent Clutter," *IEEE Transactions on Aerospace and Electronic Systems*, vol. 49, no. 1, pp. 93–117, 2013.

[17] S. Haykin, Y. Xue, and T. N. Davidson, "Optimal waveform design for cognitive radar," in *Conf. Rec. - Asilomar Conf. Signals, Syst. Comput.*, 2008, pp. 3–7.

[18] S. Boyd and L. Vandenberghe, *Convex Optimization*. Cambridge University Press, 2004.

[19] S. Haykin, "Cognitive dynamic systems: Radar, control, and radio [point of view]," *Proceedings of the IEEE*, vol. 100, no. 7, pp. 2095–2103, 2012.

[20] ——, "Cognitive Radar Networks," in *1st IEEE International Workshop on Computational Advances in Multi-Sensor Adaptive Processing, 2005*, 2005, pp. 1–3.

[21] W. Huleihel, J. Tabrikian, and R. Shavit, "Optimal Adaptive Waveform Design for Cognitive MIMO Radar," *IEEE Transactions on Signal Processing*, vol. 61, no. 20, pp. 5075–5089, 2013.

[22] P. Chavali and a Nehorai, "Scheduling and Power Allocation in a Cognitive Radar Network for Multiple-Target Tracking," *IEEE Trans. Signal Process.*, vol. 60, no. 2, pp. 715–729, 2012.

[23] U. Gunturkun, "Bivariate Empirical Mode Decomposition for Cognitive Radar Scene Analysis," *IEEE Signal Process. Lett.*, vol. 22, no. 5, pp. 603–607, 2015.

[24] R. A. Romero and N. A. Goodman, "Adaptive Beamsteering for Search-and-Track Application with Cognitive Radar Network," in *IEEE National Radar Conference - Proceedings*, 2011, pp. 1091–1095.

[25] K. L. Bell, C. J. Baker, G. E. Smith, J. T. Johnson, and M. Rangaswamy, "Fully Adaptive Radar for Target Tracking Part I: Single Target Tracking," in *2014 IEEE Radar Conference*, 2014, pp. 0303–0308.

[26] A. D. Maio, S. D. Nicola, Y. Huang, S. Zhang, and A. Farina, "Code design to optimize radar detection performance under accuracy and similarity constraints," *IEEE Trans. Signal Process.*, vol. 56, no. 11, pp. 5618–5629, 2008.

[27] A. Aubry, A. De Maio, G. Foglia, and D. Orlando, "Adaptive Radar Detection in Diffuse Multipath Environments," in *2014 IEEE Radar Conference*, 2014, pp. 1135–1138.

[28] F. Ahmad and M. G. Amin, "Matched-illumination waveform design for a multistatic through-the-wall radar system," *IEEE Journal on Selected Topics in Signal Processing*, vol. 4, no. 1, pp. 177–186, 2010.

[29] R. A. Romero and N. A. Goodman, "Cognitive radar network: Cooperative adaptive beamsteering for integrated search-and-track application," *IEEE Trans. Aerosp. Electron. Syst.*, vol. 49, no. 2, pp. 915–931, 2013.

[30] G. S. Antonio, D. R. Fuhrmann, and F. C. Robey, "MIMO radar ambiguity functions," in *Conf. Rec. - Asilomar Conference on Signals, Systems, and Computers*, 2006, pp. 36–40.

[31] C. Y. Chen and P. P. Vaidyanathan, "MIMO radar ambiguity properties and optimization using frequency-hopping waveforms," *IEEE Trans. Signal Process.*, vol. 56, no. 12, pp. 5926–5936, 2008.

[32] J. Zhang, H. Wang, and X. Zhu, "Adaptive Waveform Design for Separated Transmit/Receive ULA-MIMO Radar ," *IEEE Trans. Signal Process.*, vol. 58, no. 9, pp. 4936–4942, 2010.

[33] A. M. Haimovich, R. S. Blum, and L. J. Cimini, "MIMO Radar with Widely Separated Antennas," *IEEE Signal Processing Magazine*, vol. 25, no. 1, pp. 116–129, 2008.

[34] H. Nikookar, "Signal Design for Context Aware Distributed Radar Sensing Networks Based on Wavelets," *Selected Topics in Signal Processing, IEEE Journal of*, vol. 9, no. 2, pp. 204–215, 2015.

[35] M. R. Bell, "Information Theory and Radar Waveform Design," *IEEE Transactions on Information Theory*, vol. 39, no. 5, pp. 1578–1597, 1993.

[36] Y. Nijsure, Y. Chen, P. Rapajic, C. Yuen, Y. H. Chew, and T. F. Qin, "Information-Theoretic Algorithm for Waveform Optimization within Ultra Wideband Cognitive Radar Network," in *2010 IEEE International Conference on Ultra-Wideband*, 2010, pp. 595–598.

[37] Y. Nijsure, Y. Chen, S. Boussakta, C. Yuen, H. C. Yong, and D. Zhiguo, "Novel System Architecture and Waveform Design for Cognitive Radar Radio Networks," *IEEE Transactions on Vehicular Technology*, vol. 61, no. 8, pp. 3630–3642, 2012.

[38] H. Chen and A. B. Gershman, "Robust Adaptive Beamforming for General-Rank Signal Models Using Positive Semi-Definite Covariance

Constraint," in *2008 International Conference on Acoustics, Speech and Signal Processing (ICASSP)*, 2008, pp. 2341–2344.

[39] N. Sharaga, J. Tabrikian, and H. Messer, "Optimal Cognitive Beamforming for Target Tracking in MIMO Radar/Sonar," *IEEE Journal of Selected Topics in Signal Processing*, vol. 9, no. 8, pp. 1440–1450, 2015.

[40] S. M. Kay, *Fundamentals of Statistical Signal Processing: Estimation Theory*. Prentice Hall, 1993, vol. 1.

[41] R. A. Romero, J. Bae, and N. A. Goodman, "Theory and application of SNR and mutual information matched illumination waveforms," *IEEE Transactions on Aerospace and Electronic Systems*, vol. 47, no. 2, pp. 912–927, 2011.

[42] B. Jiu, H. Liu, L. Zhang, Y. Wang, and T. Luo, "Wideband Cognitive Radar Waveform Optimization for Joint Target Radar Signature Estimation and Target Detection," *IEEE Transactions on Aerospace and Electronic Systems*, vol. 51, no. 2, pp. 1530–1546, 2015.

[43] A. Renaux, P. Forster, P. Larzabal, and C. Richmond, "The Bayesian Abel Bound on the Mean Square Error," in *2006 IEEE International Conference on Acoustics Speech and Signal Processing Proceedings (ICASSP)*, vol. 3, 2006, pp. 9 – 12.

[44] A. Renaux, P. Forster, P. Larzabal, C. D. Richmond, and A. Nehorai, "A fresh look at the bayesian bounds of the weiss-weinstein family," *IEEE Trans. Sig. Proc.*, vol. 56, no. 11, pp. 5334 – 5352, 2008.

[45] G. Babur, O. A. Krasnov, A. Yarovoy, and P. Aubry, " Nearly orthogonal waveforms for MIMO FMCW Radar," *IEEE Trans. Aerosp. Electron. Syst.*, no. 3, pp. 1426–1437, 2013.

[46] B. J. Wysocki and T. A. Wysocki, "Modified Walsh-Hadamard sequences for DS CDMA wireless systems," *Int. J. Adapt. Control Signal Process.*, vol. 16, no. 8 SPEC., pp. 589–602, 2002.

[47] ——, "Optimization of orthogonal polyphase spreading sequences for wireless data applications," in *IEEE 54th Vehicular Technology Conference. VTC Fall 2001. Proceedings (Cat. No.01CH37211)*, vol. 3, 2001, pp. 1894–1898.

[48] M. Piezzo, A. Aubry, A. D. Maio, A. Farina, and M. Wicks, "Cognitive design of the receive filter and transmitted phase code in reverberating environment," *IET Radar, Sonar Navig.*, vol. 6, no. 9, pp. 822–833, 2012.

[49] A. D. Maio, Y. Huang, D. P. Palomar, S. Zhang, and A. Farina, "Fractional QCQP with applications in ml steering direction estimation for radar detection ," *IEEE Trans. Signal Process.*, vol. 59, no. 1, pp. 172–185, 2011.

[50] S. Shahbazpanahi, A. B. Gershman, Z. Q. Lou, and K. M. Wong, "Robust adaptive beamforming for general-rank signal models," *IEEE Transactions on Signal Processing*, vol. 51, no. 9, pp. 2257–2269, 2003.

[51] V. Sharma, I. Wajid, A. B. Gershman, H. Chen, and S. Lambotharan, "Robust downlink beamforming using positive semi-definite covariance constraints," in *International ITG Workshop on Smart Antennas, 2008 (WSA)*, 2008, pp. 36–41.

[52] K. Cumanan, R. Krishna, Z. Xiong, and S. Lambotharan, "Multiuser spatial multiplexing techniques with constraints on interference tem-

perature for cognitive radio networks," *IET Signal Processing*, vol. 4, no. 6, pp. 666 – 672, 2010.

[53] B. Chalise, S. Shahbazpanahi, A. Czylwik, and A. Gershman, "Robust Downlink Beamforming Based on Outage Probability Specifications," *IEEE Transactions on Wireless Communications*, vol. 6, no. 10, pp. 3498–3503, 2007.

[54] A. Aubry, A. De Maio, and M. M. Naghsh, "Optimizing Radar Waveform and Doppler Filter Bank via Generalized Fractional Programming," *IEEE Journal of Selected Topics in Signal Processing*, vol. 9, no. 8, pp. 1387–1399, 2015.

[55] B. Tang and J. Tang, "Robust waveform design of wideband cognitive radar for extended target detection," in *2016 IEEE International Conference on Acoustics, Speech and Signal Processing (ICASSP)*, 2016, pp. 3096–3100.

[56] L. Wang, L. Wang, Y. Zeng, and M. Wang, "Jamming power allocation strategy for MIMO radar based on MMSE and mutual information," *IET Radar, Sonar & Navigation*, vol. 11, no. 7, pp. 1081 – 1089, 2017.

[57] W. Z. Stoica, Petre and J. Li, "Robust Capon Beamforming," *IEEE Signal Processing Letters*, vol. 10, no. 6, pp. 172–175, 2003.

[58] S. A. Vorobyov, A. B. Gershman, and Z. Luo, "Robust adaptive beamforming using worst-case performance optimization via Second-Order Cone programming," in *2002 International Conference on Acoustics, Speech and Signal Processing (ICASSP)*, 2002, pp. 2901–2905.

[59] A. B. Gershman, Z. Luo, S. Shahbazpanahi, and S. A. Vorobyov, "Robust adaptive beamforming using worst-case performance optimiza-

tion," in *The Thrity-Seventh Asilomar Conference on Signals, Systems & Computers, 2003*, 2003, pp. 1353 – 1357.

[60] J. Li, P. Stoica, and Z. Wang, "On Robust Capon Beamforming and Diagonal Loading," *IEEE Trans. Sign. Proc.*, vol. 51, no. 7, pp. 1702 – 1715, 2003.

[61] R. G. Lorenz and S. P. Boyd, "Robust Minimum Variance Beamforming," *IEEE Transactions on Signal Processing*, vol. 53, no. 5, pp. 1684–1696, 2005.

[62] D. Li, Q. Yin, P. Mu, and W. Guo, "Robust MVDR Beamforming Using the DOA Matrix Decomposition," in *2011 1st International Symposium on Access Spaces (ISAS)*, 2011, pp. 105–110.

[63] Y. Li, S. A. Vorobyov, and A. Hassanien, "Robust beamforming for jammers suppression in MIMO radar," in *2014 IEEE Radar Conference*, 2014, pp. 0629 – 0634.

[64] Y. Liu, H. Wang, and J. Wang, "Robust Multiple-Input Multiple-Output Radar Waveform Design in the Presence of Clutter," *IET Radar Sonar & Navigation*, vol. 10, no. 7, pp. 1249 – 1259, 2016.

[65] A. Aubry, A. D. Maio, Y. Huang, and M. Piezzo, "Robust Multiple-Input Multiple-Output Radar Waveform Design in the Presence of Clutter," *IEEE Trans. Sign. Proc.*, vol. 64, no. 22, pp. 5848 – 5860, 2016.

[66] X. Cheng, A. Aubry, D. Ciuonzo, A. D. Maio, and X. Wang, "Robust Waveform and Filter Bank Design of Polarimetric Radar," *IEEE Trans. Aerosp. Electron. Syst.*, vol. 53, no. 1, pp. 370 – 384, 2017.

[67] N. Shahbazi, A. Abbasfar, and M. Jabbarian-Jahromi, "Robust design of measurement matrix for CS-MIMO radar in clutter," *IEEE Electron. Lett.*, vol. 53, no. 23, pp. 1548 – 1550, 2017.

[68] P.-J. Chung, H. Du, and M. Chen, "Robust transmit beamforming for multi-user MIMO systems using a probabilistic constraint approach," in *2012 IEEE 11th International Conference on Signal Processing*, vol. 2, 2012, pp. 1482 – 1485.

[69] W. Zhang and S. A. Vorobyov, "Joint Robust Transmit/Receive Adaptive Beamforming for MIMO Radar Using Probability-Constrained Optimization," *IEEE Sign. Proc. Lett.*, vol. 23, no. 1, pp. 112 – 116, 2016.

[70] S. R. Price, S. Member, J. P. Donohoe, S. Member, and J. Fairley, "Impacts of Wall and Target Interaction on Matched Illumination Waveforms for TWRI," *IEEE Geoscience and Remote Sensing Letters*, vol. 12, no. 7, pp. 1402–1405, 2015.

[71] A. Santra, R. Srinivasan, K. Jadia, and G. Alleon, "Ambiguity functions, processing gains, and Cramer-Rao bounds for matched illumination radar signals," *IEEE Trans. Aerosp. Electron. Syst.*, vol. 51, no. 3, pp. 2225 – 2235, 2015.

[72] H. Hindi, "A Tutorial on Convex Optimization," in *Proceedings of the 2004 American Control Conference*, vol. 4, 2004, pp. 3252 – 3265.

[73] Z. quan Luo and W. Yu, "An introduction to convex optimization for communications and signal processing," *IEEE J. Sel. Areas Commun.*, vol. 24, no. 8, pp. 1426 – 1438, 2006.

[74] M. Grant and S. Boyd, *CVX: Matlab software for disciplined convex programming*, September 2013, version 2.0 beta. [Online]. Available: http://cvxr.com/cvx

[75] J. F. Sturm, "Using sedumi 1.02, a matlab toolbox for optimization over symmetric cones," *Optimization Methods and Software*, vol. 11, no. 1-4, pp. 625–653, 1999.

[76] J. Lofberg, "YALMIP : a toolbox for modeling and optimization in MATLAB," in *2004 IEEE International Conference on Robotics and Automation (IEEE Cat. No.04CH37508)*, 2004, pp. 284 – 289.

[77] L. Vandenberghe and S. Boyd, "Semidefinite programming," *SIAM Rev.*, vol. 38, no. 1, pp. 49–95, 1996.

[78] J. Li, J. R. Guerci, and L. Xu, "Signal waveform's optimal-under-restriction design for active sensing," *IEEE Sign. Proc. Lett.*, vol. 13, no. 9, pp. 565–568, 2006.

[79] G. Rossetti, A. Deligiannis, and S. Lambotharan, "Waveform Design and Receiver Filter Optimization for Multistatic Cognitive Radar," in *2016 IEEE Radar Conference (RadarConf)*, 2016, pp. 1 – 5.

[80] Z. quan Luo, W. kin Ma, A. M. cho So, Y. Ye, and S. Zhang, "Semidefinite Relaxation of Quadratic Optimization Problems," *IEEE Signal Process. Mag.*, vol. 27, no. 3, pp. 20–34, 2010.

[81] G. Rossetti and S. Lambotharan, "Waveform Optimization Techniques for Bi-Static Cognitive Radars," in *Signal Processing and Its Applications (CSPA), 2016 IEEE 12th International Colloquium on*, 2016, pp. 115 – 118.

[82] ——, "Coordinated Waveform Design and Receiver Filter Optimization for Cognitive Radar Networks," in *The Ninth IEEE Sensor Array and Multichannel Signal Processing Workshop (SAM 2016)*, 2016, pp. 1 – 5.

[83] C. V. Ilioudis, C. Clemente, I. Proudler, and J. J. Soraghan, "Performance Analysis of Fractional Waveform Libraries in MIMO Radar Scenario," in *2015 IEEE Radar Conference (RadarCon)*, 2015, pp. 1119–1124.

[84] J. Li and P. Stoica, *Robust Adaptive Beamforming*, ser. Wiley Series in Telecommunications and Signal Processing. Wiley, 2005.

[85] G. Rossetti and S. Lambotharan, "Robust Optimization Techniques for Cognitive Radar Networks," *IEEE Access*, vol. PP, no. 99, pp. 1 – 1, 2017.

[86] M. Shaghaghi and R. S. Adve, "Training-based Adaptive Transmit-Receive Beamforming for Random Phase Radar Signals," in *2016 IEEE Radar Conference (RadarConf)*.

[87] D. Bertsimas, D. B. Brown, and C. Caramanis, "Theory and Applications of Robust Optimization," *SIAM Review*, vol. 53, no. 3, pp. 464–501, 2011.

[88] R. L. Harrison, "Introduction To Monte Carlo Simulation," in *AIP conference proceedings*, 2010, pp. 17 – 21.

[89] S. M. Kay, *Fundamentals of Statistical Signal Processing: Detection Theory*. Prentice Hall, 1998, vol. 2.

[90] J. Li and P. Stoica, *Robust Adaptive Beamforming*. John Wiley & Sons, 2006.

[91] R. Horn and F. Zhang, *The Schur Complement and Its Applications. Basic Properties of the Schur Complement*, ser. Numerical Methods and Algorithms. Springer, Boston, MA, 2005, vol. 4.